

1 Impact of PØD NuMu Samples in BANFF

2 Hogan, Matthew<sup>1</sup> and Toki, Walter<sup>1</sup>

3 June 10, 2019

4 <sup>1</sup>Colorado State University, Fort Collins, USA

5 **Abstract**

6 This is the abstract

# 7 **Contents**

8	<b>1 Introduction</b>	<b>10</b>
9	1.1 ND280 . . . . .	10
10	1.1.1 The PØD . . . . .	11
11	1.2 Usage of ND280 Psyche Software . . . . .	12
12	<b>2 ND280 Binned Likelihood</b>	<b>14</b>
13	2.1 Motivation . . . . .	14
14	2.2 Introduction to Conditional PDFs and Likelihoods . . . . .	15
15	2.3 BANFF Fit Test Statistic . . . . .	16
16	2.3.1 Flux, Cross Section, and Detector Systematics . . . . .	20
17	<b>3 PØD Selections and Data Samples</b>	<b>24</b>
18	3.1 Global Reconstruction . . . . .	24
19	3.2 PØD Selection Cuts . . . . .	26
20	3.2.1 Pre-Selection Cuts . . . . .	26
21	3.2.2 $\nu_\mu$ CC Inclusive in FHC Cut . . . . .	28
22	3.2.3 $\bar{\nu}_\mu$ CC Inclusive in RHC Cuts . . . . .	28
23	3.2.4 $\nu_\mu$ Background CC Inclusive in RHC Cuts . . . . .	30
24	3.3 Sample Kinematics and Validation . . . . .	30
25	3.4 PØD Water-Out Samples . . . . .	31
26	3.4.1 CC Inclusive . . . . .	32
27	3.4.1.1 $\nu_\mu$ Selection in FHC Mode: . . . . .	32
28	3.4.1.2 $\bar{\nu}_\mu$ Selection in RHC Mode: . . . . .	39
29	3.4.1.3 $\nu_\mu$ Background Selection in RHC Mode: . . . . .	46
30	3.4.2 CC 1-Track (CCQE Enhanced) . . . . .	53

31	3.4.2.1	$\nu_\mu$ Selection in FHC Mode:	53
32	3.4.2.2	$\bar{\nu}_\mu$ Selection in RHC Mode:	60
33	3.4.2.3	$\nu_\mu$ Background Selection in RHC Mode:	67
34	3.4.3	CC N-Tracks (CCnQE Enhanced)	67
35	3.4.3.1	$\nu_\mu$ Selection in FHC Mode:	67
36	3.4.3.2	$\bar{\nu}_\mu$ Selection in RHC Mode:	74
37	3.4.3.3	$\nu_\mu$ Background Selection in RHC Mode:	81
38	3.5	PØD Water-In Samples	81
39	3.5.1	CC Inclusive	82
40	3.5.1.1	$\nu_\mu$ Selection in FHC Mode:	82
41	3.5.1.2	$\bar{\nu}_\mu$ Selection in RHC Mode:	89
42	3.5.1.3	$\nu_\mu$ Background Selection in RHC Mode:	96
43	3.5.2	CC 1-Track (CCQE Enhanced)	96
44	3.5.2.1	$\nu_\mu$ Selection in FHC Mode:	96
45	3.5.2.2	$\bar{\nu}_\mu$ Selection in RHC Mode:	103
46	3.5.2.3	$\nu_\mu$ Background Selection in RHC Mode:	110
47	3.5.3	CC N-Tracks (CCnQE Enhanced)	110
48	3.5.3.1	$\nu_\mu$ Selection in FHC Mode:	110
49	3.5.3.2	$\bar{\nu}_\mu$ Selection in RHC Mode:	111
50	3.5.3.3	$\nu_\mu$ Background Selection in RHC Mode:	111
51	3.5.4	Differences Between Water-Out and Water-In Samples	111
52	<b>4</b>	<b>PØD-Only BANFF Parameterization</b>	<b>112</b>
53	4.1	PØD Samples Fit Binning	112
54	4.1.1	Fit Binning Determination	113
55	<b>5</b>	<b>Detector Systematics</b>	<b>116</b>

56	<b>6 Fitter Validation</b>	<b>117</b>
57	<b>7 Fitter Results</b>	<b>118</b>
58	<b>8 Discussion</b>	<b>119</b>
59	<b>References</b>	<b>120</b>
60	<b>Nomenclature</b>	<b>122</b>

61 **List of Figures**

62	1.1 Exploded view of the off-axis detectors of ND280 . . . . .	10
63	1.2 Cartoon of the PØD . . . . .	11
64	1.3 Cartoon of an Individual PØDule . . . . .	12
65	1.4 Fluxing Tuning Histogram for FHC Events . . . . .	13
66	2.1 BANFF Pre-fit Flux Covariance Matrix . . . . .	20
67	2.2 BANFF ND280 NuMu and ANuMu Flux Binning Parameters . . . . .	21
68	2.3 Cross Section Parameters Pre-fit Correlation Matrix . . . . .	21
69	3.1 PØD Air FHC $\nu_\mu$ CC Inc. Lepton Cand. Reco. Momentum by True Particle	33
70	3.2 PØD Air FHC $\nu_\mu$ CC Inc. Lepton Cand. Reco. $\cos\theta$ by True Particle . . .	34
71	3.3 PØD Air FHC $\nu_\mu$ CC Inc. Lepton Cand. Reco. Momentum by NEUT Mode	35
72	3.4 PØD Air FHC $\nu_\mu$ CC Inc. Lepton Cand. Reco. $\cos\theta$ by NEUT Mode . . .	36
73	3.5 PØD Air FHC $\nu_\mu$ CC Inc. Lepton Cand. Reco. Momentum by True Topology	37
74	3.6 PØD Air FHC $\nu_\mu$ CC Inc. Lepton Cand. Reco. $\cos\theta$ by True Topology . .	38
75	3.7 PØD Air FHC $\nu_\mu$ CC Inc. Lepton Cand. True $E_\nu$ by NEUT Mode . . . .	39
76	3.8 PØD Air RHC $\bar{\nu}_\mu$ CC Inc. Lepton Cand. Reco. Momentum by True Particle	40
77	3.9 PØD Air RHC $\bar{\nu}_\mu$ CC Inc. Lepton Cand. Reco. $\cos\theta$ by True Particle . . .	41
78	3.10 PØD Air RHC $\bar{\nu}_\mu$ CC Inc. Lepton Cand. Reco. Momentum by NEUT Mode	42
79	3.11 PØD Air RHC $\bar{\nu}_\mu$ CC Inc. Lepton Cand. Reco. $\cos\theta$ by NEUT Mode . . .	43
80	3.12 PØD Air RHC $\bar{\nu}_\mu$ CC Inc. Lepton Cand. Reco. Momentum by True Topology	44
81	3.13 PØD Air RHC $\bar{\nu}_\mu$ CC Inc. Lepton Cand. Reco. $\cos\theta$ by True Topology . .	45
82	3.14 PØD Air FHC $\bar{\nu}_\mu$ CC Inc. Lepton Cand. True $E_\nu$ by NEUT Mode . . . .	46
83	3.15 PØD Air RHC $\nu_\mu$ CC Inc. Lepton Cand. Reco. Momentum by True Particle	47
84	3.16 PØD Air RHC $\nu_\mu$ CC Inc. Lepton Cand. Reco. $\cos\theta$ by True Particle . . .	48
85	3.17 PØD Air FHC $\nu_\mu$ CC Inc. Lepton Cand. Reco. Momentum by NEUT Mode	49

86	3.18 PØD Air FHC $\nu_\mu$ CC Inc. Lepton Cand. Reco. $\cos\theta$ by NEUT Mode . . . . .	50
87	3.19 PØD Air FHC $\nu_\mu$ CC Inc. Lepton Cand. Reco. Momentum by True Topology	51
88	3.20 PØD Air FHC $\nu_\mu$ CC Inc. Lepton Cand. Reco. $\cos\theta$ by True Topology . . . . .	52
89	3.21 PØD Air FHC $\nu_\mu$ CC Inc. Lepton Cand. True $E_\nu$ by NEUT Mode . . . . .	53
90	3.22 PØD Air FHC $\nu_\mu$ CC Inc. Lepton Cand. Reco. Momentum by True Particle	54
91	3.23 PØD Air FHC $\nu_\mu$ CC Inc. Lepton Cand. Reco. $\cos\theta$ by True Particle . . . . .	55
92	3.24 PØD Air FHC $\nu_\mu$ CC Inc. Lepton Cand. Reco. Momentum by NEUT Mode	56
93	3.25 PØD Air FHC $\nu_\mu$ CC Inc. Lepton Cand. Reco. $\cos\theta$ by NEUT Mode . . . . .	57
94	3.26 PØD Air FHC $\nu_\mu$ CC Inc. Lepton Cand. Reco. Momentum by True Topology	58
95	3.27 PØD Air FHC $\nu_\mu$ CC Inc. Lepton Cand. Reco. $\cos\theta$ by True Topology . . . . .	59
96	3.28 PØD Air FHC $\nu_\mu$ CC Inc. Lepton Cand. True $E_\nu$ by NEUT Mode . . . . .	60
97	3.29 PØD Air RHC $\bar{\nu}_\mu$ CC Inc. Lepton Cand. Reco. Momentum by True Particle	61
98	3.30 PØD Air RHC $\bar{\nu}_\mu$ CC Inc. Lepton Cand. Reco. $\cos\theta$ by True Particle . . . . .	62
99	3.31 PØD Air RHC $\bar{\nu}_\mu$ CC Inc. Lepton Cand. Reco. Momentum by NEUT Mode	63
100	3.32 PØD Air RHC $\bar{\nu}_\mu$ CC Inc. Lepton Cand. Reco. $\cos\theta$ by NEUT Mode . . . . .	64
101	3.33 PØD Air RHC $\bar{\nu}_\mu$ CC Inc. Lepton Cand. Reco. Momentum by True Topology	65
102	3.34 PØD Air RHC $\bar{\nu}_\mu$ CC Inc. Lepton Cand. Reco. $\cos\theta$ by True Topology . . .	66
103	3.35 PØD Air FHC $\bar{\nu}_\mu$ CC Inc. Lepton Cand. True $E_\nu$ by NEUT Mode . . . . .	67
104	3.36 PØD Air FHC $\nu_\mu$ CC N-Tracks Lepton Cand. Reco. Momentum by True Particle . . . . .	68
105		
106	3.37 PØD Air FHC $\nu_\mu$ CC N-Tracks Lepton Cand. Reco. $\cos\theta$ by True Particle .	69
107	3.38 PØD Air FHC $\nu_\mu$ CC N-Tracks Lepton Cand. Reco. Momentum by NEUT Mode . . . . .	70
108		
109	3.39 PØD Air FHC $\nu_\mu$ CC N-Tracks Lepton Cand. Reco. $\cos\theta$ by NEUT Mode .	71
110	3.40 PØD Air FHC $\nu_\mu$ CC N-Tracks Lepton Cand. Reco. Momentum by True Topology . . . . .	72
111		

112	3.41 PØD Air FHC $\nu_\mu$ CC N-Tracks Lepton Cand. Reco. $\cos\theta$ by True Topology	73
113	3.42 PØD Air FHC $\nu_\mu$ CC N-Tracks Lepton Cand. True $E_\nu$ by NEUT Mode . . .	74
114	3.43 PØD Air RHC $\bar{\nu}_\mu$ CC N-Tracks Lepton Cand. Reco. Momentum by True	
115	Particle . . . . .	75
116	3.44 PØD Air RHC $\bar{\nu}_\mu$ CC N-Tracks Lepton Cand. Reco. $\cos\theta$ by True Particle .	76
117	3.45 PØD Air RHC $\bar{\nu}_\mu$ CC N-Tracks Lepton Cand. Reco. Momentum by NEUT	
118	Mode . . . . .	77
119	3.46 PØD Air RHC $\bar{\nu}_\mu$ CC N-Tracks Lepton Cand. Reco. $\cos\theta$ by NEUT Mode .	78
120	3.47 PØD Air RHC $\bar{\nu}_\mu$ CC N-Tracks Lepton Cand. Reco. Momentum by True	
121	Topology . . . . .	79
122	3.48 PØD Air RHC $\bar{\nu}_\mu$ CC N-Tracks Lepton Cand. Reco. $\cos\theta$ by True Topology	80
123	3.49 PØD Air FHC $\bar{\nu}_\mu$ CC N-Tracks Lepton Cand. True $E_\nu$ by NEUT Mode . .	81
124	3.50 PØD Water FHC $\nu_\mu$ CC Inc. Lepton Cand. Reco. Momentum by True Particle	83
125	3.51 PØD Water FHC $\nu_\mu$ CC Inc. Lepton Cand. Reco. $\cos\theta$ by True Particle .	84
126	3.52 PØD Water FHC $\nu_\mu$ CC Inc. Lepton Cand. Reco. Momentum by NEUT Mode	85
127	3.53 PØD Water FHC $\nu_\mu$ CC Inc. Lepton Cand. Reco. $\cos\theta$ by NEUT Mode .	86
128	3.54 PØD Water FHC $\nu_\mu$ CC Inc. Lepton Cand. Reco. Momentum by True Topology	87
129	3.55 PØD Water FHC $\nu_\mu$ CC Inc. Lepton Cand. Reco. $\cos\theta$ by True Topology .	88
130	3.56 PØD Water FHC $\nu_\mu$ CC Inc. Lepton Cand. True $E_\nu$ by NEUT Mode . . .	89
131	3.57 PØD Water RHC $\bar{\nu}_\mu$ CC Inc. Lepton Cand. Reco. Momentum by True Particle	90
132	3.58 PØD Water RHC $\bar{\nu}_\mu$ CC Inc. Lepton Cand. Reco. $\cos\theta$ by True Particle .	91
133	3.59 PØD Water RHC $\bar{\nu}_\mu$ CC Inc. Lepton Cand. Reco. Momentum by NEUT Mode	92
134	3.60 PØD Water RHC $\bar{\nu}_\mu$ CC Inc. Lepton Cand. Reco. $\cos\theta$ by NEUT Mode .	93
135	3.61 PØD Water RHC $\bar{\nu}_\mu$ CC Inc. Lepton Cand. Reco. Momentum by True	
136	Topology . . . . .	94
137	3.62 PØD Water RHC $\bar{\nu}_\mu$ CC Inc. Lepton Cand. Reco. $\cos\theta$ by True Topology .	95

138	3.63 PØD Water FHC $\bar{\nu}_\mu$ CC Inc. Lepton Cand. True $E_\nu$ by NEUT Mode . . . . .	96
139	3.64 PØD Water FHC $\nu_\mu$ CC 1-Track Lepton Cand. Reco. Momentum by True	
140	Particle . . . . .	97
141	3.65 PØD Water FHC $\nu_\mu$ CC 1-Track Lepton Cand. Reco. $\cos\theta$ by True Particle	98
142	3.66 PØD Water FHC $\nu_\mu$ CC 1-Track Lepton Cand. Reco. Momentum by NEUT	
143	Mode . . . . .	99
144	3.67 PØD Water FHC $\nu_\mu$ CC 1-Track Lepton Cand. Reco. $\cos\theta$ by NEUT Mode	100
145	3.68 PØD Water FHC $\nu_\mu$ CC 1-Track Lepton Cand. Reco. Momentum by True	
146	Topology . . . . .	101
147	3.69 PØD Water FHC $\nu_\mu$ CC 1-Track Lepton Cand. Reco. $\cos\theta$ by True Topology	102
148	3.70 PØD Water FHC $\nu_\mu$ CC 1-Track Lepton Cand. True $E_\nu$ by NEUT Mode . .	103
149	3.71 PØD Water RHC $\bar{\nu}_\mu$ CC Inc. Lepton Cand. Reco. Momentum by True Particle	104
150	3.72 PØD Water RHC $\bar{\nu}_\mu$ CC Inc. Lepton Cand. Reco. $\cos\theta$ by True Particle . .	105
151	3.73 PØD Water RHC $\bar{\nu}_\mu$ CC Inc. Lepton Cand. Reco. Momentum by NEUT Mode	106
152	3.74 PØD Water RHC $\bar{\nu}_\mu$ CC Inc. Lepton Cand. Reco. $\cos\theta$ by NEUT Mode . .	107
153	3.75 PØD Water RHC $\bar{\nu}_\mu$ CC Inc. Lepton Cand. Reco. Momentum by True	
154	Topology . . . . .	108
155	3.76 PØD Water RHC $\bar{\nu}_\mu$ CC Inc. Lepton Cand. Reco. $\cos\theta$ by True Topology .	109
156	3.77 PØD Water FHC $\bar{\nu}_\mu$ CC Inc. Lepton Cand. True $E_\nu$ by NEUT Mode . . . .	110
157	4.1 PØD Momenta Resolutions Used for Fit Binning . . . . .	114
158	4.2 PØD Angular Residuals Used for Fit Binning . . . . .	115

159 **List of Tables**

160      3.1 PØD WT FV and Corridor Definition . . . . .	28
161      3.2 POT Used in This Analysis . . . . .	31

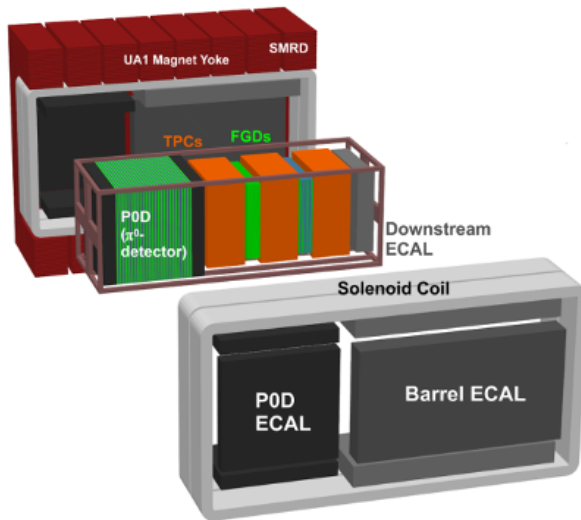


Figure 1.1: Exploded view of the off-axis detectors of ND280. The neutrino beam is directed from left to right along the figure.

## 162 1 Introduction

163 The primary goal of an oscillation experiment is to measure the parameters in a neutrino  
 164 mixing matrix. All other parameters, with some having some theoretical importance to  
 165 fundamental physics, are nuisance parameters. To understand the methodology of Beam  
 166 and Near detector Flux task Force (BANFF) fit, it is relevant to understand how likelihood  
 167 fitting works.

### 168 1.1 ND280

169 The T2K near detector (ND) complex consists of on-axis and off-axis detectors at 280m away  
 170 from the secondary beamline proton target. The off-axis detector is used in this analysis  
 171 which consists of several subdetectors housed inside the UA1/NOMAD magnet yoke as  
 172 shown in figure 1.1. A similar analysis was also performed with the on-axis detector and is  
 173 available in T2K-TN-335[13]. . The magnet provides a 0.2T magnetic field which is designed  
 174 to provide momentum and particle identification for the tracker region.

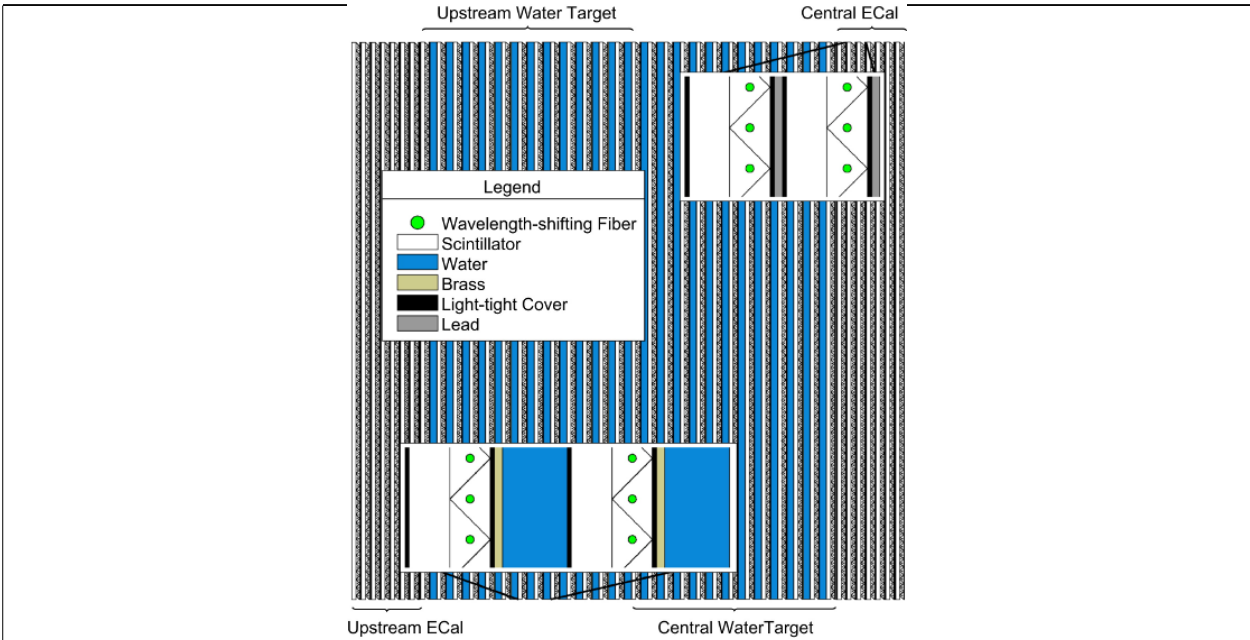


Figure 1.2: This cartoon illustrates the concept design of the PØD where the neutrino beam is approaching from the left.

### <sup>175</sup> 1.1.1 The PØD

<sup>176</sup> The PØD, short for  $\pi^0$  Detector, is a plastic scintillator based tracking calorimeter inside the  
<sup>177</sup> ND280 basket. The PØD is constructed as many sandwiches of active and inactive materials  
<sup>178</sup> designed to fully contain  $\pi^0$  decay photons. The four primary regions inside the PØD in  
<sup>179</sup> order of upstream to downstream of the neutrino beam are the upstream ECal (USECal),  
<sup>180</sup> upstream water target (WT), central WT, and central ECal (CECal). A representation of  
<sup>181</sup> the entire PØD can be seen in Figure 1.2. Each active module, also called a PØDule, consists  
<sup>182</sup> of two orthogonally oriented sheets of triangular, scintillator-doped plastic bars as shown in

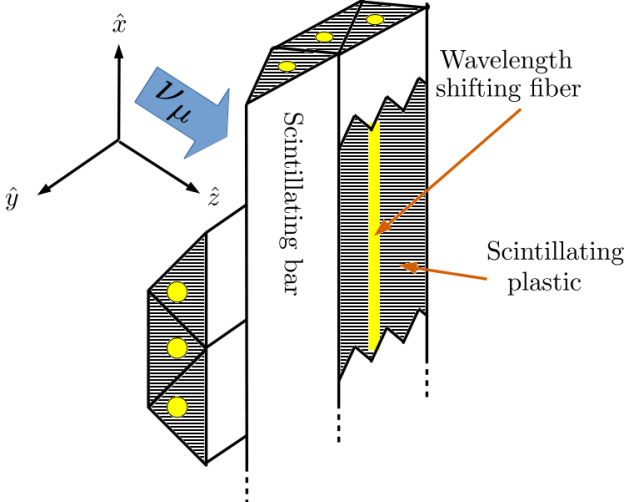


Figure 1.3: This cartoon illustrates the design of a PØDule with orthogonal layers of scintillating, triangular bars. When a charged particle travels through the bar such as a muon from CC interaction, the scintillation light is captured and wavelength shifted inside a fiber bored in the center of each bar. The wavelength shifted light is later observed by a photon counter.

183     Figure 1.3. The ECal regions are designed to contain decay photons inside the PØD by  
 184     alternating the scintillator planes with lead sheets. The WT regions, as compared to the lead  
 185     sheets in the ECals, alternate a thin brass sheet and water filled bags between the PØDules.  
 186     A unique feature of the PØD is that the water can be drained out resulting in two detector  
 187     configurations: water-in and water-out.

## 188     1.2 Usage of ND280 Psyche Software

189     Psyche is a general framework for data handling, event selections, and systematic evaluations  
 190     with toy experiments. Psyche is a “lean” package from the perspective of analyzing MC  
 191     events since that functionality is built heavily into Highland2. The analysis performed in  
 192     this technical note required making additions to psyche in order replicate features available  
 193     in Highland2. It would be wise for future analyses to build a selection in Highland2 and  
 194     migrate that psyche once mature.

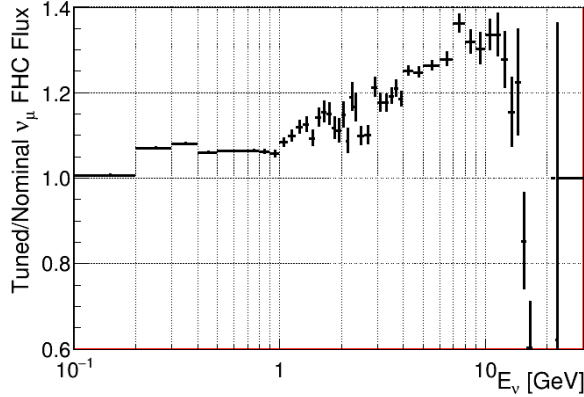


Figure 1.4: Fluxing tuning histogram for  $\nu_\mu$  FHC events taken from the 13av3 flux release.

BANFF uses a psyche package called psycheSteering that interfaces with all the psyche tools to manage the migration of samples into its analysis code. New PØD selections were added to the psycheSelections package and validated using the psycheSteering AnalysisManager class. The AnalysisManager provides the functionality to get the true and reconstructed detector observables from each reconstructed event along with the flux tuning and detector systematic weights.

Flux tuning is the process of applying an event weight based on the true neutrino energy, flavor, and run period. Since the ND280 MC uses a series of models to describe the expected neutrino flux, it cannot perfectly model the true flux nor know the beam conditions at run time. The beam group is responsible for releasing the expected and measured neutrino flux in order to account for these differences. To flux tune an event, the relevant neutrino flavor flux histogram must be referenced. The weight is extracted by taking the ratio of the tuned flux to the nominal flux in the MC for a given neutrino energy. As an example Figure 1.4 shows the flux tuning weights for true  $\nu_\mu$  FHC events.

209 **2 ND280 Binned Likelihood**

210 The BANFF likelihood maximization procedure is a binned likelihood maximization of the  
211 ND280 data. In a ND280 and Super-Kamiokande (SK) joint fit, the measurements from both  
212 detectors are considered along with their respective nuisance parameters. This approach  
213 is more computationally expensive compared to the Markov Chain Monte Carlo analysis  
214 (MaCh3) which will not be explained here. The BANFF likelihood maximization, hitherto  
215 referred to as the “BANFF-fit”, includes nuisance parameters that affect the measurement of  
216 the oscillation parameters, but are not physics goals of the T2K experiment. The BANFF-  
217 fit parameters and their respective covariances are then used as inputs in the oscillation  
218 analysis. This “divide-and-conquer” approach allows for more rapidly completed studies  
219 on the effects of model parameters and biases present. Also this approach should provide  
220 the same result with a joint ND280 and SK analysis as is performed in MaCh3. However,  
221 information encoded in the ND280 measurements for shared nuisance parameters like the  
222 neutrino flux is inevitably lost in the BANFF-fit.

223 The modern BANFF-fit likelihood is described in detail in TN-220[10]. It uses a fre-  
224 quentist approach to find the best nuisance parameter set to maximize a binned likelihood.  
225 Subsequent updates to the BANFF analysis[11, 4, 3] increase the sample sizes and systematic  
226 parameterizations.

227 **2.1 Motivation**

228 Curve fitting is commonly found in the particle physics community literature due to the  
229 need to compare two models or constrain unknown model parameters using one or more  
230 histograms. For the first case, this involves two competing models,  $H_0$  and  $H_1$ , in order to  
231 establish if the data supports new Physics ( $H_1$ ) not predicted in the Standard Model ( $H_0$ ).  
232 The second case finds the “best” set of the model predictions,  $\theta$ , that match the data as is the

233 case for the BANFF-fit. In both cases, chi-squared tests are performed to provide goodness  
234 of fit, parameter estimation (also referred to as “best fit parameters”), and error/confidence  
235 estimation.

## 236 2.2 Introduction to Conditional PDFs and Likelihoods

237 Consider the problem of extracting physics parameters  $\vec{y}$  given some data vector  $\vec{N}$ . The  
238 conditional probability density function (PDF)  $\mathcal{P}$  to measure these parameters is given as

$$\mathcal{P}(\vec{y}|\vec{N}) = \frac{\mathcal{L}(\vec{N}|\vec{y})\mathcal{P}(\vec{y})}{\int \mathcal{L}(\vec{N}|\vec{x})\mathcal{P}(\vec{x})d\vec{x}}, \quad (2.1)$$

239 where anything right of a vertical line represents a condition on the probability,  $\mathcal{L}(\vec{N}|\vec{y})$   
240 is the likelihood of the model with parameters  $\vec{y}$ ,  $\mathcal{P}(\vec{y})$  is the probability for the model,  
241 and the denominator is the normalization over all possible constraints on the observations.  
242 A frequentist interpretation of a PDF is a proportion of outcomes of repeated trials or  
243 experiments. A likelihood function is an expression of the probability of observing data as a  
244 function of the model parameters in their appropriate ranges.

245 One arrives at (2.1) by using the definition of compound probabilities

$$\mathcal{P}(A, B) = \mathcal{P}(B|A)\mathcal{P}(A) \quad (2.2)$$

246 to evaluate  $\mathcal{P}(\vec{y}|\vec{N})$  as

$$\mathcal{P}\left(\underbrace{\vec{y}}_B \middle| \underbrace{\vec{N}}_A\right) = \frac{\mathcal{P}(\vec{N}, \vec{y})}{\mathcal{P}(\vec{N})} \quad (2.3)$$

247 with the denominator here is recognized as the normalization of the PDF. The compound

248 PDF  $\mathcal{P}(\vec{N}, \vec{y})$  can expanded using Bayes' theorem which states

$$\mathcal{P}(A|B)\mathcal{P}(B) = \mathcal{P}(B|A)\mathcal{P}(A), \quad (2.4)$$

249 and combined with (2.2) yielding

$$\mathcal{P}\left(\underbrace{\vec{N}}_A, \underbrace{\vec{y}}_B\right) = \mathcal{P}(\vec{N}|\vec{y}) \times \mathcal{P}(\vec{y}), \quad (2.5)$$

250 where the PDFs to the left and right of the  $\times$  operator are recognized as the likelihoods and  
251 priors, respectively. Combining resulting in (2.3) and (2.5) reproduces the original expression  
252 of (2.1).

### 253 2.3 BANFF Fit Test Statistic

254 For the BANFF fit, one considers the problem of trying to maximize the agreement between  
255 measured and predicted data histograms. This is equivalent to maximizing a binned likeli-  
256 hood function  $\mathcal{L}$  of the data given the a set of parameters that predict the measured rate.  
257 The use of likelihood functions in fits to histogram is explained further in reference [2] and  
258 the PDG review on Statistics. By invoking Wilks' theorem, also known as the likelihood ratio  
259 theorem, the likelihood maximization procedure is converted into a minimization problem  
260 involving a test statistic denoted as a chi-squared. Below is an explanation of the BANFF  
261 test statistic,  $\Delta\chi^2$ , and its systematic model terms.

262 Consider many binned samples that select different charged current topologies. A conve-  
263 nient choice of observables for all the samples are the outgoing charged lepton  $l$  momentum  $P_l$   
264 and angle  $\cos\theta_l$  as measured in ND280. Much of this is also documented in TN-220[10] where  
265 additional details can be found. For each  $(P_l, \cos\theta_l)$  analysis bin  $i = 1, 2, \dots, M - 1, M$ , the

266 likelihood is given by

$$\mathcal{L}(\vec{N}^d | \vec{N}^p) = \left( \prod_{i=1}^M \left( \vec{N}_i^p \right)^{\vec{N}_i^d} \frac{e^{-\vec{N}_i^p}}{\vec{N}_i^p!} \right) \quad (2.6)$$

267 where  $\vec{N}_i^d$  is the number of observed data events in the  $i$ th bin and  $\vec{N}_i^p$  is the number of  
 268 predicted events as a function of nuisance parameters in the  $i$ th bin. One recognizes the  
 269 likelihood function in (2.6) as a product of Poisson distributions with each corresponding  
 270 to bins  $i = 1, 2, \dots, M - 1, M$ . The sets of dependent nuisance parameters, also sometimes  
 271 called systematics, that affect the predicted event rate are

- 272 • cross section physics models, labeled as “xsec”,
- 273 • neutrino flux, and
- 274 • detector biases and inefficiencies.

275 Given these three sets of systematics, the number of predicted CC events from any neutrino  
 276 flavor  $\nu_l$  at ND280 is calculated using the general formula

$$N_{\nu_l} = \Phi_{\nu_l} \sum_t (\sigma_{\nu_l}^t M_t) \epsilon_{\nu_l}, \quad (2.7)$$

277 where  $\Phi_{\nu_l}$  is the flux of  $l$  flavor neutrinos,  $\sigma_{\nu_l}^t$  is the cross section of the interaction for  
 278 neutrino flavor  $l$  on target  $t$ ,  $M_t$  is the number of  $t$  targets, and  $\epsilon_{\nu_l}$  is the total efficiency  
 279 to reconstruct and properly identify the event as  $\nu_l$ CC interactions. Each term in (2.7) is  
 280 modeled carefully and the efficiency term is estimated using Monte Carlo (MC) simulations  
 281 and control samples. The number of predicted events from the MC for a given analysis bin  
 282  $i$  is given by

$$\vec{N}_i^p(\vec{b}, \vec{x}, \vec{d}) = w_i^{\text{POT}} (\vec{d})_i^{\text{Det}} \sum_{j=1}^{N_i^{\text{MC}}} \left[ \sum_{k=1}^{N^{\text{Flux}}} \left( \delta_{j,k}^{\text{Flux}} (\vec{b})_k^{\text{Flux}} \right) \prod_{l=1}^{N^{\text{xSyst}}} w_{j,l}((\vec{x})_l^{\text{xsec}}) \right]. \quad (2.8)$$

283 Here  $w_i^{\text{POT}}$  is the protons on target (POT) weight for the  $i$ th analysis which normalizes  
 284 the MC statistics to expected data statistics. To account for the detector inefficiencies, the  
 285  $(\vec{d})_i^{\text{Det}}$  parameters are normalization parameters that vary the total number of predicted  
 286 events in the  $i$ th bin. Each  $(\vec{d})_i^{\text{Det}}$  is determined prior to the fit by surveying over a large  
 287 number of toy experiments with the detector systematics varied in each. The sum over  
 288  $j = 1, 2, \dots, N_i^{\text{MC}} - 1, N_i^{\text{MC}}$  considers the contribution of all MC events in the  $i$ th analysis  
 289 bin. The  $(\vec{b})_k^{\text{Flux}}$  parameters, out of a total of  $N^{\text{Flux}}$ , are flux normalization systematics  
 290 for each flux bin. Since the flux bins are categorized not only by neutrino energy, but also  
 291 by flavor and horn current, the  $\delta_{j,k}^{\text{Flux}}$  term in the sum over  $k$  selects the correct flux bin.  
 292 The parameters  $w_{j,l}$  are pre-calculated weights as a function for the  $l$ th cross section model,  
 293  $(\vec{x})_l^{\text{xsec}}$ , with a total of  $N^{\text{xSyst}}$  cross section model terms. Different  $t$  target materials have  
 294 separate cross section parameters. Also the number of targets  $M_t$  can vary via detector  
 295 systematics.

296 Using the likelihood ratio test theorem, a test statistic is defined as taking -2 times the  
 297 natural logarithm of the ratio of predicted to observed likelihoods

$$\Delta\chi_{\text{LLR}}^2 = -2 \log \frac{\mathcal{L}(\vec{N}^d | \vec{N}^p)}{\mathcal{L}(\vec{N}^d | \vec{N}^d)}, \quad (2.9)$$

298 where this test statistic  $\Delta\chi_{\text{LLR}}^2$  obeys a true chi-squared distribution for asymptotically  
 299 large statistics and the likelihood functions are of the form (2.6). The denominator in (2.9)  
 300 is the MC predicted probability which assumes the best maximum likelihood estimate is  
 301 the number of observed events. Penalty terms from the cross section, flux, and detector  
 302 systematics are included in order to prevent overfitting of the data. The new test statistic

303 for all of ND280,  $\Delta\chi^2_{\text{ND280}}$ , is given by

$$\begin{aligned}\Delta\chi^2_{\text{ND280}} &= \Delta\chi^2_{\text{LLR}} + \Delta\chi^2_{\text{xsec}} + \Delta\chi^2_{\text{Flux}} + \Delta\chi^2_{\text{Det}} \\ &\quad - 2 \left( \log \frac{\mathcal{L}(\vec{N}^d | \vec{N}^p)}{\mathcal{L}(\vec{N}^d | \vec{N}^d)} + \underbrace{\log \pi(\vec{x})}_{\text{xsec}} + \underbrace{\log \pi(\vec{b})}_{\text{Flux}} + \underbrace{\log \pi(\vec{d})}_{\text{Det}} \right),\end{aligned}\quad (2.10)$$

304 where each of the PDFs  $\pi(\vec{y} = \vec{x}, \vec{b}, \vec{d})$  are assumed multivariate normal distributions

$$\pi(\vec{y}) = C_y e^{\left(-\frac{1}{2} \Delta \vec{y} \cdot V_y^{-1} \cdot \Delta \vec{y}^T\right)}, \quad (2.11)$$

305  $\Delta \vec{y}$  is a vector with the difference between the current/explored and nominal set of vector  
306 parameters  $\vec{y}$ ,  $T$  corresponds to the transpose operator, and the normalization is given by

$$C_y = ((2\pi)^{k_y} \det(V_y))^{-\frac{1}{2}} \quad (2.12)$$

307 with  $V_y$  being the covariance matrix for a vector  $\vec{y}$  with  $k_y$  rows. The expanded form of the  
308 test statistic  $\Delta\chi^2_{\text{ND280}}$  is given by

$$\begin{aligned}\Delta\chi^2_{\text{ND280}} &= 2 \sum_{i=1}^M \left[ \vec{N}_i^p - \vec{N}_i^d + \vec{N}_i^d \log \left( \frac{\vec{N}_i^d}{\vec{N}_i^p} \right) \right] \\ &\quad + \Delta \vec{x} \cdot (V_x^{-1}) \cdot \Delta \vec{x}^T + \Delta \vec{b} \cdot (V_b^{-1}) \cdot \Delta \vec{b}^T + \Delta \vec{d} \cdot (V_d^{-1}) \cdot \Delta \vec{d}^T\end{aligned}\quad (2.13)$$

309 where the “ $\cdot$ ” is the matrix multiplication operator. It must be stated that the test statistic  
310 (2.13) purposefully *excludes normalization terms*. Once the global minimum of the test  
311 statistic is found, the postfit covariance matrix  $V$  is calculated as the inverse of the Hessian  
312 matrix  $H$

$$V_{i,j}(\hat{\vec{y}}) = (H_{i,j})^{-1} = \left( \frac{\partial^2}{\partial y_i \partial y_j} (\Delta\chi^2_{\text{ND280}}) \Big|_{\vec{y}=\hat{\vec{y}}} \right)^{-1} \quad (2.14)$$

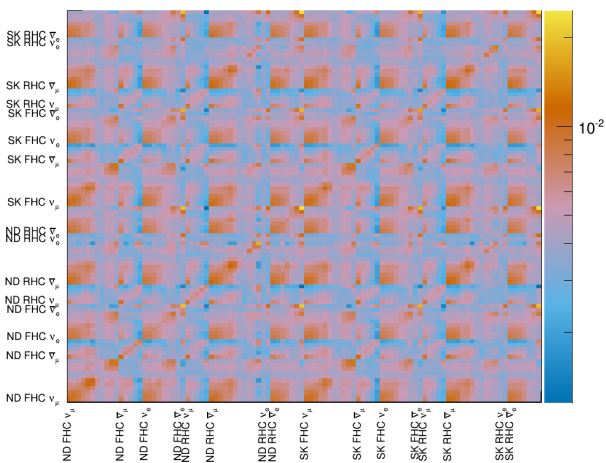


Figure 2.1: BANFF pre-fit flux covariance matrix shown with respective detector, horn current, and neutrino flavor.

313 where  $y_i, y_j \in \vec{y}$  and  $\hat{y}$  is the maximum likelihood estimate for the parameters  $\vec{y}$ .

### 314 2.3.1 Flux, Cross Section, and Detector Systematics

315 Below is a description for each of the systematics in the BANFF likelihood and test statistic  
 316 penalty terms. First is a description of flux, followed by the cross section, and finally the  
 317 detector systematics.

318 **Flux:** The flux weight is binned as a function of neutrino energy, horn current/polarity  
 319 (FHC and RHC), and neutrino flavor ( $\nu_\mu$ ,  $\bar{\nu}_\mu$ ,  $\nu_e$ , and  $\bar{\nu}_e$ ). There are 50 ND280 and 50 SK  
 320 parameters with an associated covariance matrix as shown in Figure 2.1. The binning and  
 321 covariance matrix is provided by the T2K flux group prior to the BANFF analysis. Each  
 322 flux bin is assigned a normalization parameter with initial value of one (1) for all events in  
 323 that neutrino energy bin. A value of 1.1 indicates that any event in that energy bin has an  
 324 additional weight of 1.1, or 10% increase in events. An example of the flux normalizations  
 325 and uncertainties used in the 2017 analysis are shown in Figure 2.2.

326 **Cross Section:** There are a number of cross section model systematics implemented in  
 327 BANFF to account for the uncertainties in cross section measurements. The cross section

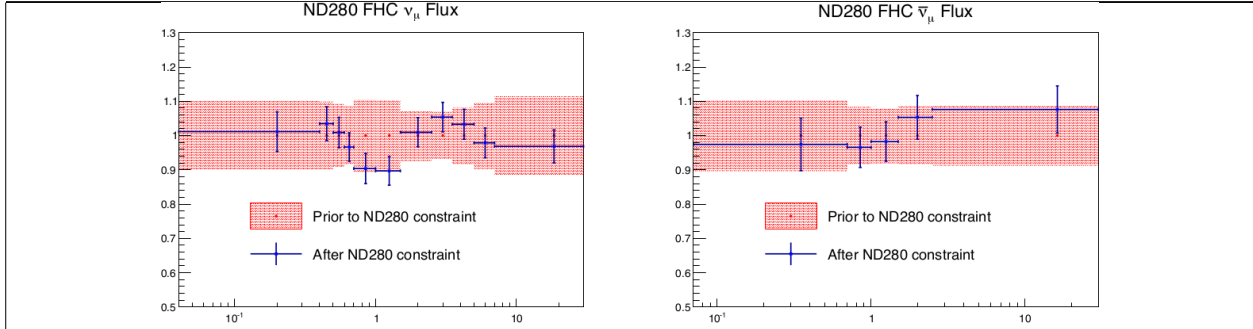


Figure 2.2: BANFF ND280 flux  $\nu_\mu$  and  $\bar{\nu}_\mu$  binning parameters from T2K-TN-324 data post-fit results. The uncertainties are extracted from the pre-fit and post-fit covariance matrices.

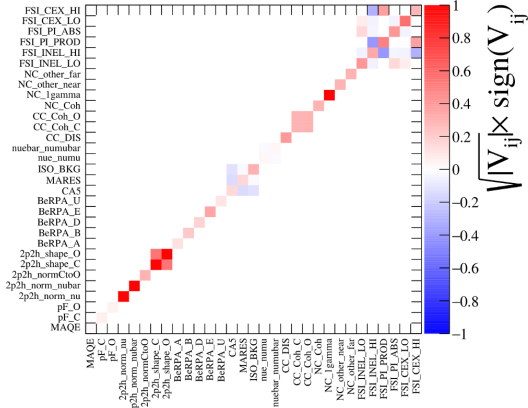


Figure 2.3: Cross section parameters pre-fit correlation matrix from the 2017 BANFF analysis.

models used in this analysis are the 2017 Neutrino Interactions Working Group (NIWG) parameterization, which is a canonical set of parameters and covariance matrix shared among all analyses in T2K. A technical description of the 2017 parameterization is given in TN-315[5] and TN-307[14]. There are a total of 25 cross section parameters for interactions like meson exchange current that affect the shape and normalization of the cross section. The cross section correlation matrix is shown in Figure 2.3[4].

**334 Detector Systematic Errors:** Detector systematics are implemented in BANFF to  
335 account for uncertainties in detector efficiencies. Since neutrino interaction events can mi-  
336 grate from sample-to-sample, bin-to-bin, or both depending on the relevant systematics,  
337 numerous toy experiments are performed by varying parameters that model known detector

338 systematics.

339 After many toy experiments, a covariance matrix among the bins is constructed con-  
340 sidering correlations and statistical errors. This detector covariance matrix is fractional to  
341 be consistent with the definitions for the flux and cross section covariance matrices. The  
342 detector covariance matrix,  $\sigma_{\text{Det}}^2$ , between bins  $x$  and  $y$  given explicitly as

$$\sigma_{\text{Det}}^2(x, y) = \frac{1}{x_{\text{Nom}}} \frac{1}{y_{\text{Nom}}} (\sigma_{\text{Cov}}^2(x, y) + \sigma_{\text{Stat}}^2(x, y)), \quad (2.15)$$

343 where ‘‘Nom’’, ‘‘Cov’’, and ‘‘Stat’’ refer to the nominal MC prediction, covariance, and sta-  
344 tistical uncertainties for bins  $x$  and  $y$ , respectively. The nominal bin expectation for bin  $x$   
345 is

$$x_{\text{Nom}} = \sum_{k=1}^{N_x^{\text{MC}}} w_k, \quad (2.16)$$

346 where  $N_x^{\text{MC}}$  being the number of predicted MC events in the bin and  $w_k$  being the product  
347 of all the weights applied to the  $k$ th event (see (2.8) for all possible weights). The covariance  
348 and statistical terms are given by

$$\begin{aligned} \sigma_{\text{Cov}}^2(x, y) &= \frac{1}{N_{\text{Toy}}} \sum_{t=1}^{N_{\text{Toy}}} (x_t - \bar{x})(y_t - \bar{y}) \\ \sigma_{\text{Stat}}^2(x, y) &= \delta(x, y) \sum_{k=1}^{N_x^{\text{MC}}} w_k^2, \end{aligned} \quad (2.17)$$

349 where  $N_{\text{Toy}}$  is the number of toy experiments,  $\bar{x}$  is the mean of the all the toy experiments  
350 in bin  $x$ , and  $\delta(x, y)$  is the Kronecker delta function. Additional uncertainties like fake data  
351 contributions are added to the covariance in quadrature.

352 While there could be one detector systematic normalization for each analysis bin, also  
353 called a observable normalization, a single one can be assigned to multiple analysis bins to  
354 reduce the number of fit parameters. This procedure requires careful consideration of the

355 shared detector systematics among analysis bins. A considerable drawback to designing nor-  
356 malizations in this way is that not all detector systematics are Gaussian with respect to the  
357 observables ( $P_l, \cos \theta_l$ ), and so the covariance matrix may not be an accurate representation  
358 of the detector systematics.

359 **3 PØD Selections and Data Samples**

360 This section describes the development of  $\nu_\mu$  and  $\bar{\nu}_\mu$  CC Inclusive selections in both FHC  
361 and RHC beam configuration for PØD-based analyses. These selections are the continuation  
362 of previous works that developed  $\nu_\mu$  CC Inclusive selections between the PØD and TPC1.  
363 The first such analyses were T2K-TN-80 and T2K-TN-100 which described the  $\nu_\mu$  CC In-  
364 clusive event selection and, later, cross-section analysis using ND280 Production 5 software,  
365 respectively[7, 8]. These analyzes relied on each sub-detector’s reconstruction software and  
366 developed a track matching algorithm since the ND280 “Global” reconstruction matching  
367 was problematic in Production 5. As the inter-detector matching reconstruction improved in  
368 “Global”, two CC-0 $\pi$  cross section analyzes, T2K-TN-258 and T2K-TN-328, were developed  
369 that also used the CC Inclusive selection as pre-selection cuts[16, 6]. The selections described  
370 in this technical note also employ the same pre-selection cuts. What follows from here in  
371 this section is a layout of the following topic discussions.

372 The first topic discussed in this section is a description of the  $\pi^0$  Detector (PØD). The  
373 next topic is the event reconstruction using the “Global” reconstruction software. Following  
374 that is the pre-selection cut flow. With the pre-selection cuts established, each of the three  
375 CC Inclusive selection’s cut flow is described. Concluding this section is a discussion of the  
376 three samples in the following order:  $\nu_\mu$  in FHC mode,  $\bar{\nu}_\mu$  in RHC, and  $\nu_\mu$  background in  
377 RHC.

378 **3.1 Global Reconstruction**

379 The task of the Global reconstruction is to combine all the ND280 information into a com-  
380 bined reconstructed object. It was originally designed to analyze “CCQE-like” events in the  
381 Tracker region and has been extended to operate with all of ND280. A brief description  
382 of the Global reconstruction is described below. First the specific detector technologies and

383 electronics of ND280 are explained. That is followed by the calibration procedure to properly  
384 tune each detector’s response. And finally a general outline of the reconstruction algorithms  
385 to form tracks and vertices in ND280 is presented.

386 ND280 events are first collected in the form of electronic signals from either multipixel  
387 photon counters (MPPCs) in the scintillator-based sub-detectors or charge collection planes  
388 of the time projection chambers (TPCs). MPPCs were chosen for the scintillator-based sub-  
389 detectors since they are insensitive to the strong 0.2T magnetic field present in ND280. The  
390 PØD, ECals, and SMRD all share the same “Trip-T” frontend board (TFB) electronics of  
391 which collect the photoelectrons released when photons interact with a pixel in the MPPCs.  
392 The FGDs operate with the same MPPC technology while using different frontend electron-  
393 ics. The TPCs utilize a locally strong electric field to collect ionization electrons from an  
394 Argon-based gas. Collected charge in the TPCs are collected and enhanced using micromega  
395 technology[1]. With the collected information from each sub-detector, the next step is the  
396 data calibration.

397 Data calibration in ND280 is the process where the charge and timing information col-  
398 lected from each sub-detector is adjusted to match with expected parameters. This is an  
399 important process that takes into account environmental changes, aging effects, and other  
400 behavior that might be present. Calibration data is collected frequently before and during  
401 operational runtime and is stored in a database for later use. A common calibration is to  
402 measure the detector’s cosmic ray response since most cosmic rays deposit the same energy  
403 per unit length. After the data has been calibrated, reconstruction algorithms now attempt  
404 to find charged particle tracks in the data.

405 The Global reconstruction is a software package that attempts to recognize patterns of  
406 data to form tracks and find vertices for those tracks. Particle shower reconstruction in  
407 Global will not be discussed in this TN since no shower objects are used. Each sub-detector  
408 reconstruction is run to seeds Global’s track matching algorithms. Global attempts to then

409 re-fit sub-detector tracks using a Kalman filter while correcting for particle energy loss as a  
410 function of length ( $dE/dx$ ) and multi-scattering processes. A vertex is then associated with  
411 the re-fit track using another Kalman filter algorithm. A further detailed description of the  
412 track matching and vertex finding algorithms for Global is described in T2K-TN-46[15].

## 413 **3.2 PØD Selection Cuts**

414 The selection of CC Inclusive events use a series of cuts to select the primary lepton. The  
415 pre-selection cuts (“precuts”) are applied first to extract events that start in the PØD FV.  
416 A MIP is more likely to reach TPC1 from the PØD FV since the PØD is constructed out  
417 of heavy materials especially in the CECal. So the main track each selection is designed to  
418 select a muon.

419 This following sections will describe the precuts common to all CC Inclusive selections  
420 and the branching of different cuts, after the precuts, to select the main track.

### 421 **3.2.1 Pre-Selection Cuts**

422 The pre-selection (“precuts”) were initially developed to select  $\nu_\mu$ CC Inclusive using the PØD  
423 and TPC sub-detector reconstruction softwares separately[7]. They were then used with the  
424 Global reconstruction software for the  $\nu_\mu$ CC-0 $\pi$  selection in the FHC beam configuration as  
425 described in technical note T2K-TN-258[16]. The description and flow of the precuts are  
426 described here as well since there is an incomplete description of the selection precuts.

427 The precuts are performed on each bunch per beam spill as follows

- 428 1. The event has a “good” data quality flag.
  - 429 • An event is rejected if any sub-detector or electronics in ND280 reported as “bad”  
430 during that bunch.
- 431 2. There is at least one (1) track reconstructed in TPC1.

- 432     • There are no restrictions on the number of tracks fully contained in the PØD or  
433            exiting into other sub-detectors.

434     3. The track in TPC1 must have more than 18 nodes.

- 435     • The TPC reconstruction gathers vertical and horizontal hits into clusters of hits.  
436         The charge distribution of the cluster is used to get a vertical (horizontal) position  
437         that is more accurate than the individual readout pads. A node is constructed  
438         out of each cluster with associated track state information. The set of nodes are  
439         used to fit the track helix[12].

440     4. The reconstructed vertex is within the PØD WT FV.

- 441     • The PØD FV is defined to include as much as the WT regions as possible. Its  
442         X and Y borders are 25 cm away from the PØDule edges while its Z borders  
443         intersect the last and first half downstream PØDule in the USECal and CECal,  
444         respectively. The enumerated volume edges are shown in table 3.1. This volume,  
445         while used for track-based analyzes in the past, was optimized for  $\pi^0$  and  $\nu_e$   
446         analyzes[9].

447     5. All tracks that enter TPC1 pass the veto cut

- 448     • An event is rejected if any PØD track enters TPC1 from outside the “corridor”  
449         volume. This cut was designed to eliminate broken tracks between the PØD and  
450         TPC1 when the separate sub-detector reconstructions were used[7]. In practice,  
451         this cut ensures that Global tracks entering TPC1 away from its X and Y edges.  
452         The corridor definition is the same as defined in T2K-TN-208 and shown in Ta-  
453         ble 3.1.

PØD WT FV			Corridor Volume		
-836	< X <	764	-988	< X <	910
-871	< Y <	869	-1020	< Y <	1010
-2969	< Z <	1264	-3139	< Z <	-900

Table 3.1: The PØD WT FV (left) and veto corridor volume (right) in the ND280 coordinate system. The corridor spans from the 5th (8th) to 40th (80th) PØDule (scintillator layer). All the units are given in millimeters.

After passing all the precuts, a single, global track, which is observed in TPC1, is assigned as the “main track” of a selection. The main track for  $\nu_\mu$  selections is the highest momentum, negatively-charged track (HMNT). Similarly the highest momentum, positively-charged track (HMPT) is assigned the main track for  $\bar{\nu}_\mu$  selections.

This concludes the application of precuts to all the CC Inclusive selections. The following subsubsections describe the CC Inclusive selection cuts, first in FHC mode and then RHC mode.

### 3.2.2 $\nu_\mu$ CC Inclusive in FHC Cut

- The highest momentum negatively charged track (HMNT) is the lepton candidate

As discussed in Section section 3.2.1 on page 26, this selection is the basis for the  $\nu_\mu$  CC-0 $\pi$  PØD+TPC1 analysis. In FHC mode, the vast majority of neutrino interactions are  $\nu_\mu$ CC events producing an outgoing, negatively charged muon. So if there is no negatively charged track in the TPC, the event is rejected.

### 3.2.3 $\bar{\nu}_\mu$ CC Inclusive in RHC Cuts

- The highest momentum positively charged track (HMPT) is the lepton candidate
- The HMPT must be the highest momentum track (HMT)

470 In RHC, the majority of neutrinos in the beam is  $\bar{\nu}_\mu$  since the horn focuses negatively charged  
 471 pions. To select  $\bar{\nu}_\mu$  CC interaction events by selecting positively charged muons, the lepton  
 472 candidate is the HMPT in the TPC. The event is rejected if there is no positively charged  
 473 track. However, since the RHC mode beam is not as  $\bar{\nu}_\mu$  pure as the FHC beam, another cut  
 474 was added to reduce this effect.

475 Since RHC neutrino beam can be described as a  $\bar{\nu}_\mu$ -enhanced beam, the HMPT must  
 476 also be the HMT due to the significant “wrong-sign”  $\nu_\mu$  background. This effect is two  
 477 fold due to the nature of the neutrino source and the cross section between neutrinos and  
 478 antineutrinos.

479 Firstly the neutrino flux is larger in RHC mode due to neutrino production at the tar-  
 480 get. The source of neutrinos are from protons, which have positive charge, on a graphite  
 481 target. This method is more likely to produce positively charged pions in the target than  
 482 negatively charged one. While the horns are designed to select the negatively charged pions  
 483 in RHC mode, the excess amount of positively charged pions will penetrate the horns’ filter.  
 484 Therefore there are many more  $\pi^+ \rightarrow \mu^+ + \nu_\mu$  decays in RHC compared to FHC mode.

485 Secondly, antineutrino interactions on matter are suppressed compared to neutrinos due  
 486 to helicity considerations. Consider neutrino-electron scattering, the cross section for  $\nu_e + e^-$   
 487 is given by

$$\frac{d\sigma}{d\Omega} = \frac{G^2 s}{4\pi^2}, \quad (3.1)$$

488 where  $G$  is the Fermi constant and  $s$  is the center of mass energy squared. The outgoing  
 489 particles are isotropic since the initial and final spin state of the system is  $J = 0$ . Compare  
 490 (3.1) with the cross section for  $\bar{\nu}_e + e^-$

$$\frac{d\sigma}{d\Omega} = \frac{G^2 s}{16\pi^2} (1 - \cos \theta)^2, \quad (3.2)$$

491 where  $\theta$  is the observed scattering angle of the electron. Since the total spin of the  $\bar{\nu}_e + e^-$

492 system is  $J = 1$  with the  $J_z = 1$ , the antineutrino is preferentially forward scattered.

493 Integrating over all angles, the cross sections come out to

$$\sigma(\bar{\nu}_e + e^-) = \frac{1}{3}\sigma(\nu_e + e^-).$$

494 The factor  $1/3$  arises from the fact that angular momentum conservation forbids the  $J_z = -1$

495 and  $0$  states for  $\bar{\nu}_e + e^-$  scattering. The same  $1/3$  factor arises with  $e^-$  replaced with quarks.

496 Therefore the cross sections for neutrinos are larger than antineutrinos.

#### 497 **3.2.4 $\nu_\mu$ Background CC Inclusive in RHC Cuts**

- 498
- The highest momentum negative track (HMNT) is the lepton candidate
  - The HMNT must be the highest momentum track (HMT)

500 As discussed in section 3.2.3 on page 28, the RHC neutrino beam has a significant wrong-

501 sign  $\nu_\mu$  background. The selection of the HMNT is designed to select the negatively charged

502 muons. To prevent selecting the antineutrino events, the HMNT must also be the HMT.

503 The event is rejected if there is no negatively charged track. If there are both positively and

504 negatively charged tracks, the HMT cut discriminates if the event originates from a  $\nu_\mu$  or

505  $\bar{\nu}_\mu$ .

### 506 **3.3 Sample Kinematics and Validation**

507 This section examines the kinematics for each of selections while differentiating between

508 water-in and water-out mode. The selection cuts were implemented in Psyche which is the

509 software interface that BANFF uses to select events. An analysis of the kinematics are care-

510 fully cross validated with the same selection cuts in the T2K high level analysis framework

511 called Highland. Comparing the results between Highland and Psyche is important since

Run Period	Horn Current	PØD Status	Data POT ( $\times 10^{20}$ )	MC POT ( $\times 10^{20}$ )
2	+250 kA	Water	0.4339	12.03
		Air	0.3591	9.239
3b	+205 kA		0.2172	4.478
3c	+250 kA		1.364	26.32
4			1.782	34.99
		Water	1.642	34.97
5c	-250 kA		0.4346	22.77
6b		Air	1.288	14.17
6c			0.5058	5.275
6d			0.7753	6.884
6e			0.8479	8.594
7b		Water	2.436	33.70
8	+250 kA		1.580	26.46
		Air	4.148	36.06
Sand	FHC		-	11.19
Sand	RHC		-	12.92
2, 3b, 3c, 4, 8		FHC	Air	7.872
2, 4, 8			Water	3.657
6b, 6c, 6d, 6e		RHC	Air	3.417
5c, 7b			Water	2.871
				56.48

Table 3.2: T2K MC and data POT divided by run periods. The bottom four rows are the aggregated periods grouped by horn current and PØD status which is how the data analysis is performed.

512 they are complementary frameworks within T2K. The data sets used in this analysis are  
513 runs 2-8 in both PØD water-in and water-out (air) modes as shown in Table 3.2.

### 514 3.4 PØD Water-Out Samples

515 This section shows the kinematic distributions for the PØD water-out samples. First an  
516 examination of the CC Inclusive samples and the effects of the systematic weights will be  
517 explored. The samples are then examined as CC 1-track and CC N-tracks.

518 **3.4.1 CC Inclusive**

519 The CC Inclusive sample cuts are discussed 3.2.1. Since both flux and systematic weights  
520 are applied to all MC events in BANFF, it is important to validate the event weights. Using  
521 neither set of weights is referred to as the nominal MC.

522 **3.4.1.1  $\nu_\mu$  Selection in FHC Mode:** Shown in Figures 3.1 to 3.7 are the momentum  
523 and  $\cos\theta$  distributions for  $\nu_\mu$ CC Inclusive events in FHC mode. There are three pairs of  
524  $P, \theta$  figures with the same truth information break down accompanied by one of neutrino  
525 energy. The truth information categories are lepton candidate particle, NEUT reaction, and  
526 topology. Each figure consists of a set of four sub-figures which illustrate the application of  
527 flux and detector systematic weights.

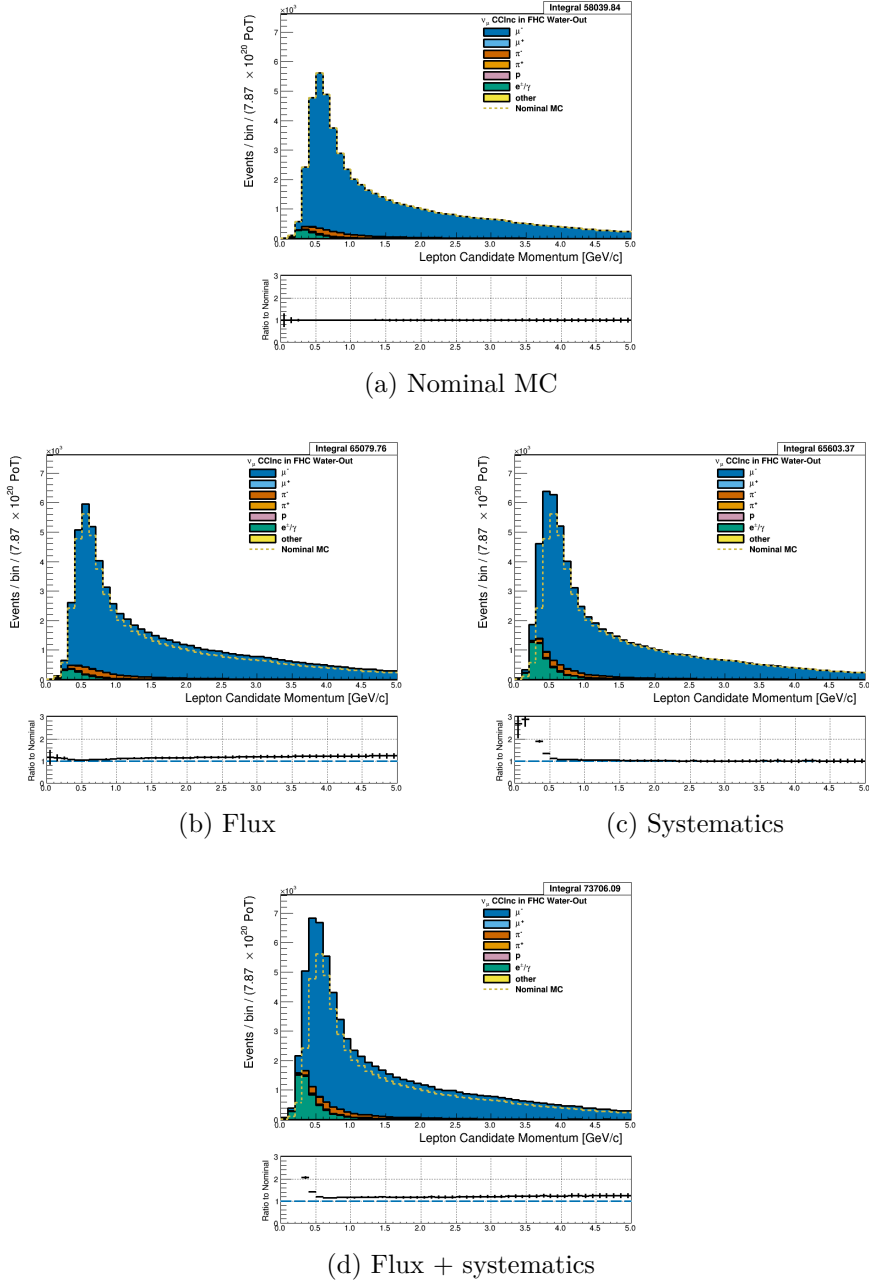


Figure 3.1: Reconstructed lepton candidate momentum separated by true particle species for FHC  $\nu_\mu$  CC Inc. events occurring in the PØD in water-out mode. (a) The nominal MC prediction without any weights applied. (b) The flux tuning are applied. (c) The systematic weighting are applied. (d) Both flux and systematic weighting are applied.

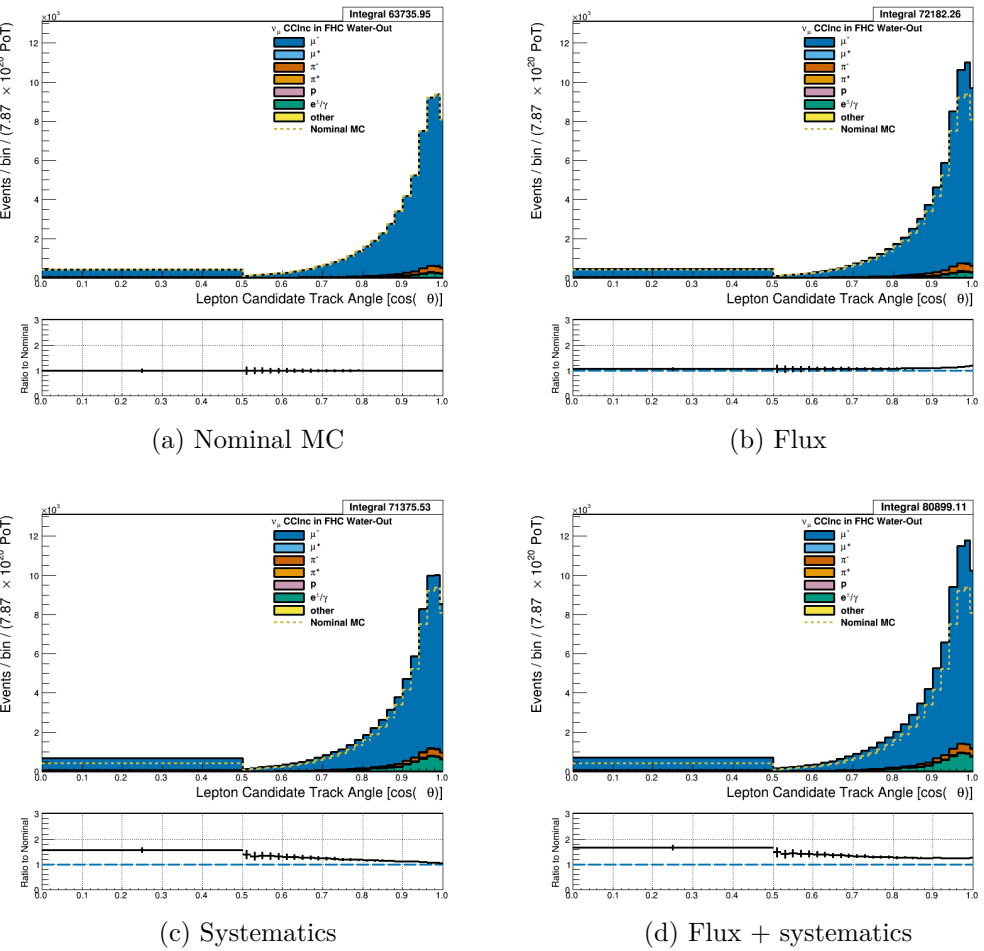


Figure 3.2: Reconstructed lepton candidate angle separated by true particle species for FHC  $\nu_\mu$  CC Inc. events occurring in the PØD in water-out mode. (a) The nominal MC prediction without any weights applied. (b) The flux tuning are applied. (c) The systematic weighting are applied. (d) Both flux and systematic weighting are applied.

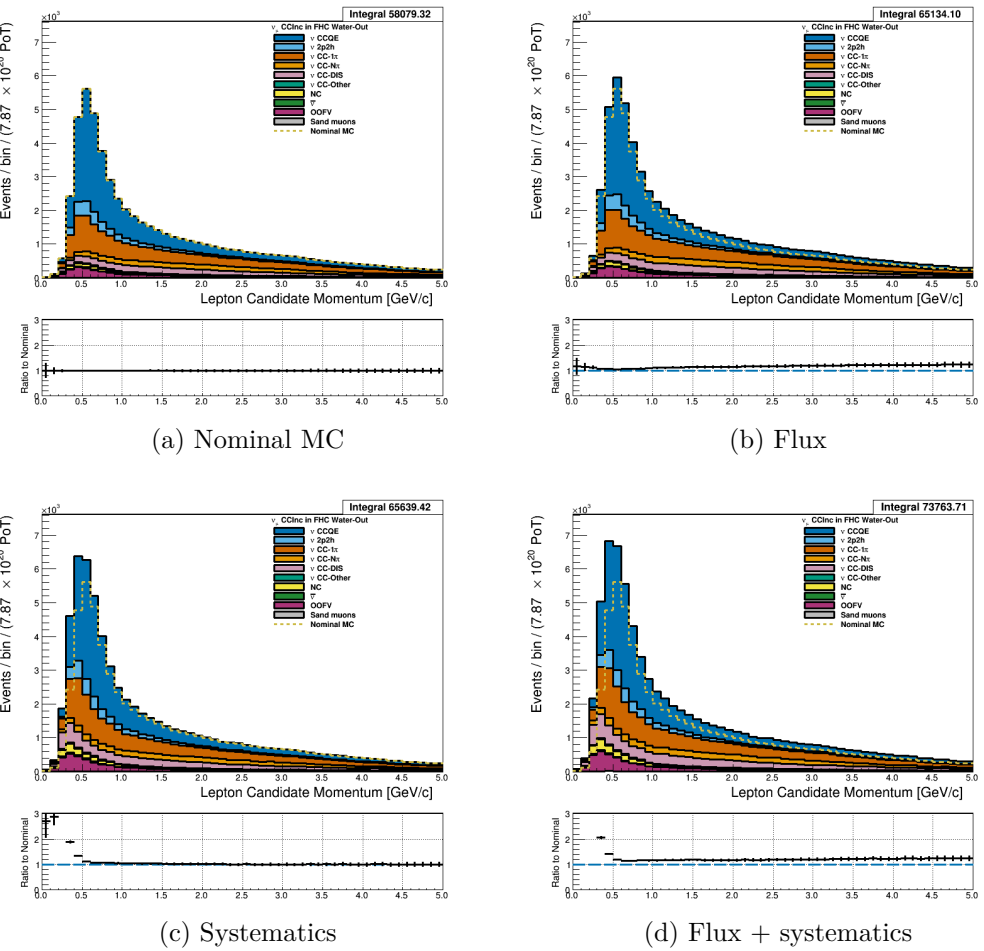


Figure 3.3: Reconstructed lepton candidate momentum separated by NEUT model interaction mode for FHC  $\nu_\mu$  CC Inc. events occurring in the PØD in water-out mode. (a) The nominal MC prediction without any weights applied. (b) The flux tuning are applied. (c) The systematic weighting are applied. (d) Both flux and systematic weighting are applied.

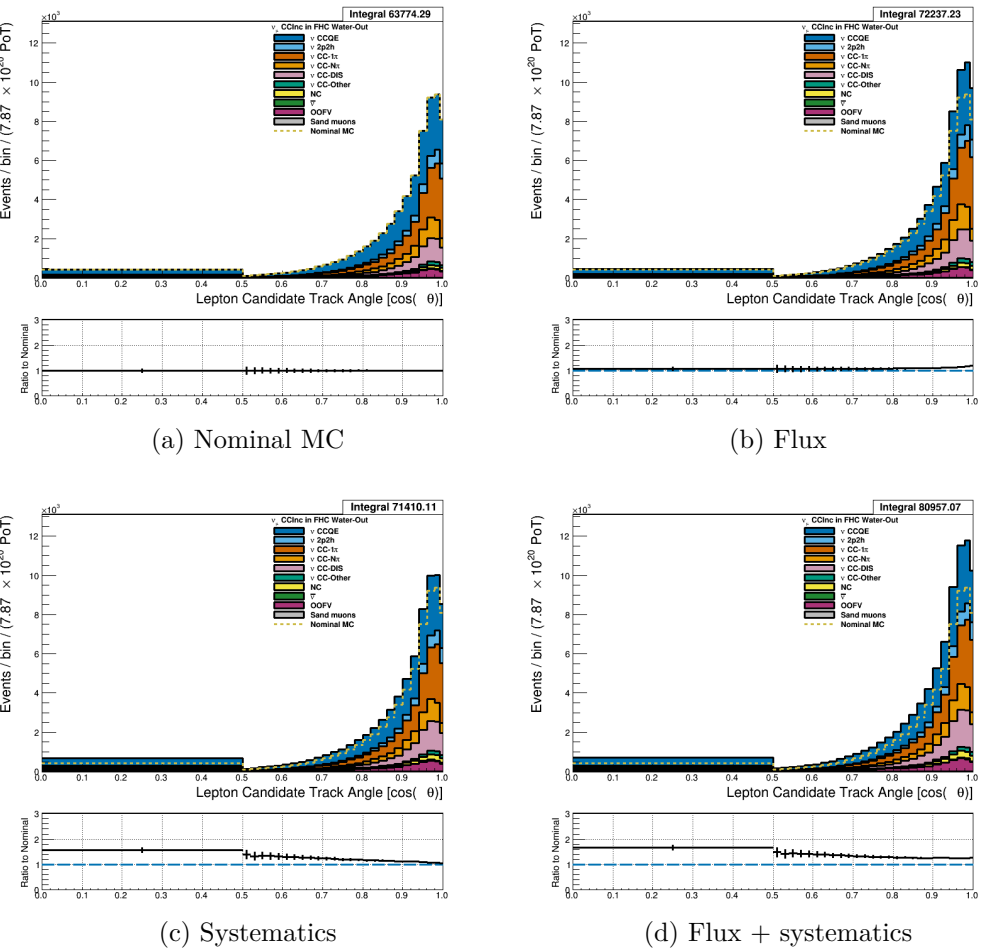


Figure 3.4: Reconstructed lepton candidate  $\cos\theta$  separated by NEUT model interaction mode for FHC  $\nu_\mu$  CC Inc. events occurring in the PØD in water-out mode. (a) The nominal MC prediction without any weights applied. (b) The flux tuning are applied. (c) The systematic weighting are applied. (d) Both flux and systematic weighting are applied.

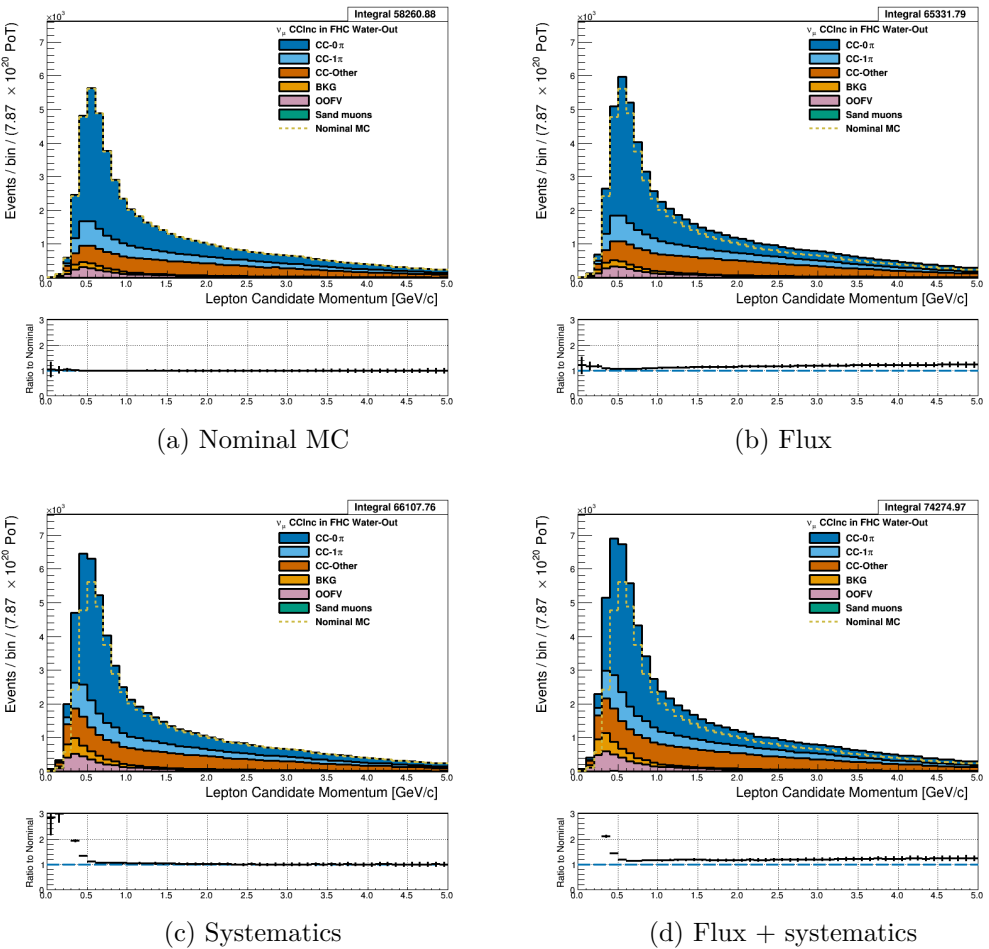


Figure 3.5: Reconstructed lepton candidate momentum separated by topology for FHC  $\nu_\mu$  CC Inc. events occurring in the PØD in water-out mode. (a) The nominal MC prediction without any weights applied. (b) The flux tuning are applied. (c) The systematic weighting are applied. (d) Both flux and systematic weighting are applied.

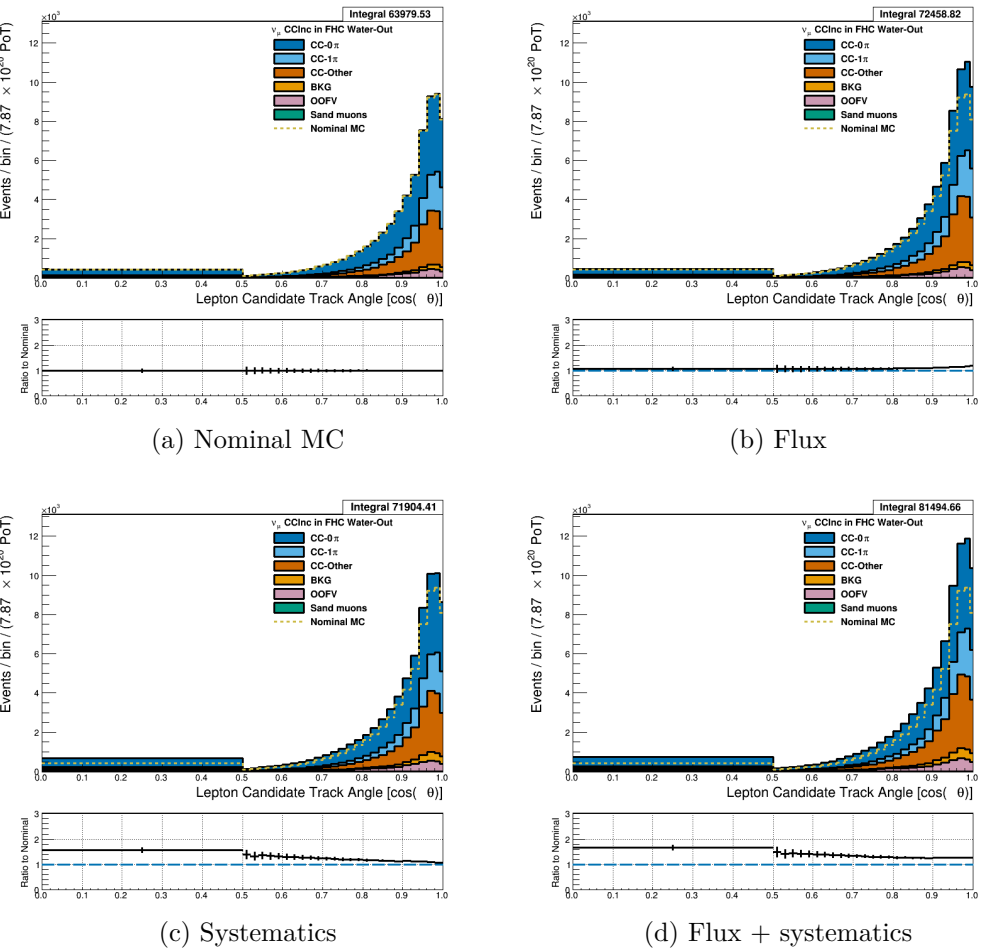


Figure 3.6: Reconstructed lepton candidate  $\cos \theta$  separated by topology for FHC  $\nu_\mu$  CC Inc. events occurring in the PØD in water-out mode. (a) The nominal MC prediction without any weights applied. (b) The flux tuning are applied. (c) The systematic weighting are applied. (d) Both flux and systematic weighting are applied.

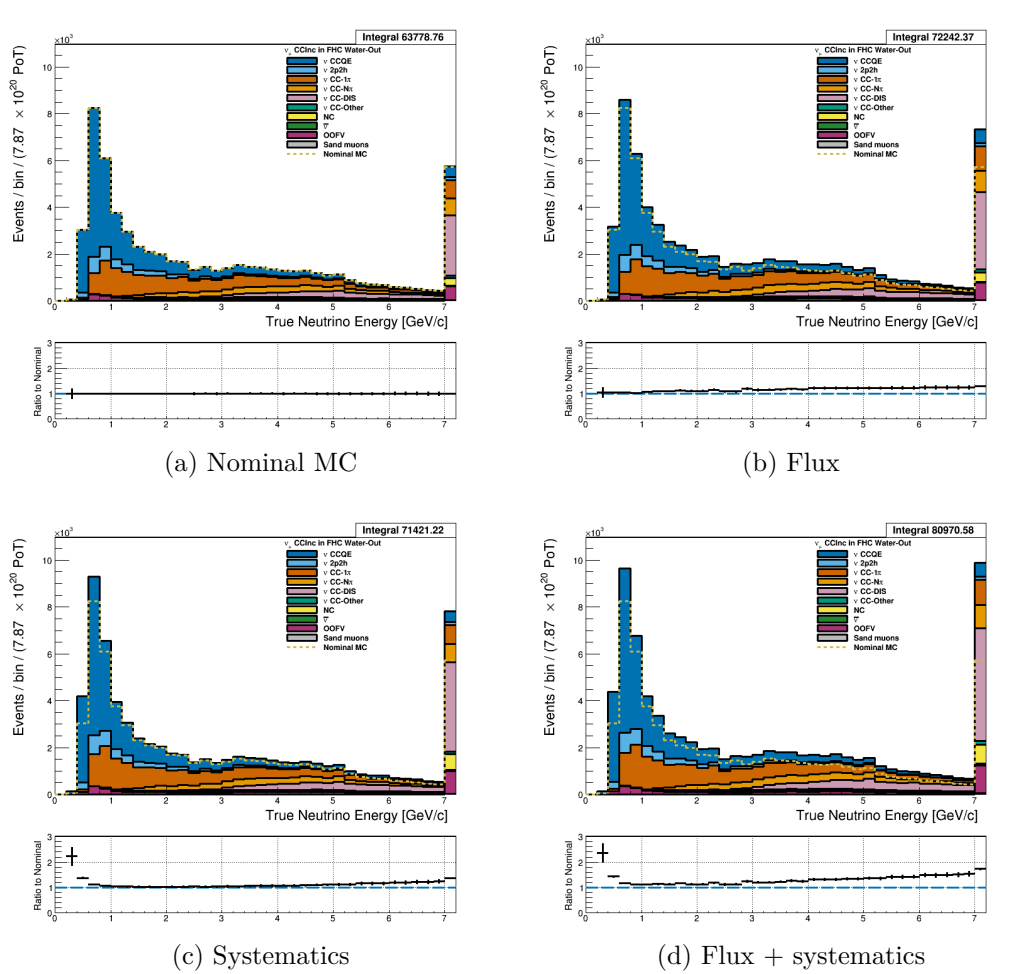


Figure 3.7: True neutrino energy associated with the lepton candidate separated by NEUT model interaction mode for FHC  $\nu_\mu$  CC Inc. events occurring in the PØD in water-out mode. (a) The nominal MC prediction without any weights applied. (b) The flux tuning are applied. (c) The systematic weighting are applied. (d) Both flux and systematic weighting are applied.

528 **3.4.1.2  $\bar{\nu}_\mu$  Selection in RHC Mode:** Shown in Figures 3.8 to 3.14 for  $\bar{\nu}_\mu$  CC Inclusive  
 529 events in RHC mode. There are three pairs of  $P, \theta$  figures with the same truth information  
 530 break down accompanied by one of neutrino energy. The truth information categories are  
 531 lepton candidate particle, NEUT reaction, and topology. Each figure consists of a set of four  
 532 sub-figures which illustrate the application of flux and detector systematic weights.

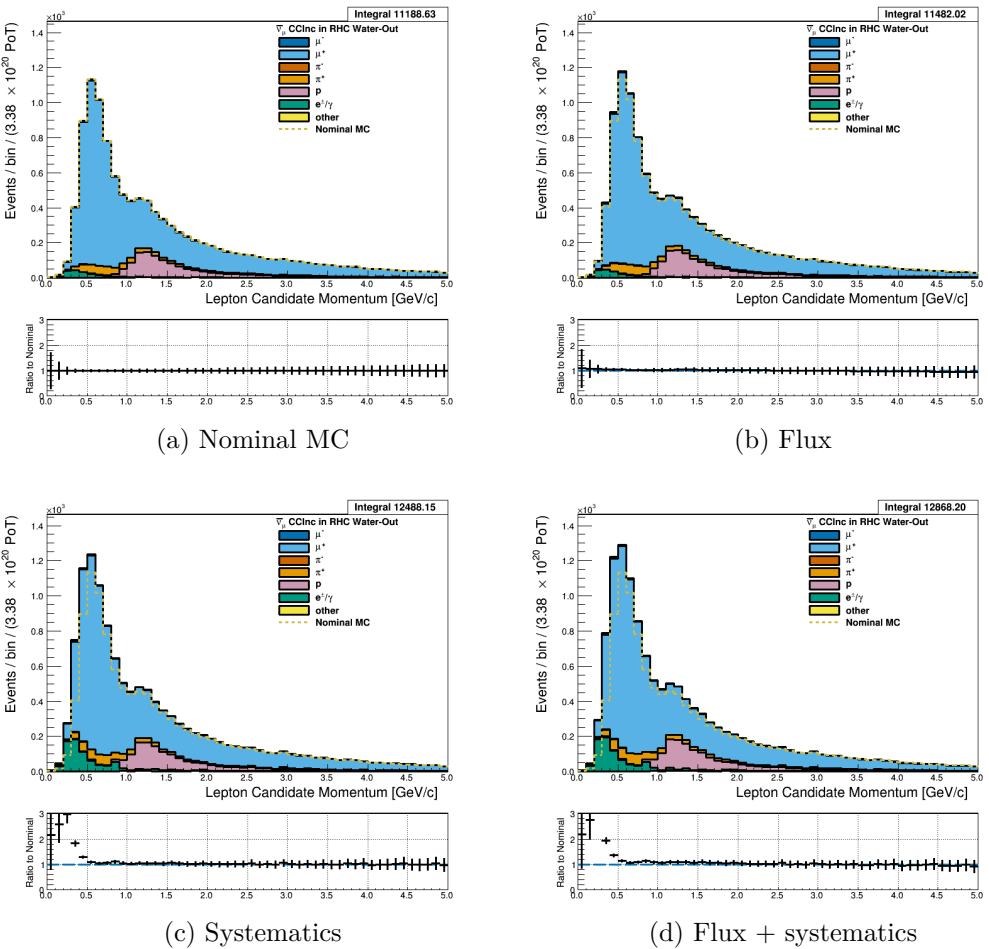


Figure 3.8: Reconstructed lepton candidate momentum separated by true particle species for RHC  $\bar{\nu}_\mu$  CC Inc. events occurring in the PØD in water-out mode. Reconstructed lepton candidate angle separated by true particle species for RHC  $\bar{\nu}_\mu$  CC Inc. events occurring in the PØD in water-in mode. (a) The nominal MC prediction without any weights applied. (b) The flux tuning are applied. (c) The systematic weighting are applied. (d) Both flux and systematic weighting are applied.

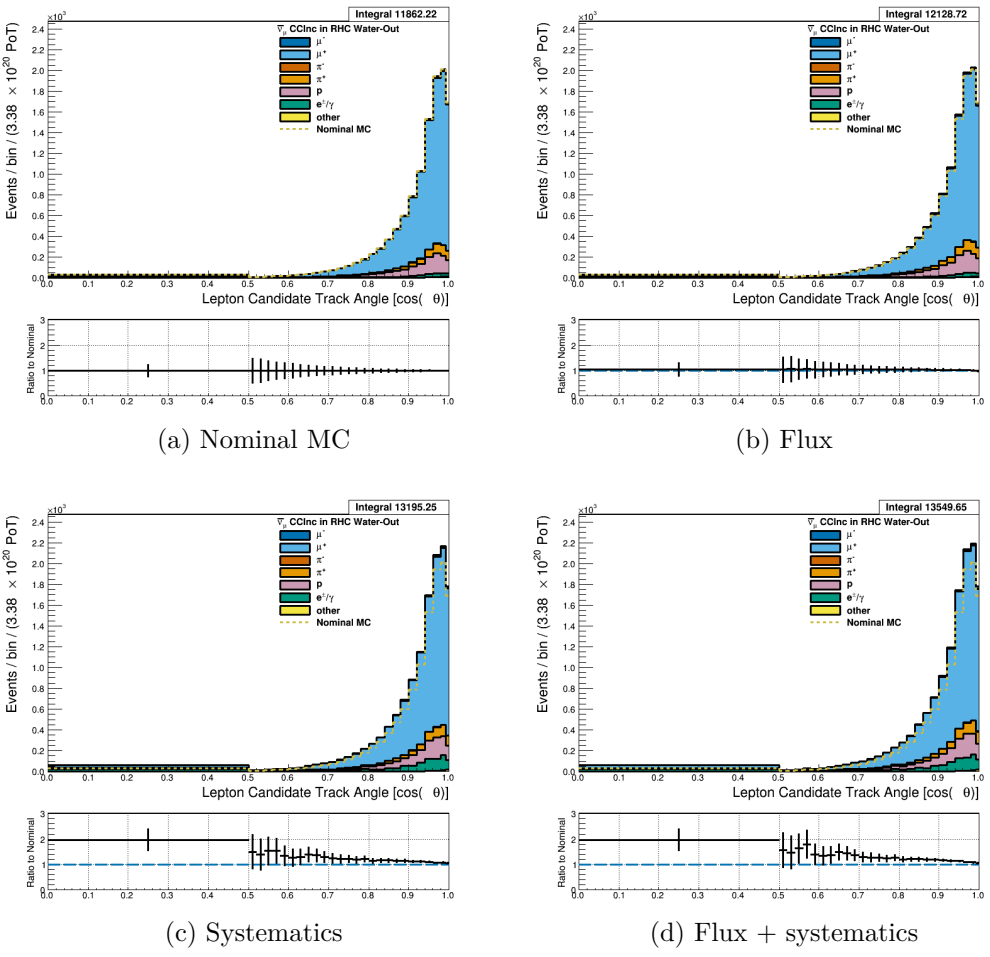


Figure 3.9: Reconstructed lepton candidate angle separated by true particle species for RHC  $\bar{\nu}_\mu$  CC Inc. events occurring in the PØD in water-out mode. (a) The nominal MC prediction without any weights applied. (b) The flux tuning are applied. (c) The systematic weighting are applied. (d) Both flux and systematic weighting are applied.

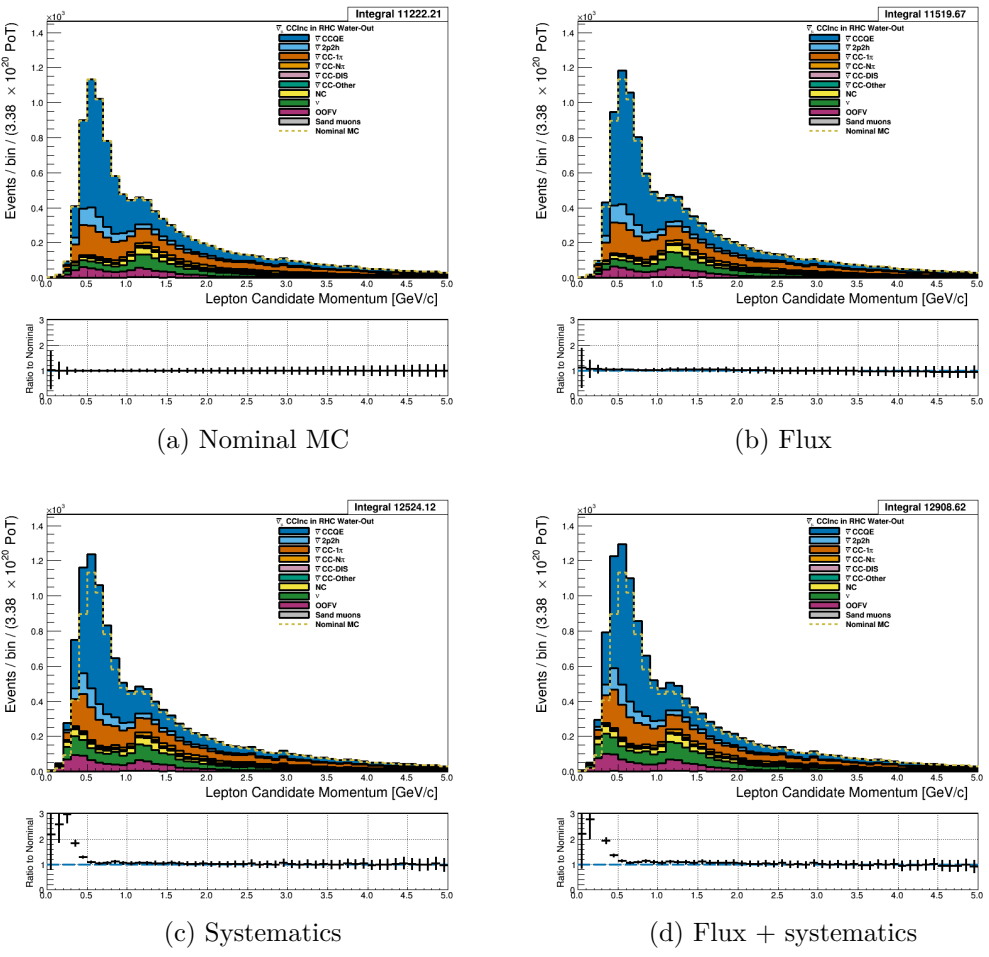


Figure 3.10: Reconstructed lepton candidate momentum separated by NEUT model interaction mode for RHC  $\bar{\nu}_\mu$  CC Inc. events occurring in the PØD in water-out mode. (a) The nominal MC prediction without any weights applied. (b) The flux tuning are applied. (c) The systematic weighting are applied. (d) Both flux and systematic weighting are applied.

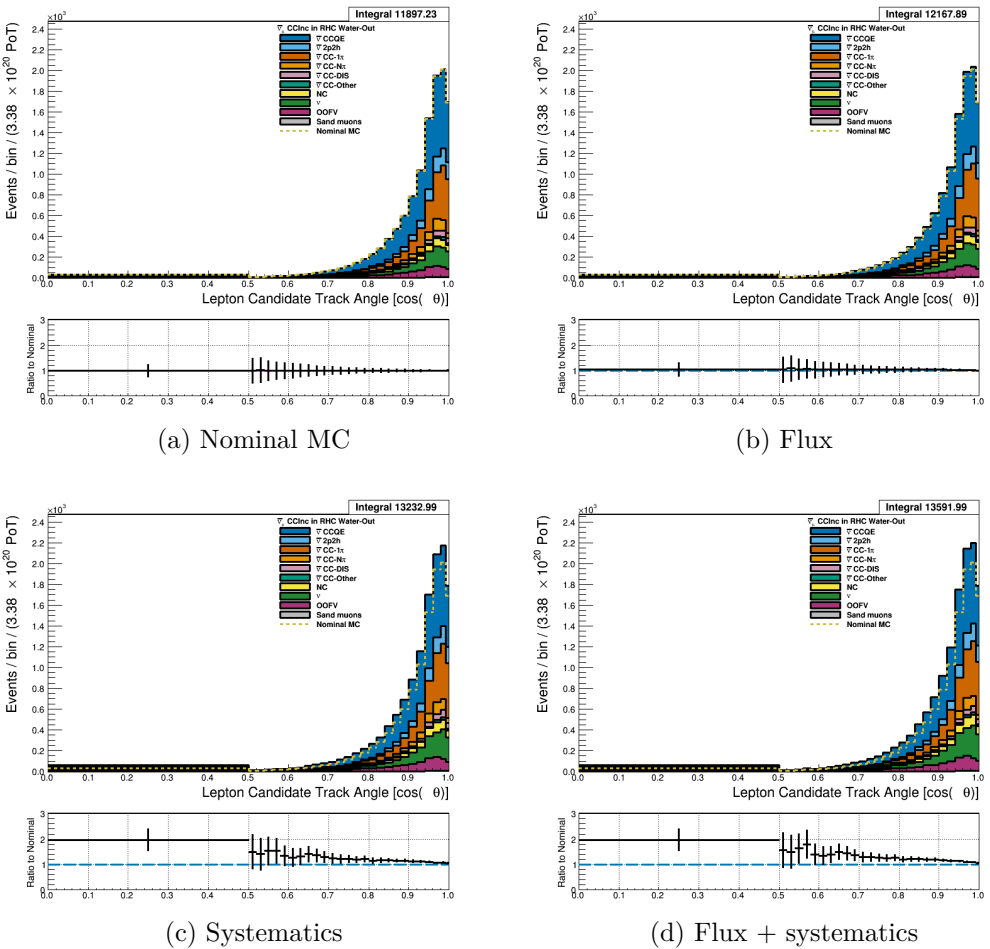


Figure 3.11: Reconstructed lepton candidate  $\cos \theta$  separated by NEUT model interaction mode for RHC  $\bar{\nu}_\mu$  CC Inc. events occurring in the PØD in water-out mode. (a) The nominal MC prediction without any weights applied. (b) The flux tuning are applied. (c) The systematic weighting are applied. (d) Both flux and systematic weighting are applied.

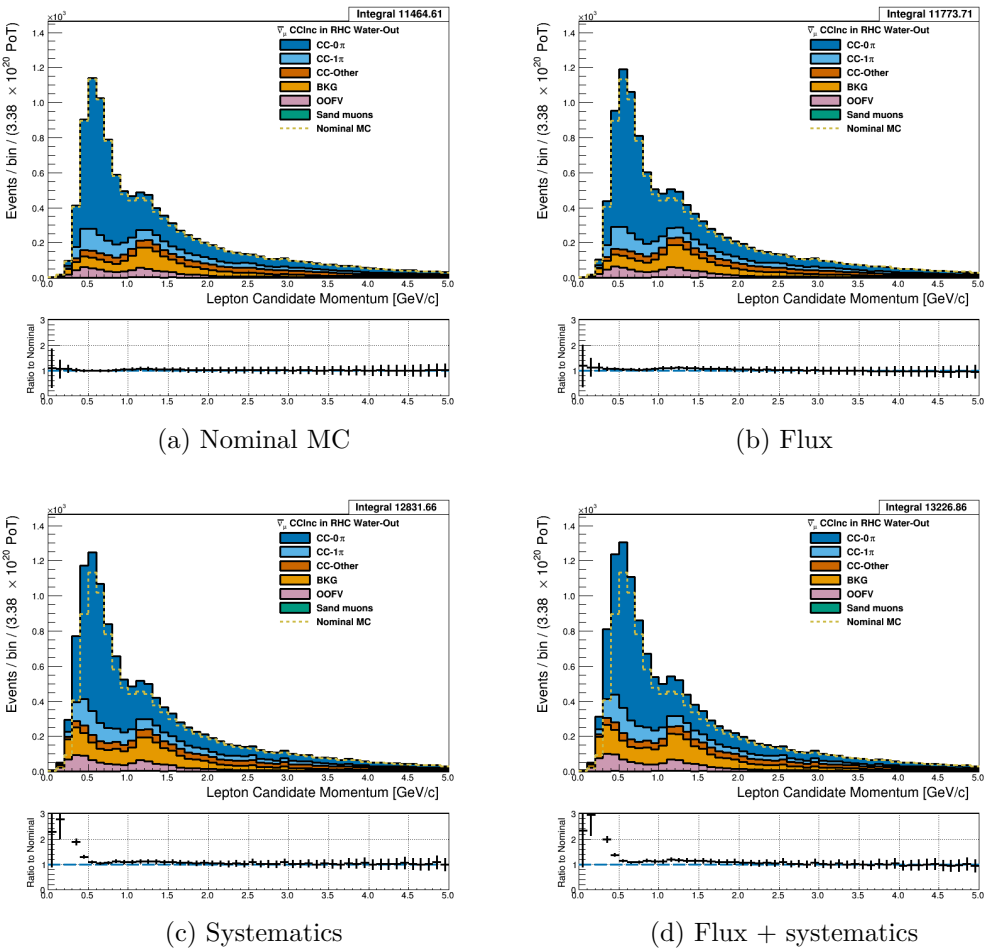


Figure 3.12: Reconstructed lepton candidate momentum separated by topology for RHC  $\bar{\nu}_\mu$  CC Inc. events occurring in the PØD in water-out mode. (a) The nominal MC prediction without any weights applied. (b) The flux tuning are applied. (c) The systematic weighting are applied. (d) Both flux and systematic weighting are applied.

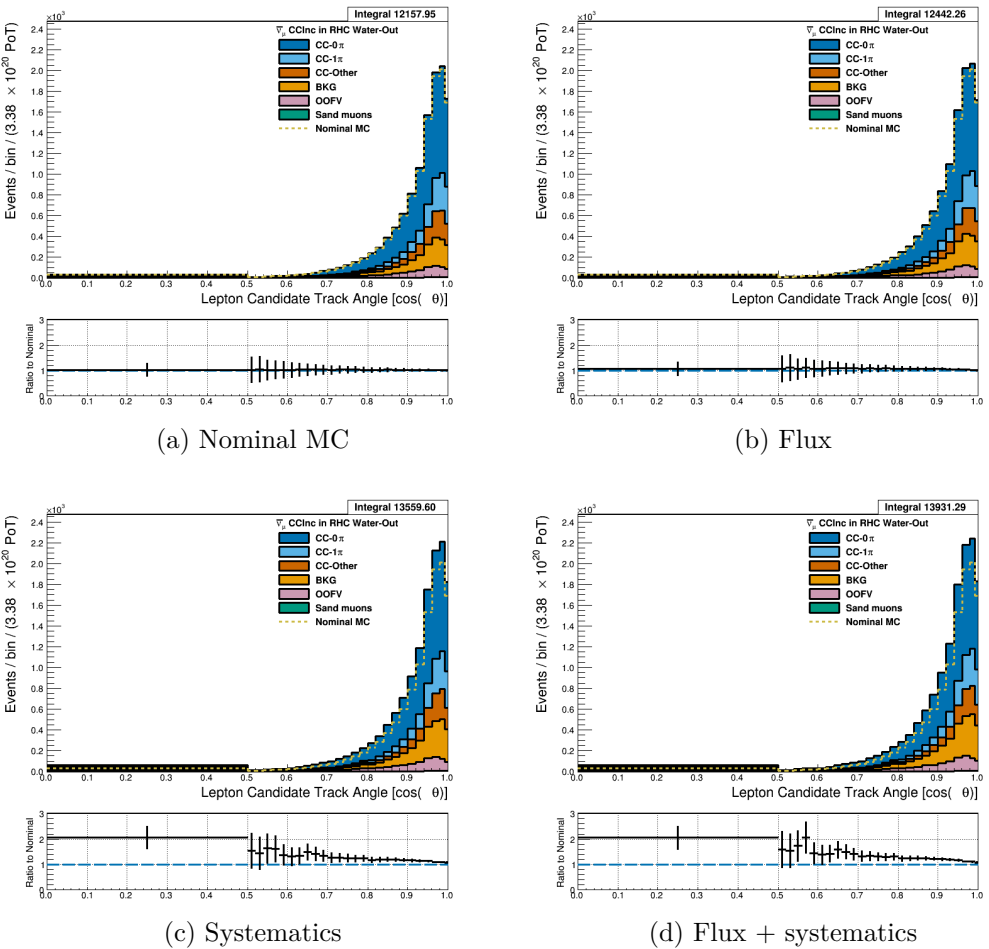


Figure 3.13: Reconstructed lepton candidate  $\cos \theta$  separated by topology for RHC  $\bar{\nu}_\mu$  CC Inc. events occurring in the PØD in water-out mode. (a) The nominal MC prediction without any weights applied. (b) The flux tuning are applied. (c) The systematic weighting are applied. (d) Both flux and systematic weighting are applied.

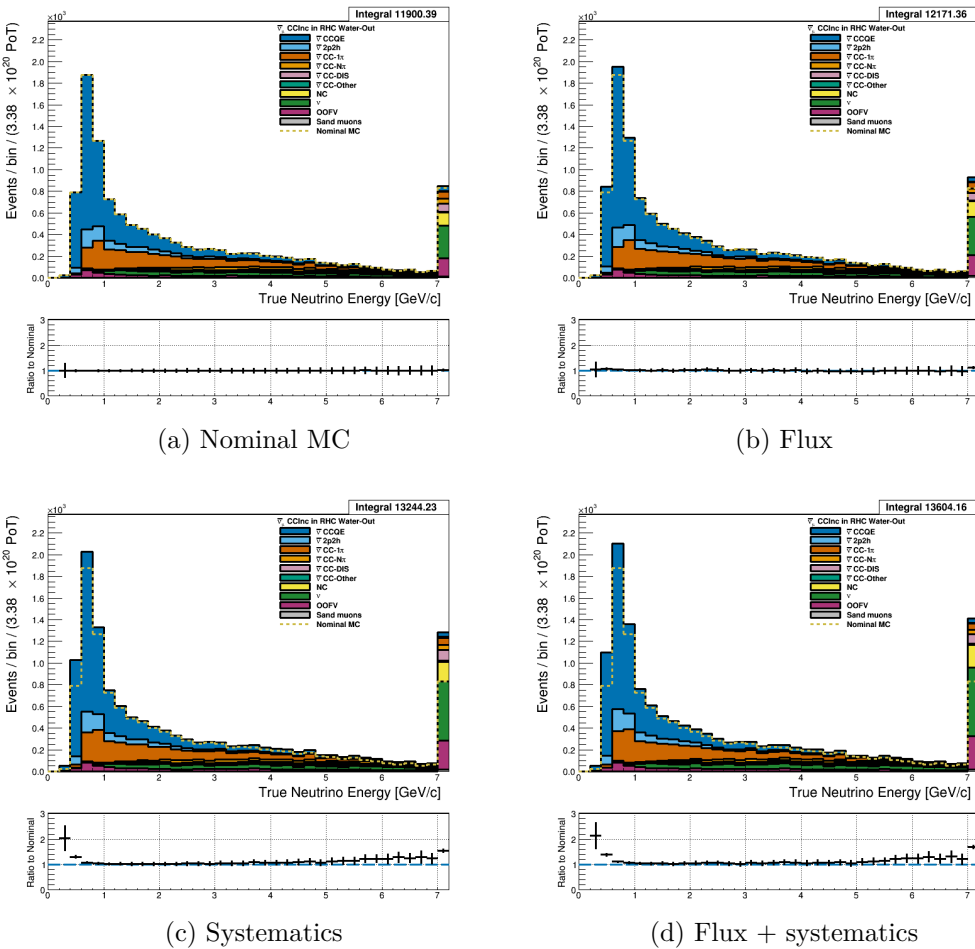


Figure 3.14: True neutrino energy associated with the lepton candidate separated by NEUT model interaction mode for RHC  $\bar{\nu}_\mu$  CC Inc. events occurring in the PØD in water-out mode. (a) The nominal MC prediction without any weights applied. (b) The flux tuning are applied. (c) The systematic weighting are applied. (d) Both flux and systematic weighting are applied.

533 **3.4.1.3  $\nu_\mu$  Background Selection in RHC Mode:** Shown in Figures 3.15, 3.16 and 3.19

534 to 3.21 and ????

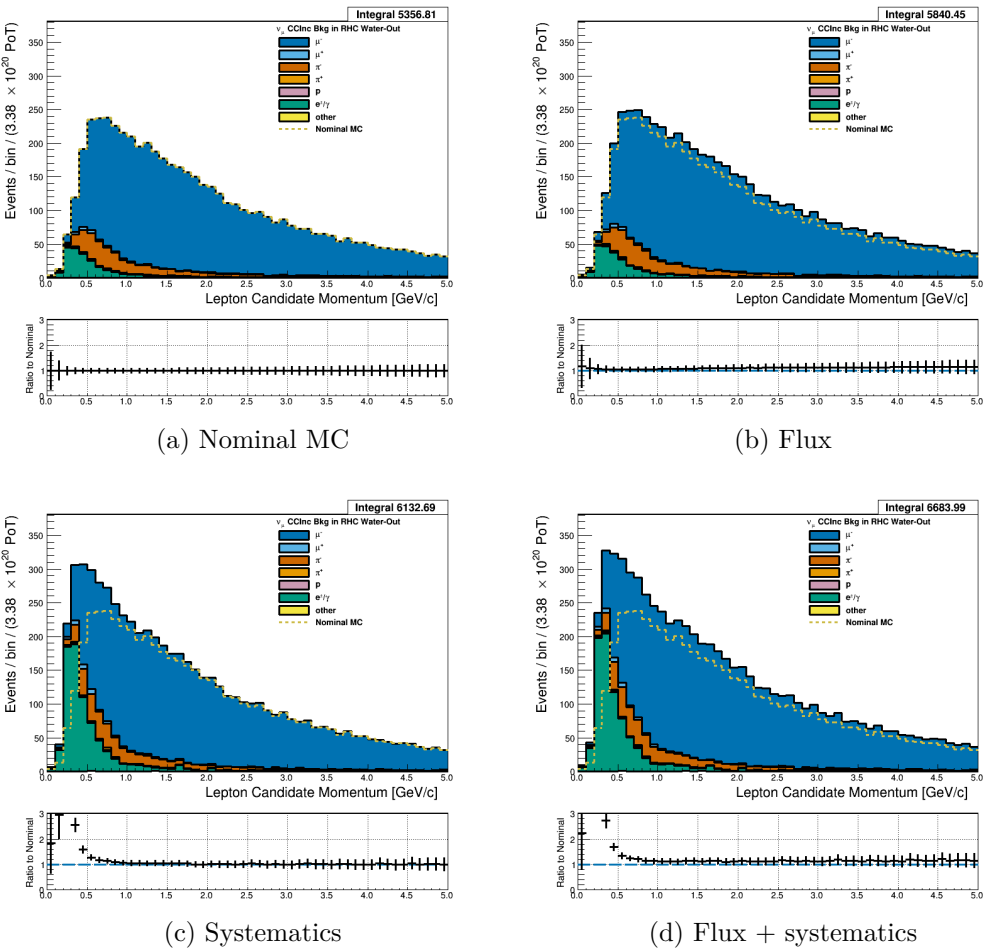


Figure 3.15: Reconstructed lepton candidate momentum separated by true particle species for RHC  $\nu_\mu$  CC Inc. events occurring in the PØD in water-out mode. (a) The nominal MC prediction without any weights applied. (b) The flux tuning are applied. (c) The systematic weighting are applied. (d) Both flux and systematic weighting are applied.

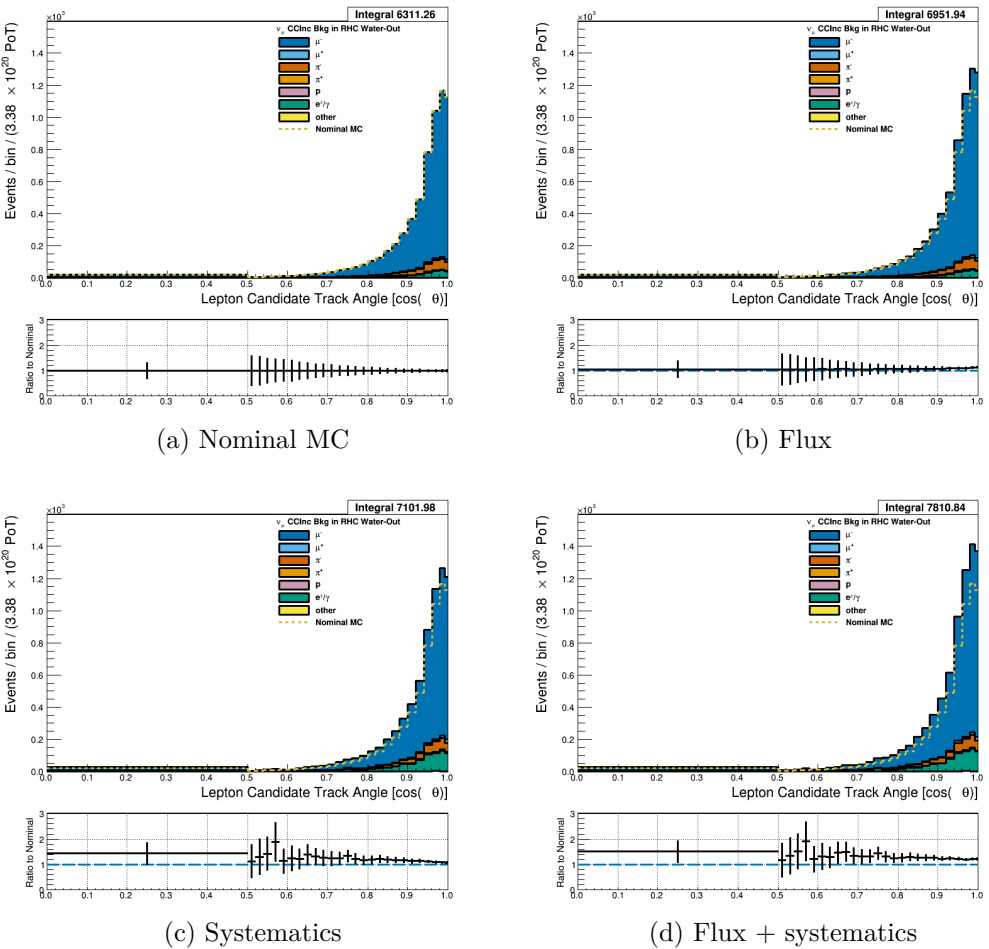


Figure 3.16: Reconstructed lepton candidate angle separated by true particle species for RHC  $\nu_\mu$  CC Inc. events occurring in the PØD in water-out mode. (a) The nominal MC prediction without any weights applied. (b) The flux tuning are applied. (c) The systematic weighting are applied. (d) Both flux and systematic weighting are applied.

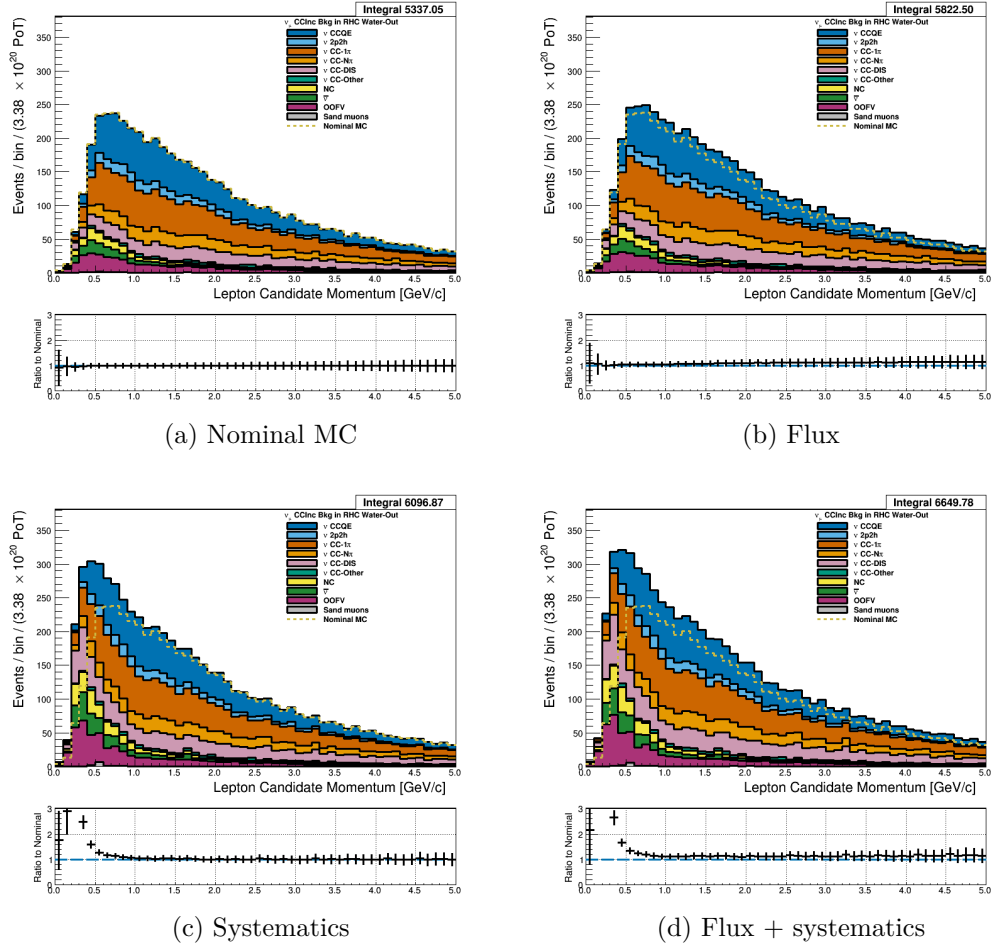


Figure 3.17: Reconstructed lepton candidate momentum separated by NEUT model interaction mode for RHC  $\nu_\mu$  CC Inc. events occurring in the PØD in water-out mode. (a) The nominal MC prediction without any weights applied. (b) The flux tuning are applied. (c) The systematic weighting are applied. (d) Both flux and systematic weighting are applied.

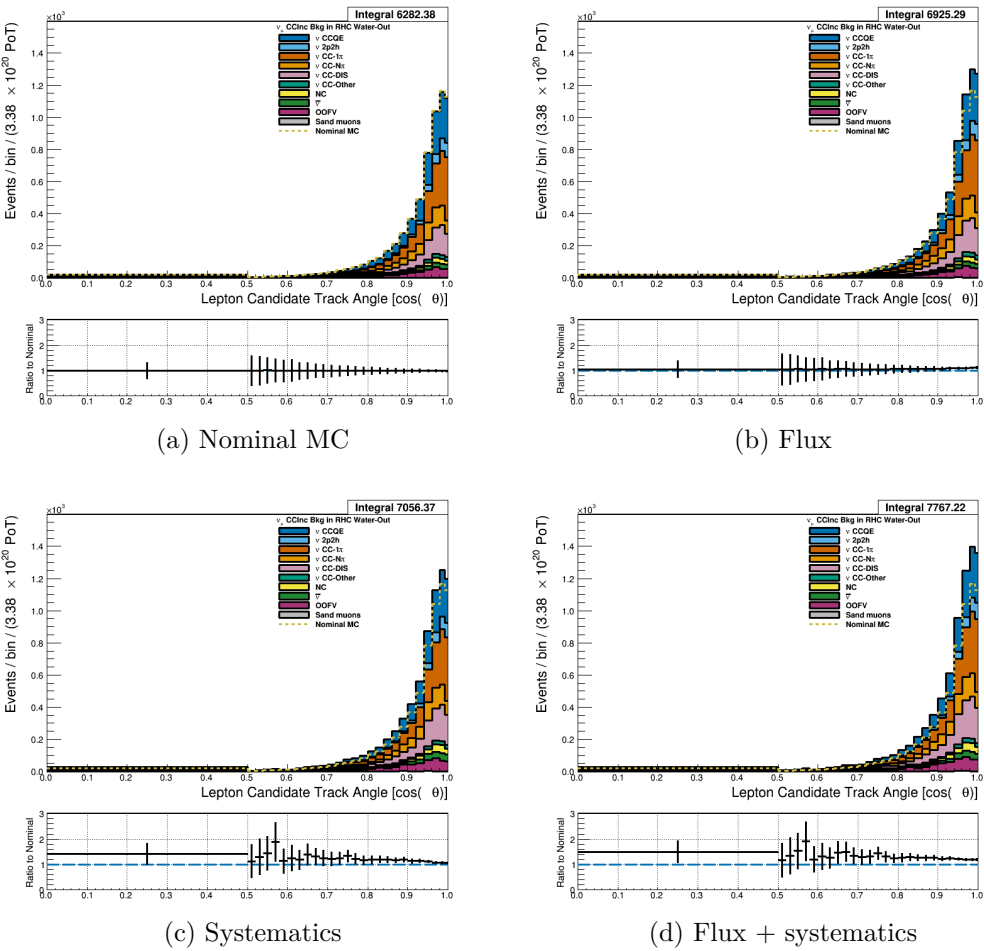


Figure 3.18: Reconstructed lepton candidate  $\cos \theta$  separated by NEUT model interaction mode for FHC  $\nu_\mu$  CC Inc. events occurring in the PØD in water-out mode. (a) The nominal MC prediction without any weights applied. (b) The flux tuning are applied. (c) The systematic weighting are applied. (d) Both flux and systematic weighting are applied.

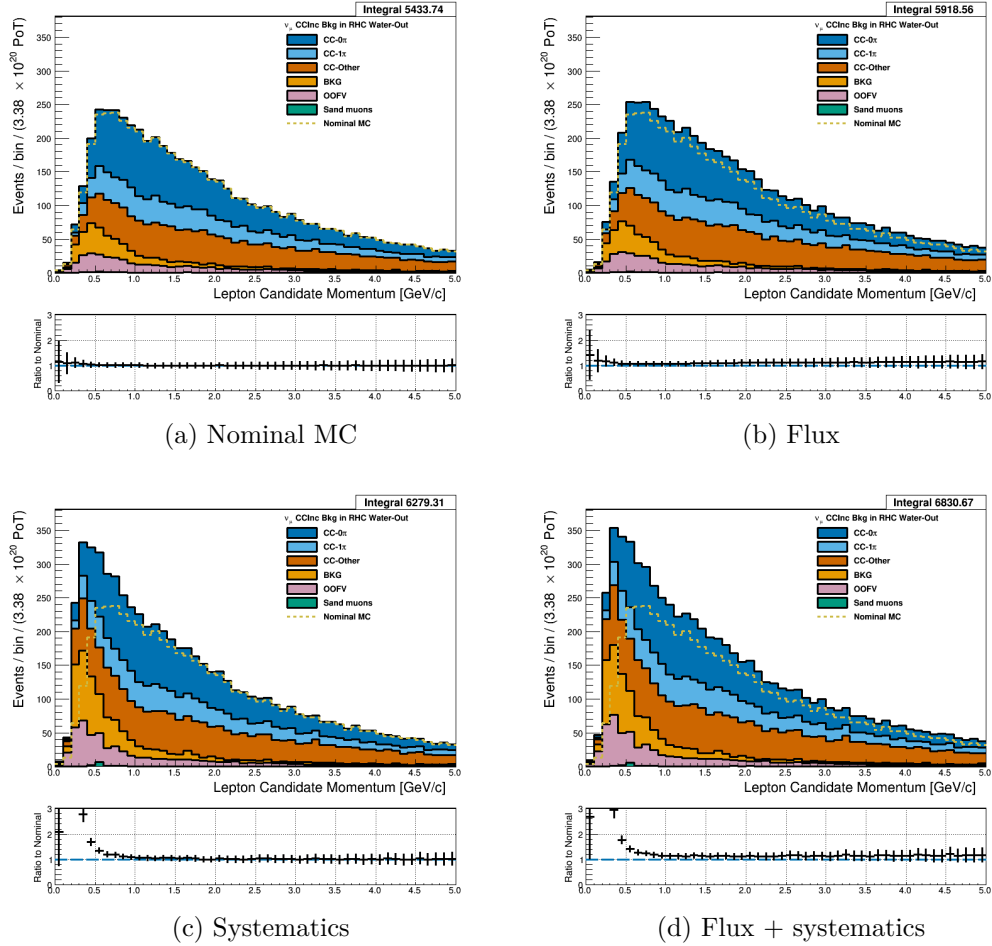


Figure 3.19: Reconstructed lepton candidate momentum separated by topology for FHC  $\nu_\mu$  CC Inc. events occurring in the PØD in water-out mode. (a) The nominal MC prediction without any weights applied. (b) The flux tuning are applied. (c) The systematic weighting are applied. (d) Both flux and systematic weighting are applied.

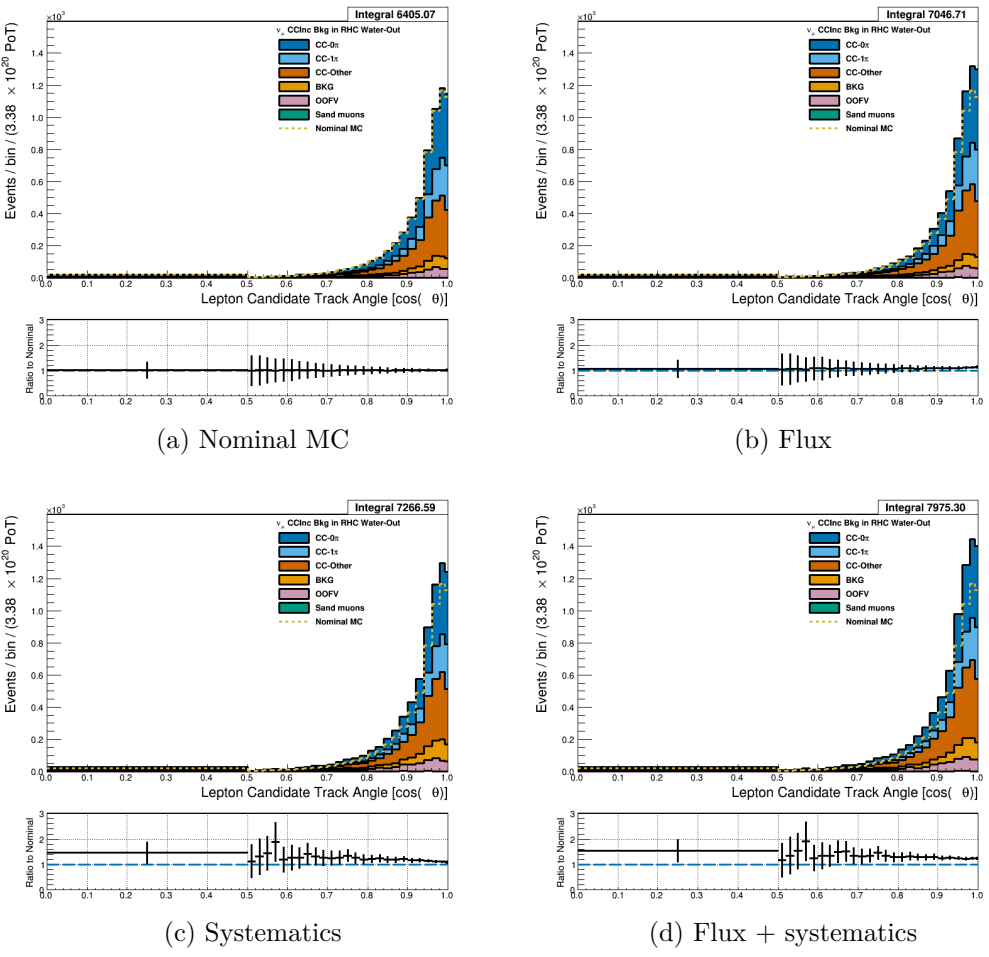


Figure 3.20: Reconstructed lepton candidate  $\cos \theta$  separated by topology for FHC  $\nu_\mu$  CC Inc. events occurring in the PØD in water-out mode. (a) The nominal MC prediction without any weights applied. (b) The flux tuning are applied. (c) The systematic weighting are applied. (d) Both flux and systematic weighting are applied.

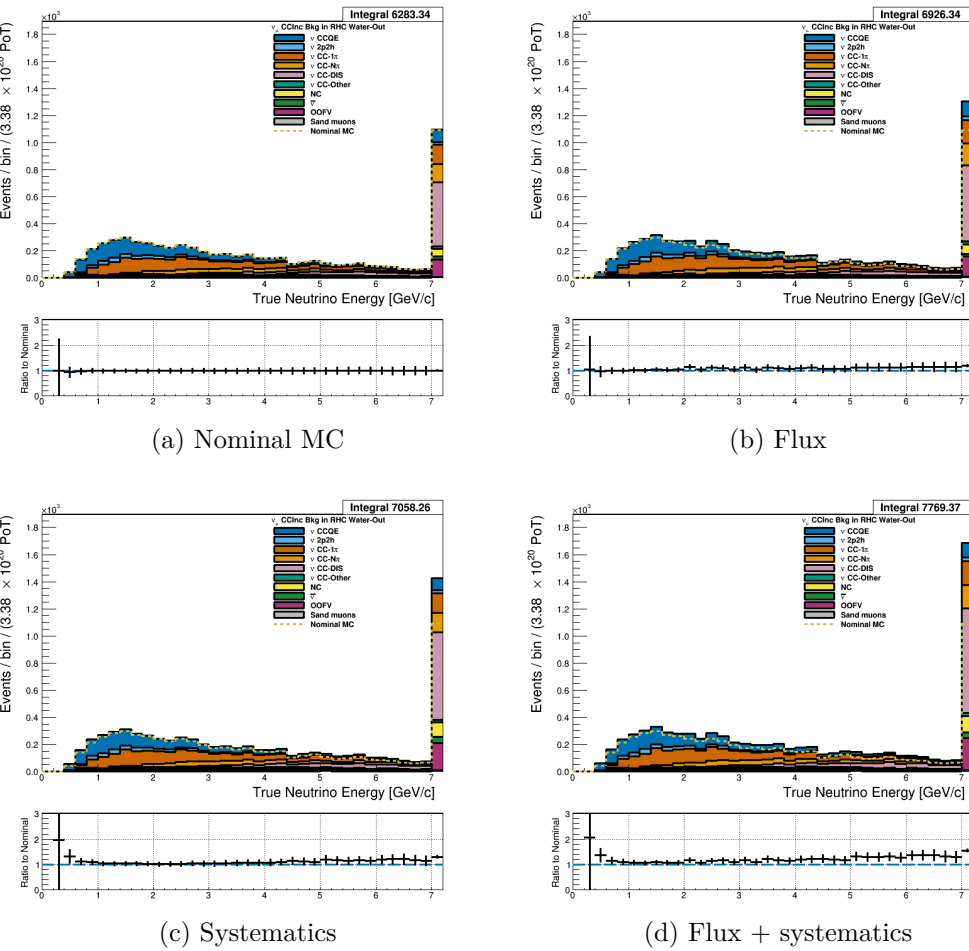


Figure 3.21: True neutrino energy associated with the lepton candidate separated by NEUT model interaction mode for FHC  $\nu_\mu$  CC Inc. events occurring in the PØD in water-out mode. (a) The nominal MC prediction without any weights applied. (b) The flux tuning are applied. (c) The systematic weighting are applied. (d) Both flux and systematic weighting are applied.

### 535 3.4.2 CC 1-Track (CCQE Enhanced)

536 **3.4.2.1  $\nu_\mu$  Selection in FHC Mode:** Shown in

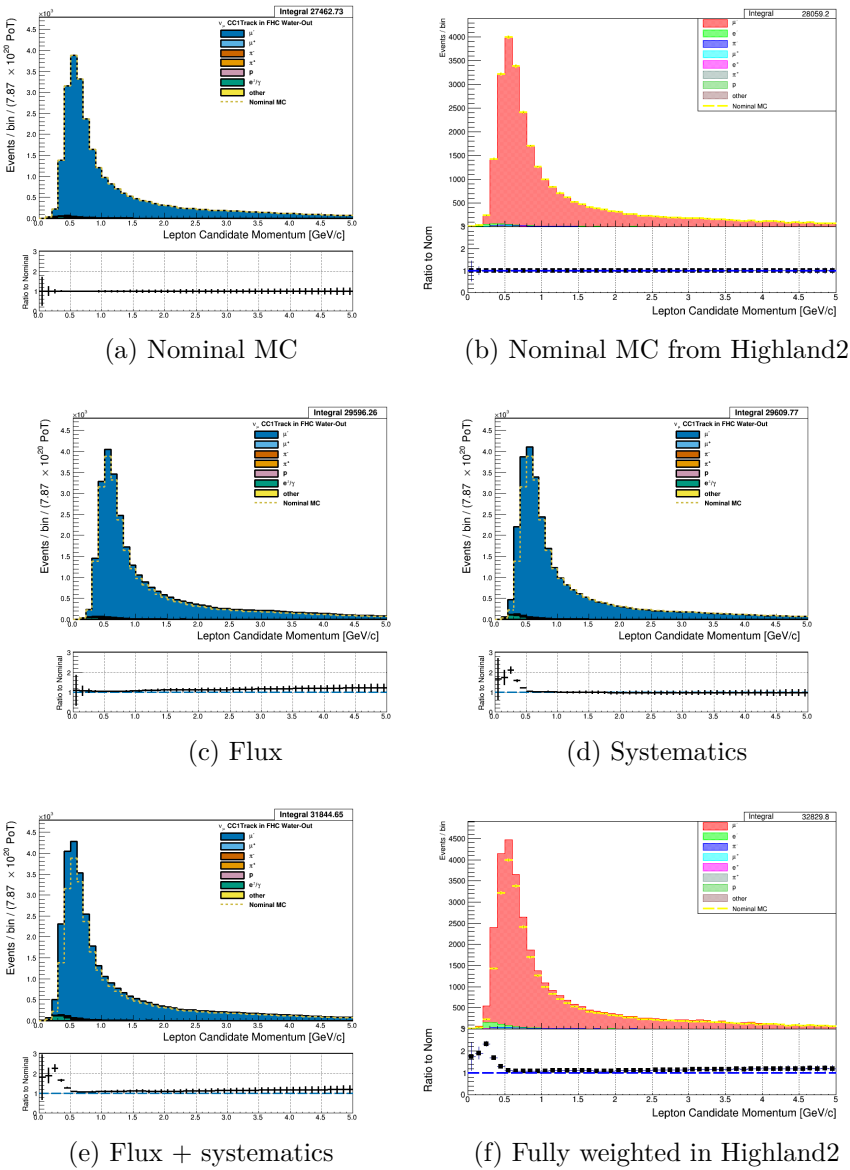


Figure 3.22: Reconstructed lepton candidate momentum separated by true particle species for FHC  $\nu_\mu$  CC 1-Track events occurring in the PØD in water-out mode. (a) The nominal MC prediction without any weights applied. (b) The same POT-normalized plot as (a) using a subset of the water-out MC in Highland. (c) The flux tuning are applied. (d) The systematic weighting are applied. (e) Both flux and systematic weighting are applied. (f) The same POT-normalized plot as (e) using a subset of the water-out MC in Highland. There is a  $\sim 1\%$  difference between Highland2 and BANFF since a subset of the MC was used to generate Highland plots.

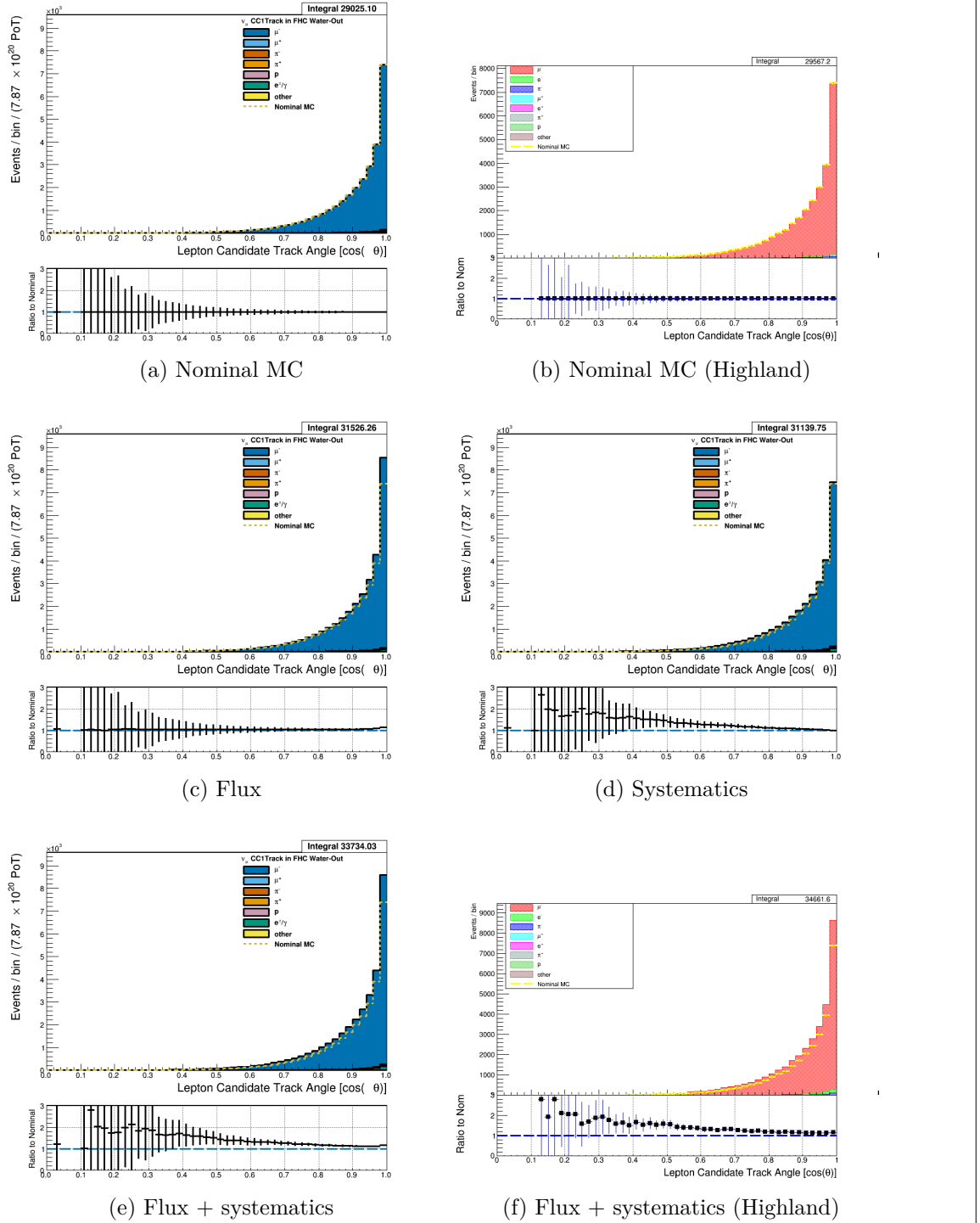


Figure 3.23: Reconstructed lepton candidate angle separated by true particle species for FHC  $\nu_\mu$  CC 1-Track events occurring in the PØD in water-out mode. (a) The nominal MC prediction without any weights applied. (b) The same POT-normalized plot as (a) using a subset of the water-out MC in Highland. (c) The flux tuning are applied. (d) The systematic weighting are applied. (e) Both flux and systematic weighting are applied. (f) The same POT-normalized plot as (e) using a subset of the water-out MC in Highland. There is a ~1% difference between Highland2 and BANFF since a subset of the MC was used to generate Highland plots.

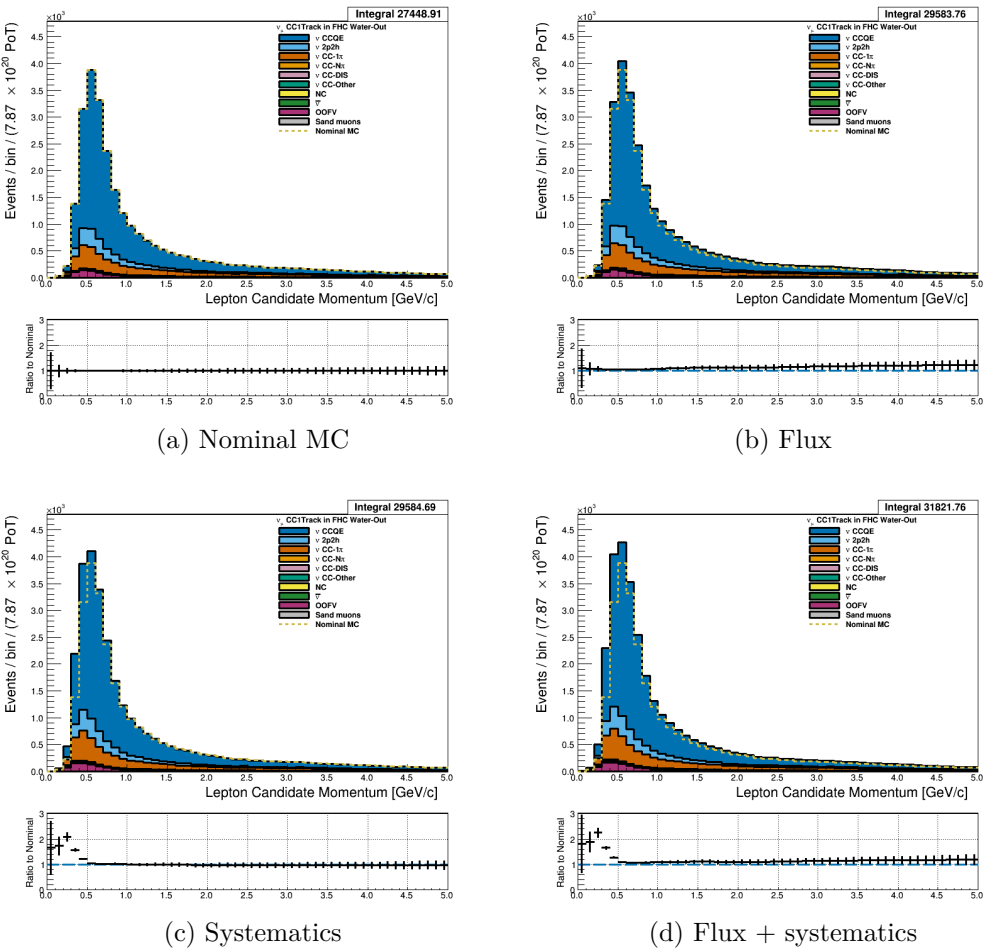


Figure 3.24: Reconstructed lepton candidate momentum separated by NEUT model interaction mode for FHC  $\nu_\mu$  CC 1-Track events occurring in the PØD in water-out mode. (a) The nominal MC prediction without any weights applied. (b) The flux tuning are applied. (c) The systematic weighting are applied. (d) Both flux and systematic weighting are applied.

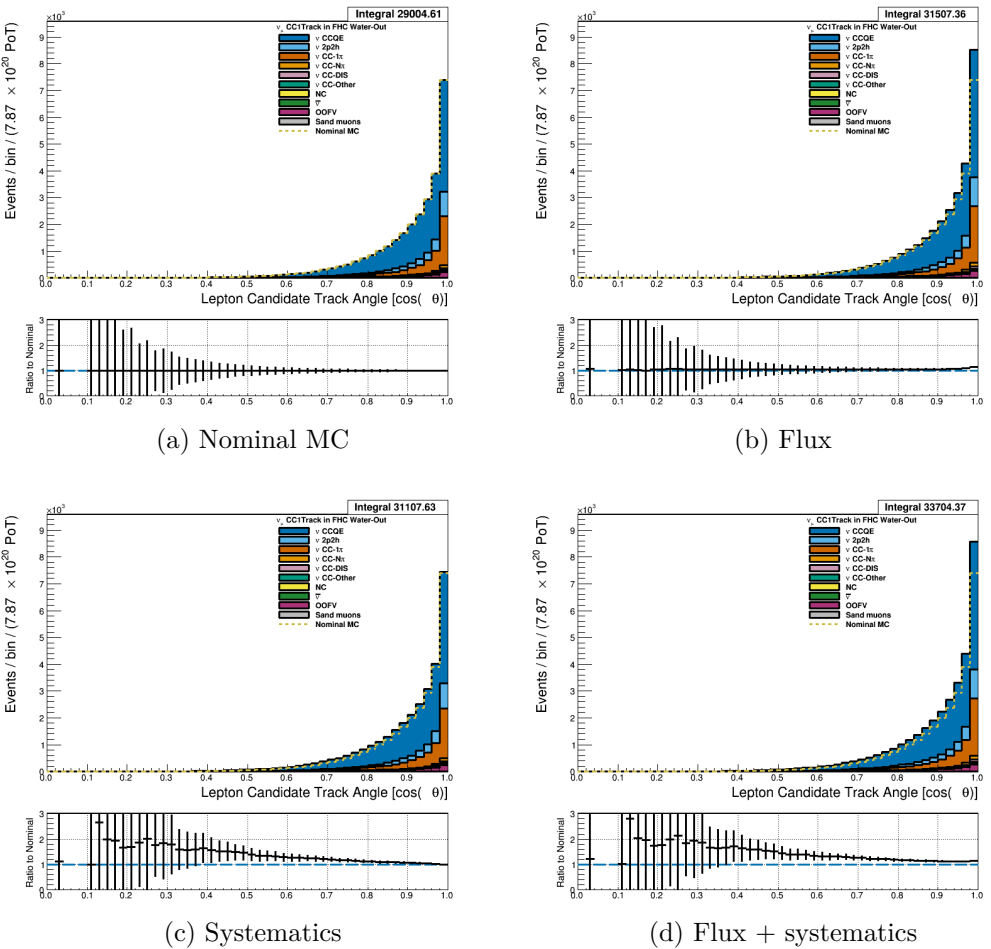


Figure 3.25: Reconstructed lepton candidate  $\cos \theta$  separated by NEUT model interaction mode for FHC  $\nu_\mu$  CC 1-Track events occurring in the PØD in water-out mode. (a) The nominal MC prediction without any weights applied. (b) The flux tuning are applied. (c) The systematic weighting are applied. (d) Both flux and systematic weighting are applied.

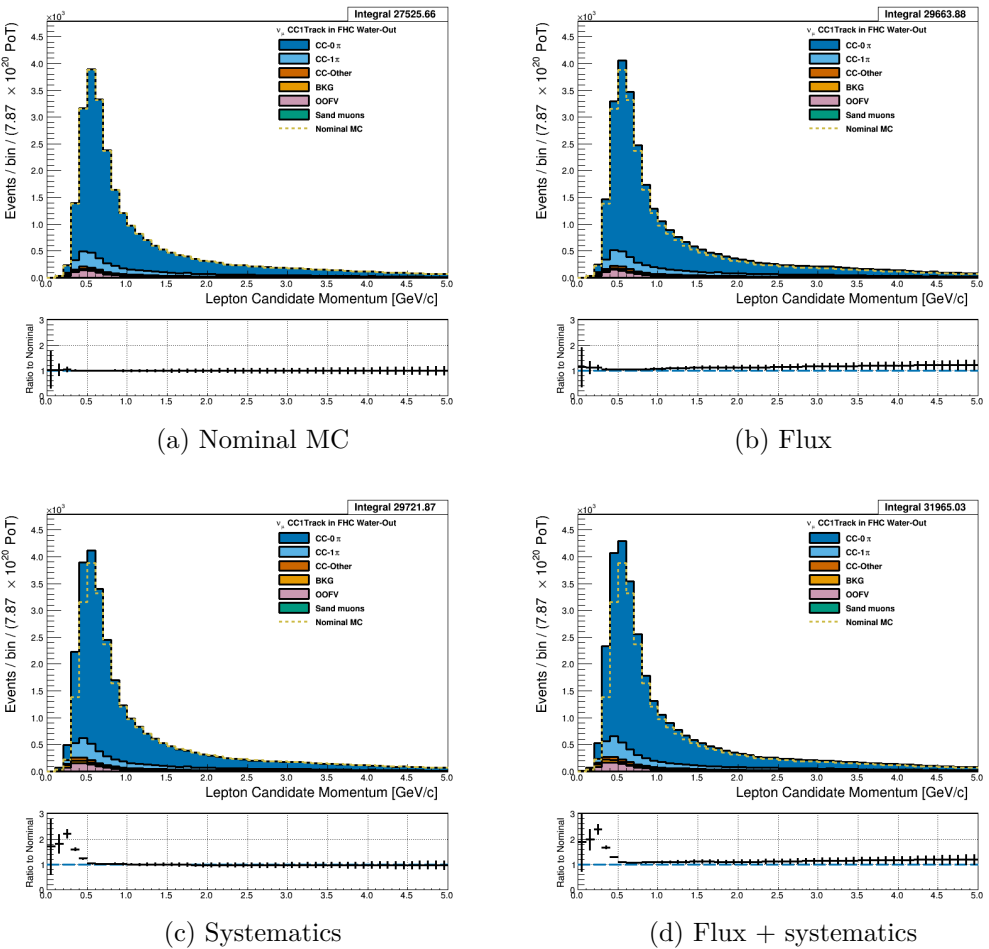


Figure 3.26: Reconstructed lepton candidate momentum separated by topology for FHC  $\nu_\mu$  CC 1-Track events occurring in the PØD in water-out mode. (a) The nominal MC prediction without any weights applied. (b) The flux tuning are applied. (c) The systematic weighting are applied. (d) Both flux and systematic weighting are applied.

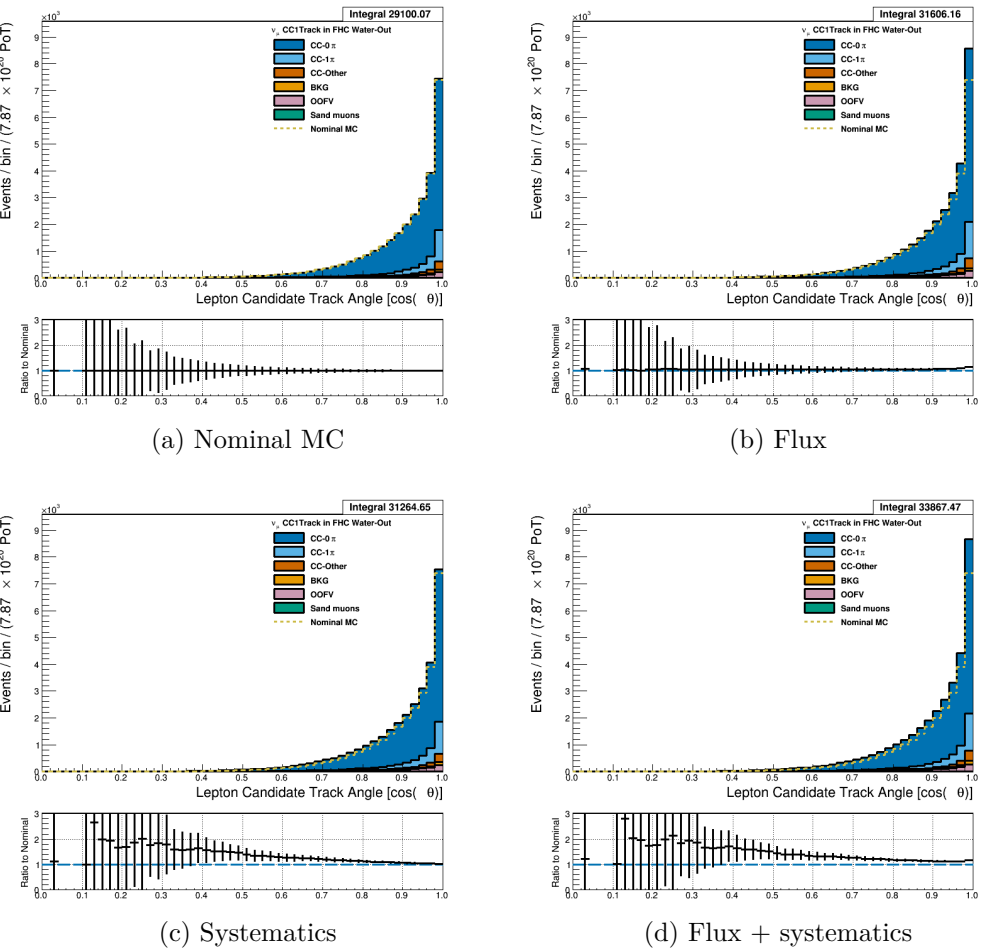


Figure 3.27: Reconstructed lepton candidate  $\cos \theta$  separated by topology for FHC  $\nu_\mu$  CC 1-Track events occurring in the PØD in water-out mode. (a) The nominal MC prediction without any weights applied. (b) The flux tuning are applied. (c) The systematic weighting are applied. (d) Both flux and systematic weighting are applied.

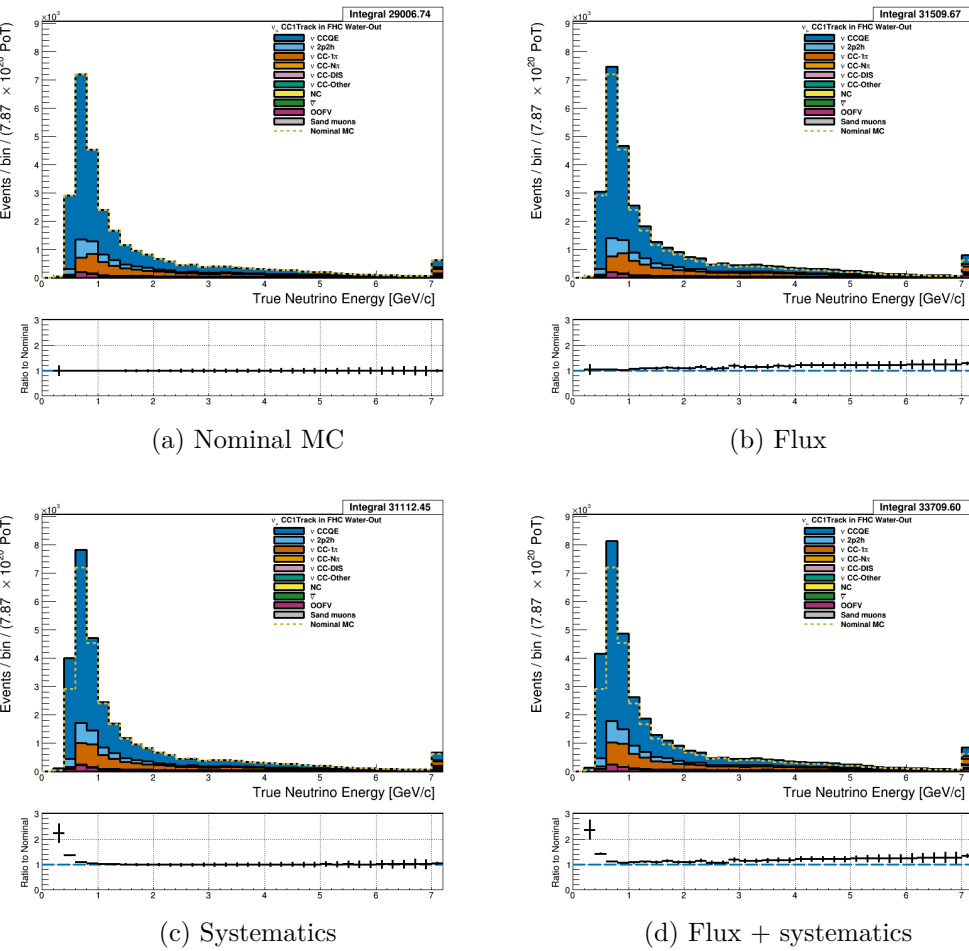


Figure 3.28: True neutrino energy associated with the lepton candidate separated by NEUT model interaction mode for FHC  $\nu_\mu$  CC 1-Track events occurring in the PØD in water-out mode. (a) The nominal MC prediction without any weights applied. (b) The flux tuning are applied. (c) The systematic weighting are applied. (d) Both flux and systematic weighting are applied.

#### 3.4.2.2 $\bar{\nu}_\mu$ Selection in RHC Mode: Figures

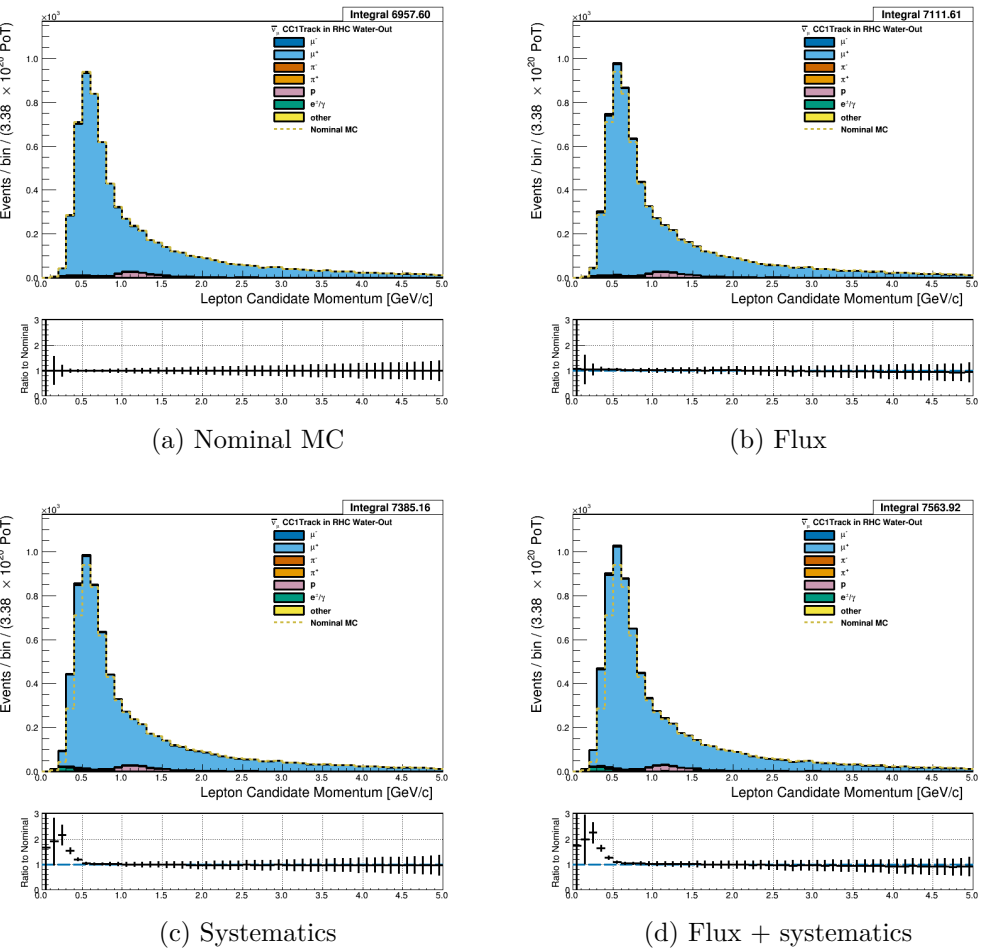


Figure 3.29: Reconstructed lepton candidate momentum separated by true particle species for RHC  $\bar{\nu}_\mu$  CC 1-Track events occurring in the PØD in water-out mode. Reconstructed lepton candidate angle separated by true particle species for RHC  $\bar{\nu}_\mu$  CC Inc. events occurring in the PØD in water-in mode. (a) The nominal MC prediction without any weights applied. (b) The flux tuning are applied. (c) The systematic weighting are applied. (c) Both flux and systematic weighting are applied.

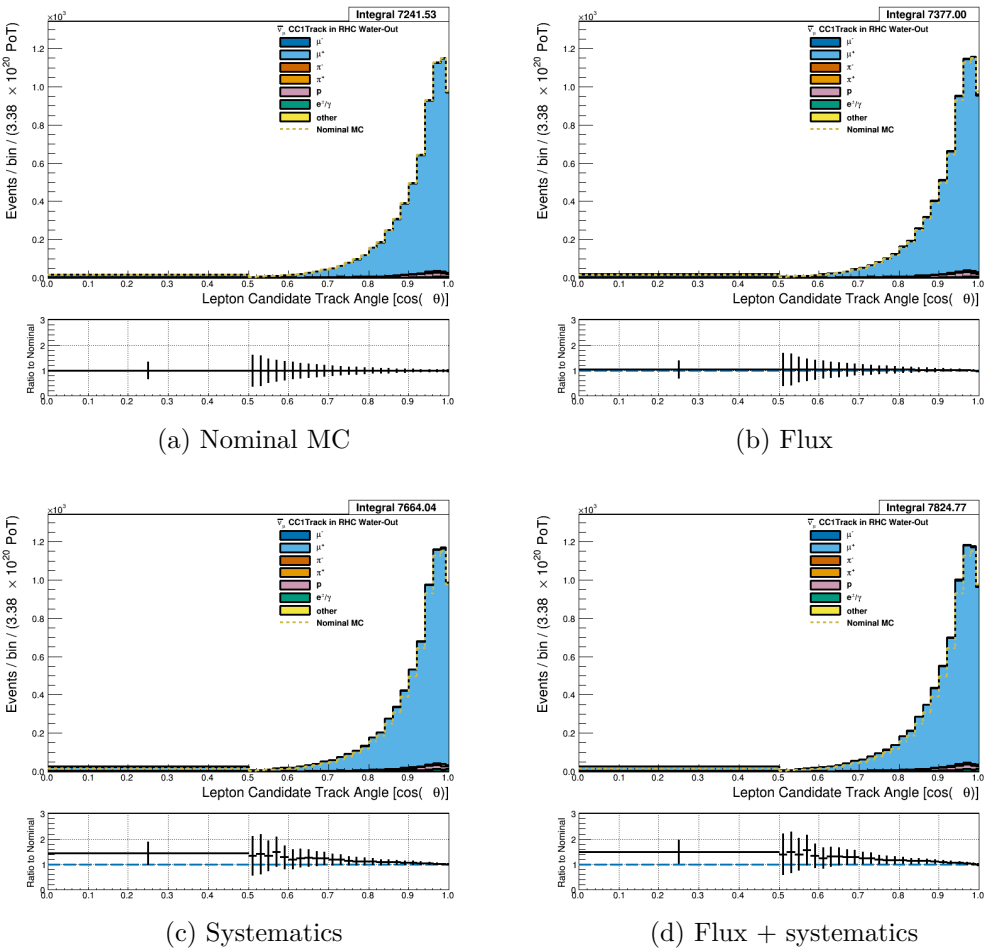


Figure 3.30: Reconstructed lepton candidate angle separated by true particle species for RHC  $\bar{\nu}_\mu$  CC 1-Track events occurring in the PØD in water-out mode. (a) The nominal MC prediction without any weights applied. (b) The flux tuning are applied. (c) The systematic weighting are applied. (d) Both flux and systematic weighting are applied.

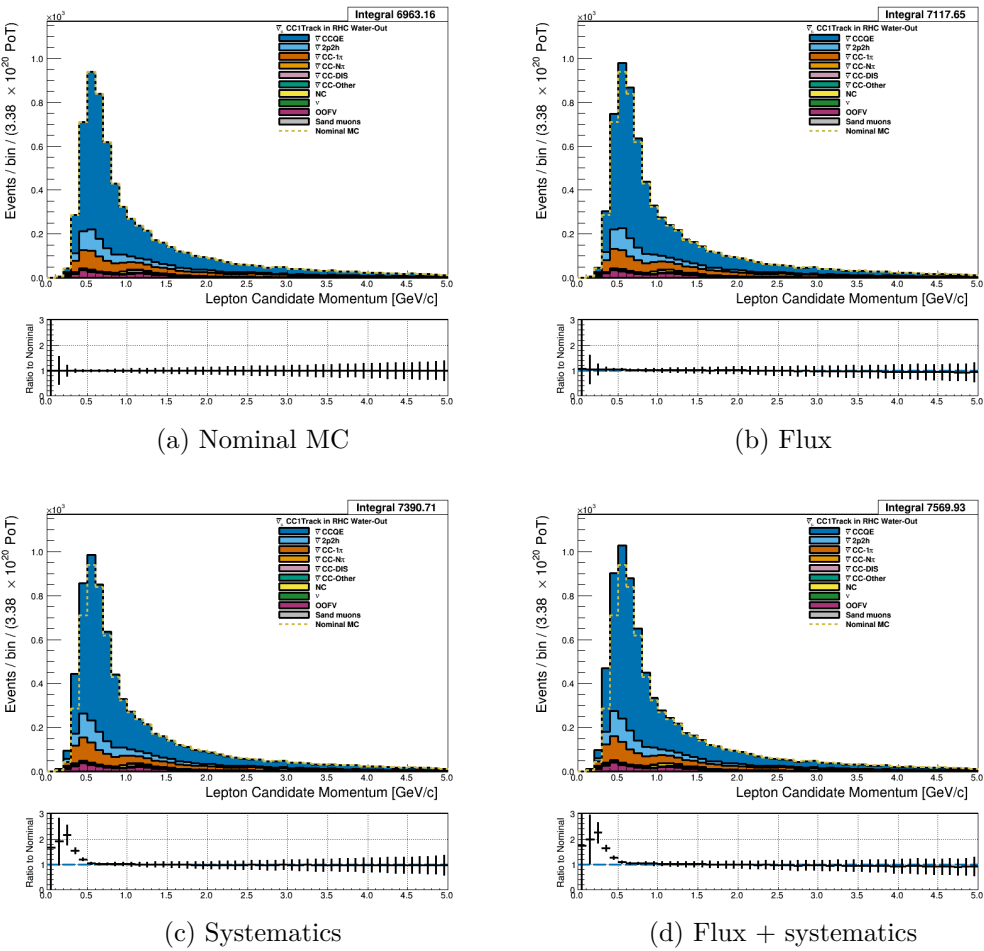


Figure 3.31: Reconstructed lepton candidate momentum separated by NEUT model interaction mode for RHC  $\bar{\nu}_\mu$  CC 1-Track events occurring in the PØD in water-out mode. (a) The nominal MC prediction without any weights applied. (b) The flux tuning are applied. (c) The systematic weighting are applied. (d) Both flux and systematic weighting are applied.

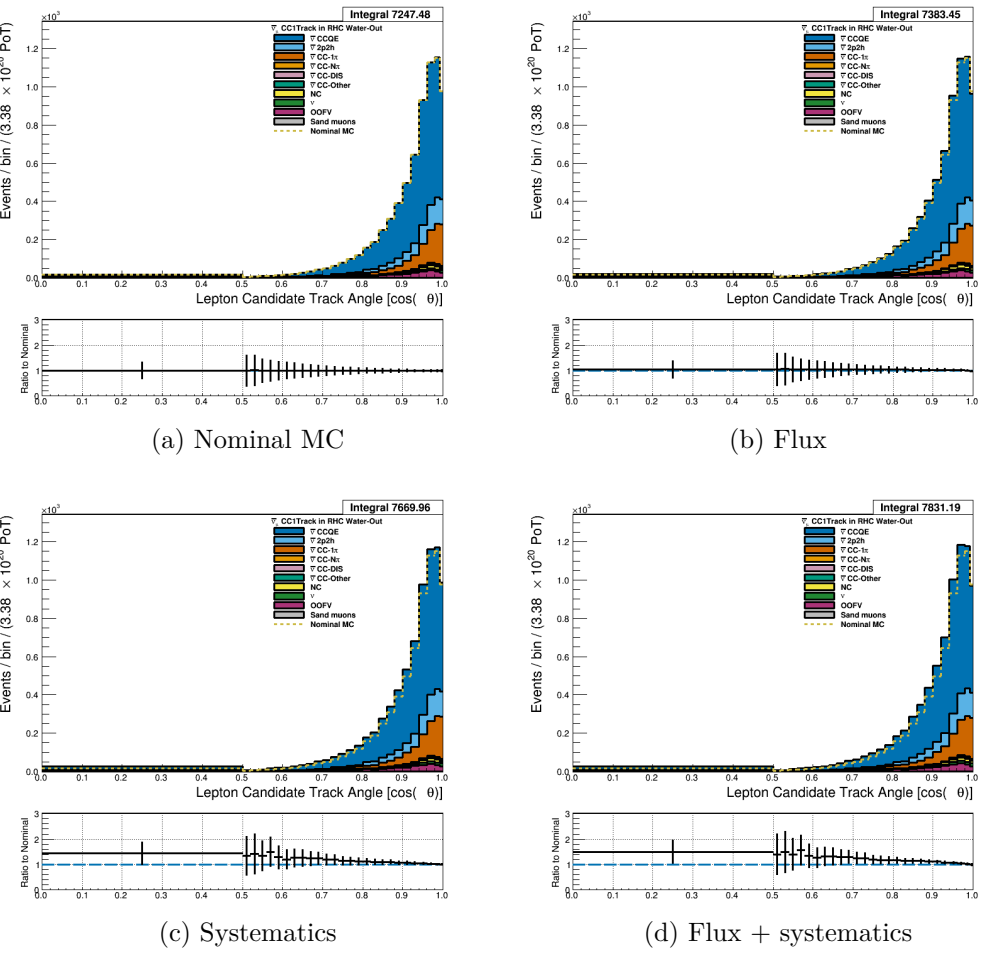


Figure 3.32: Reconstructed lepton candidate  $\cos \theta$  separated by NEUT model interaction mode for RHC  $\bar{\nu}_\mu$  CC 1-TracI events occurring in the P0D in water-out mode. (a) The nominal MC prediction without any weights applied. (b) The flux tuning are applied. (c) The systematic weighting are applied. (d) Both flux and systematic weighting are applied.

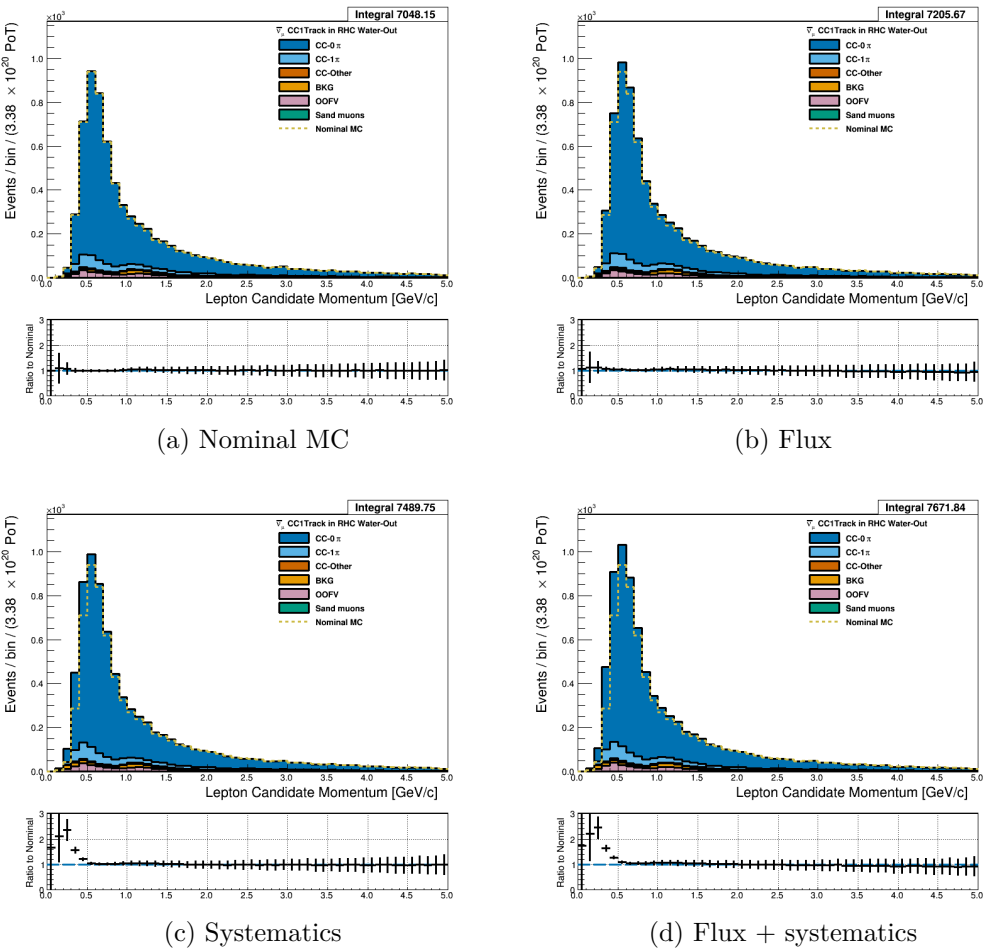


Figure 3.33: Reconstructed lepton candidate momentum separated by topology for RHC  $\bar{\nu}_\mu$  CC 1-Track events occurring in the PØD in water-out mode. (a) The nominal MC prediction without any weights applied. (b) The flux tuning are applied. (c) The systematic weighting are applied. (d) Both flux and systematic weighting are applied.

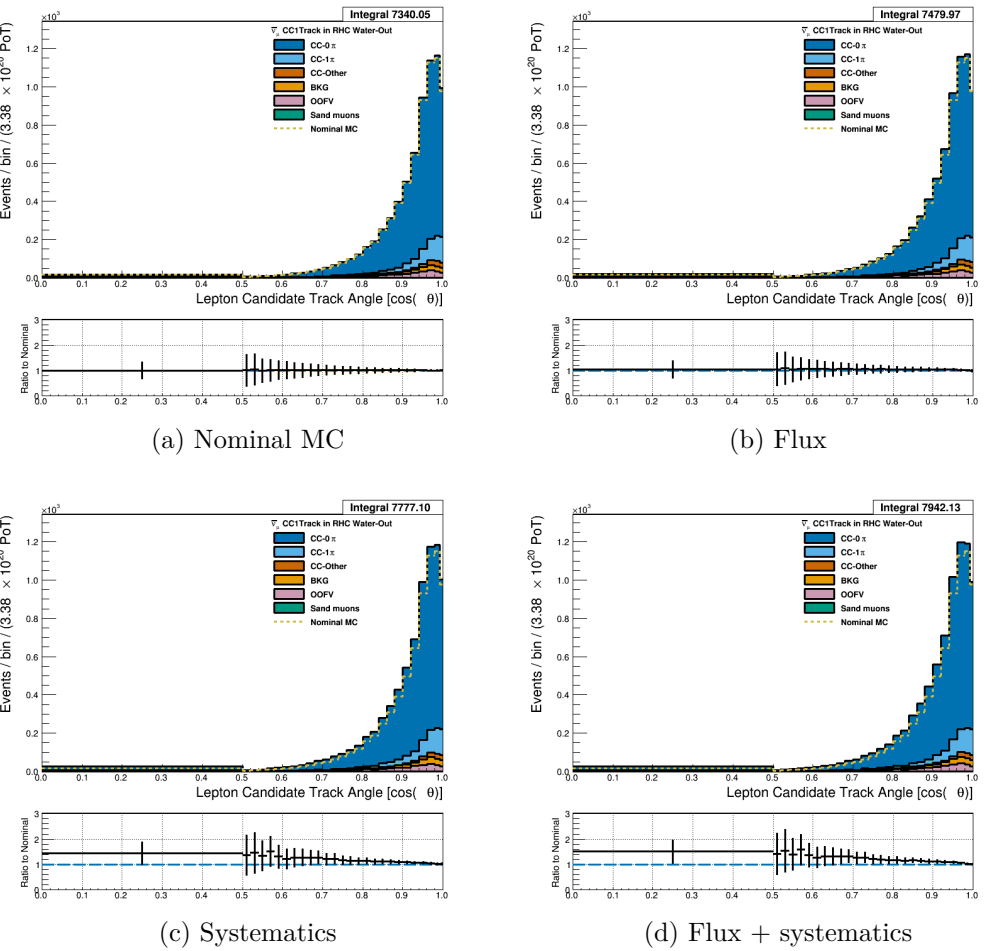


Figure 3.34: Reconstructed lepton candidate  $\cos \theta$  separated by topology for RHC  $\bar{\nu}_\mu$  CC 1-Track events occurring in the PØD in water-out mode. (a) The nominal MC prediction without any weights applied. (b) The flux tuning are applied. (c) The systematic weighting are applied. (d) Both flux and systematic weighting are applied.

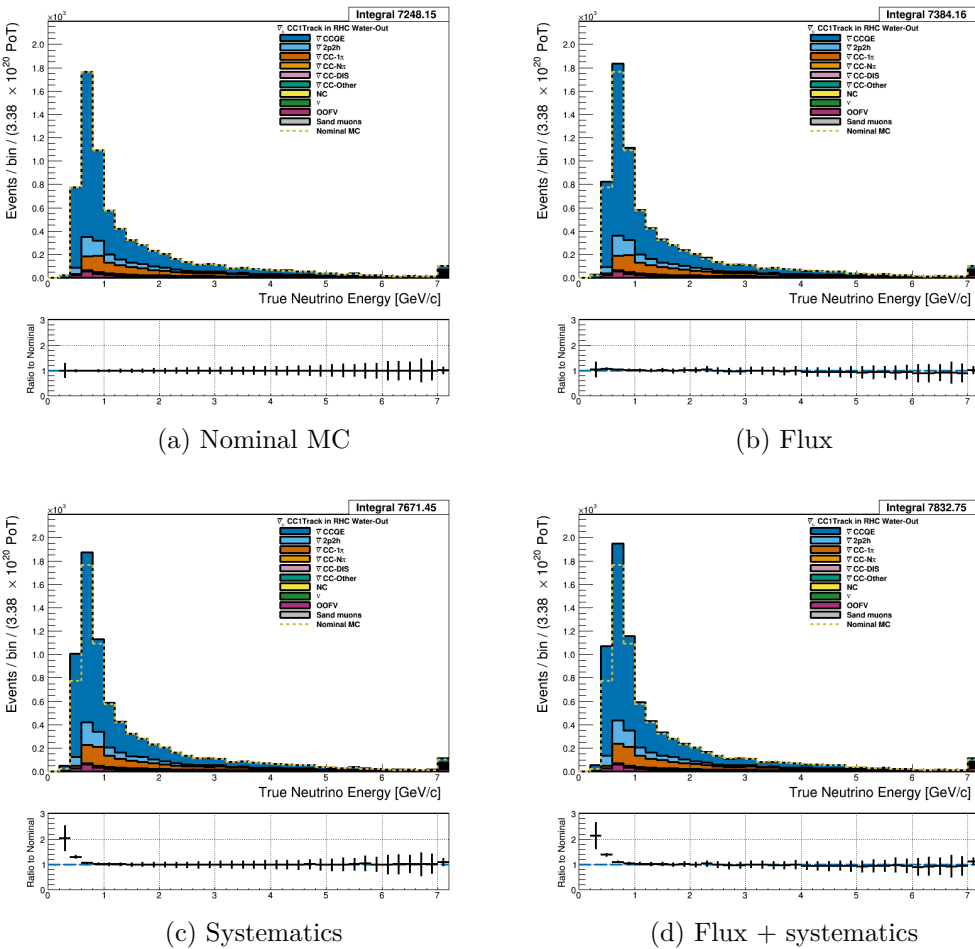


Figure 3.35: True neutrino energy associated with the lepton candidate separated by NEUT model interaction mode for RHC  $\bar{\nu}_\mu$  CC 1-Track events occurring in the PØD in water-out mode. (a) The nominal MC prediction without any weights applied. (b) The flux tuning are applied. (c) The systematic weighting are applied. (d) Both flux and systematic weighting are applied.

538     **3.4.2.3  $\nu_\mu$  Background Selection in RHC Mode:** Text [Add figures here](#)

539     **3.4.3 CC N-Tracks (CCnQE Enhanced)**

540     Text [Add figures here](#)

541     **3.4.3.1  $\nu_\mu$  Selection in FHC Mode:** Text

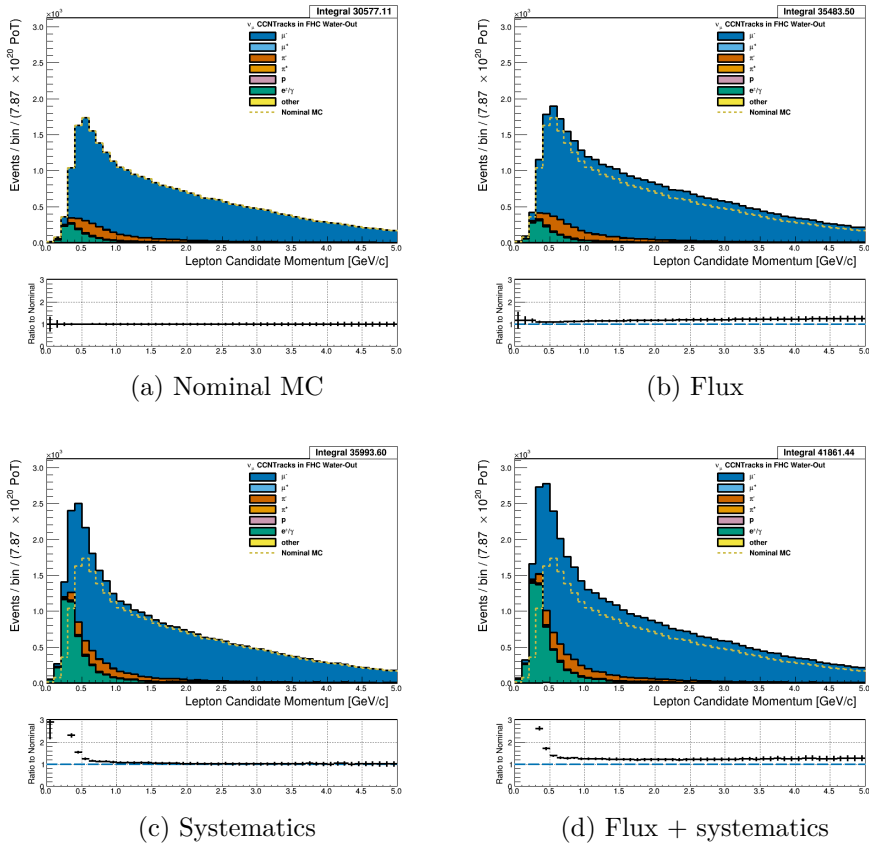


Figure 3.36: Reconstructed lepton candidate momentum separated by true particle species for FHC  $\nu_\mu$  CC N-Tracks events occurring in the PØD in water-out mode. (a) The nominal MC prediction without any weights applied. (b) The flux tuning are applied. (c) The systematic weighting are applied. (e) Both flux and systematic weighting are applied.

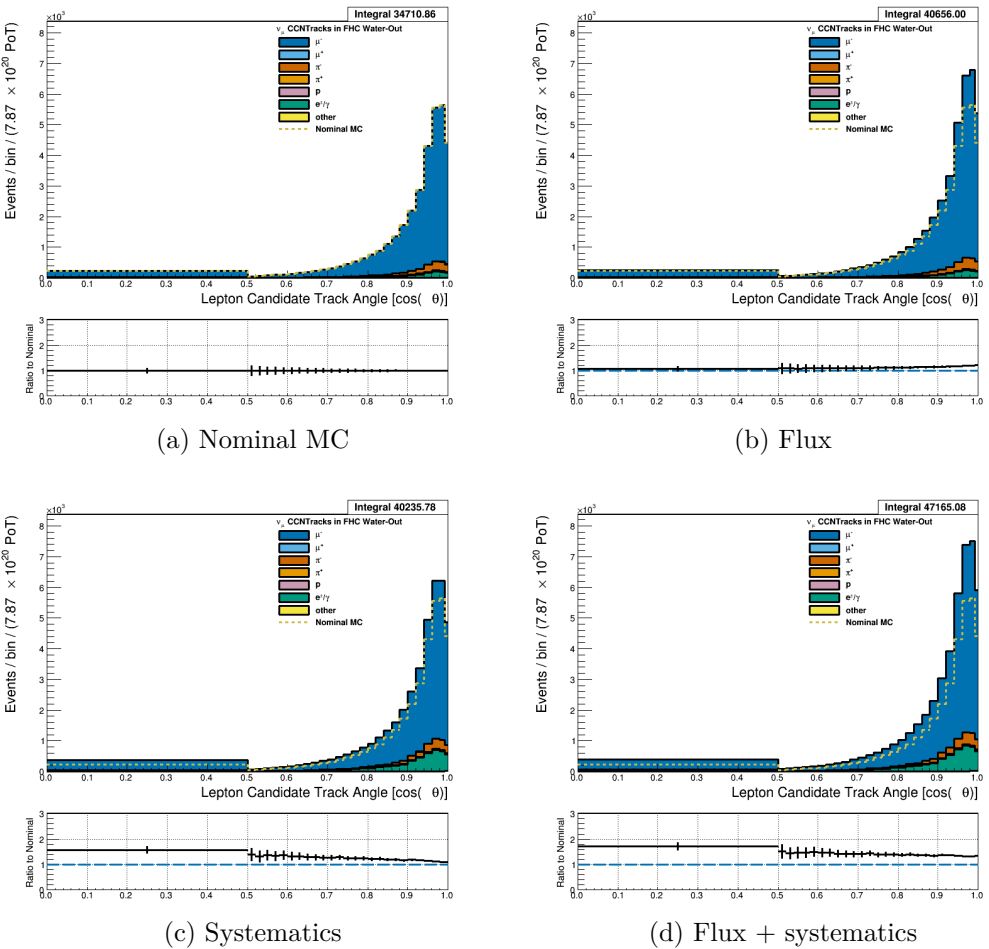


Figure 3.37: Reconstructed lepton candidate angle separated by true particle species for FHC  $\nu_\mu$  CC N-Tracks events occurring in the PØD in water-out mode. (a) The nominal MC prediction without any weights applied. (b) The flux tuning are applied. (c) The systematic weighting are applied. (d) Both flux and systematic weighting are applied.

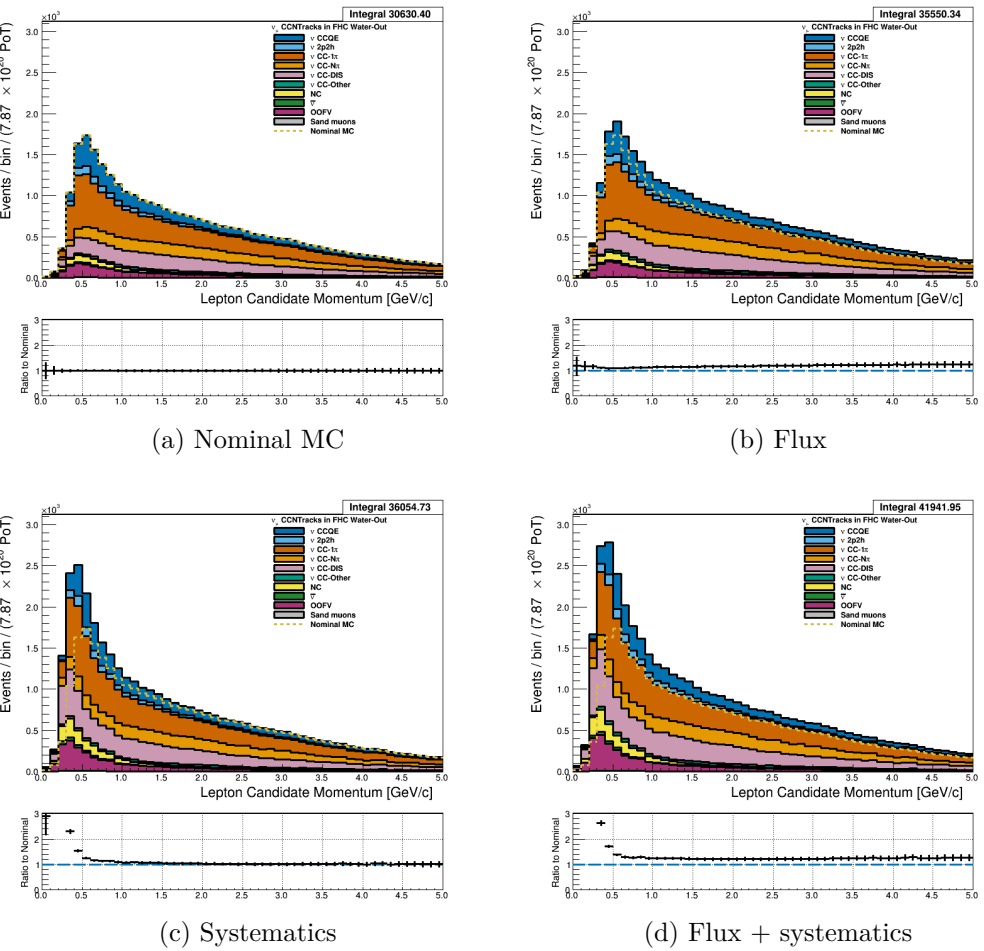


Figure 3.38: Reconstructed lepton candidate momentum separated by NEUT model interaction mode for FHC  $\nu_\mu$  CC N-Tracks events occurring in the PØD in water-out mode. (a) The nominal MC prediction without any weights applied. (b) The flux tuning are applied. (c) The systematic weighting are applied. (d) Both flux and systematic weighting are applied.

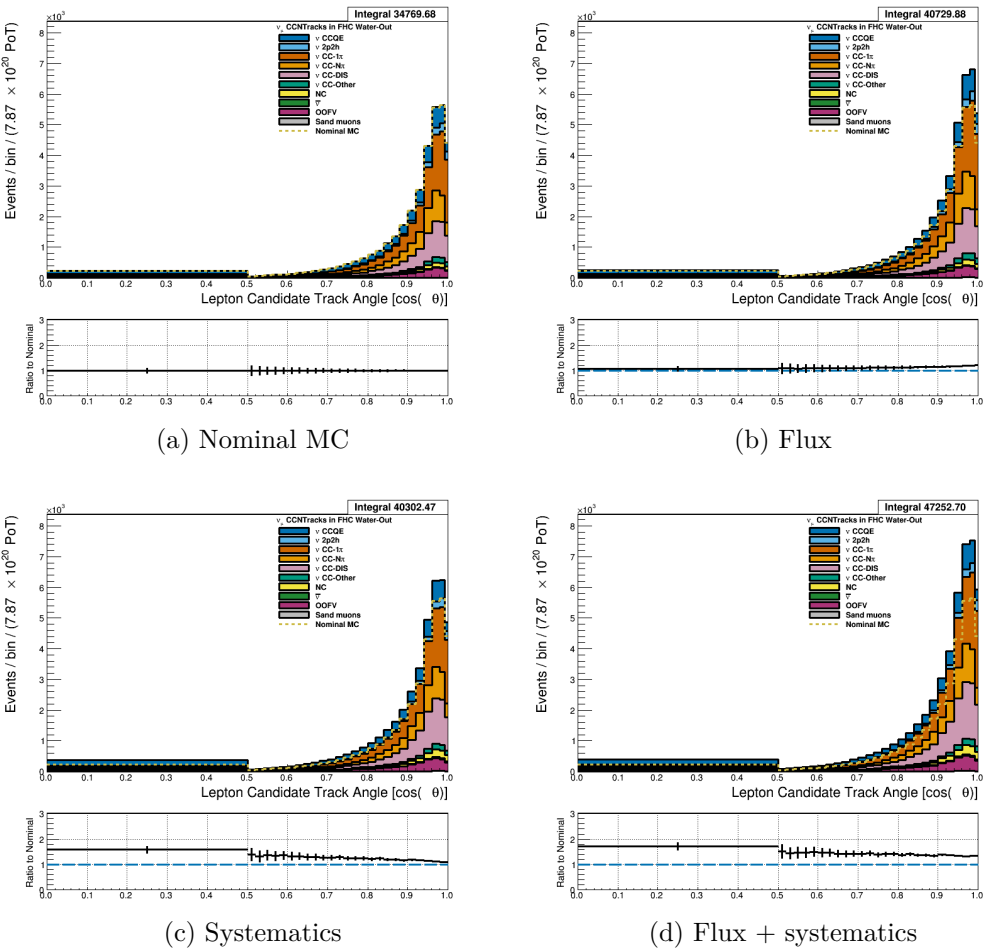


Figure 3.39: Reconstructed lepton candidate  $\cos \theta$  separated by NEUT model interaction mode for FHC  $\nu_\mu$  CC N-Tracks events occurring in the PØD in water-out mode. (a) The nominal MC prediction without any weights applied. (b) The flux tuning are applied. (c) The systematic weighting are applied. (d) Both flux and systematic weighting are applied.

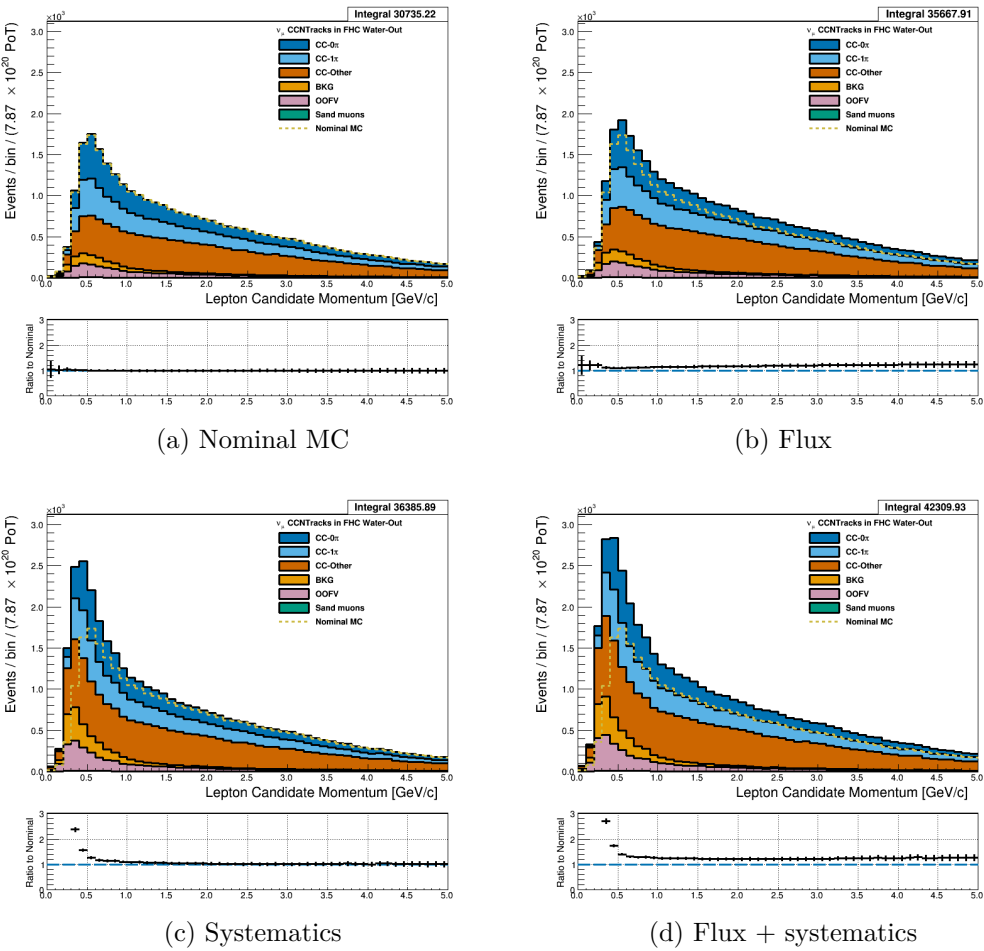


Figure 3.40: Reconstructed lepton candidate momentum separated by topology for FHC  $\nu_\mu$  CC N-Tracks events occurring in the PØD in water-out mode. (a) The nominal MC prediction without any weights applied. (b) The flux tuning are applied. (c) The systematic weighting are applied. (d) Both flux and systematic weighting are applied.

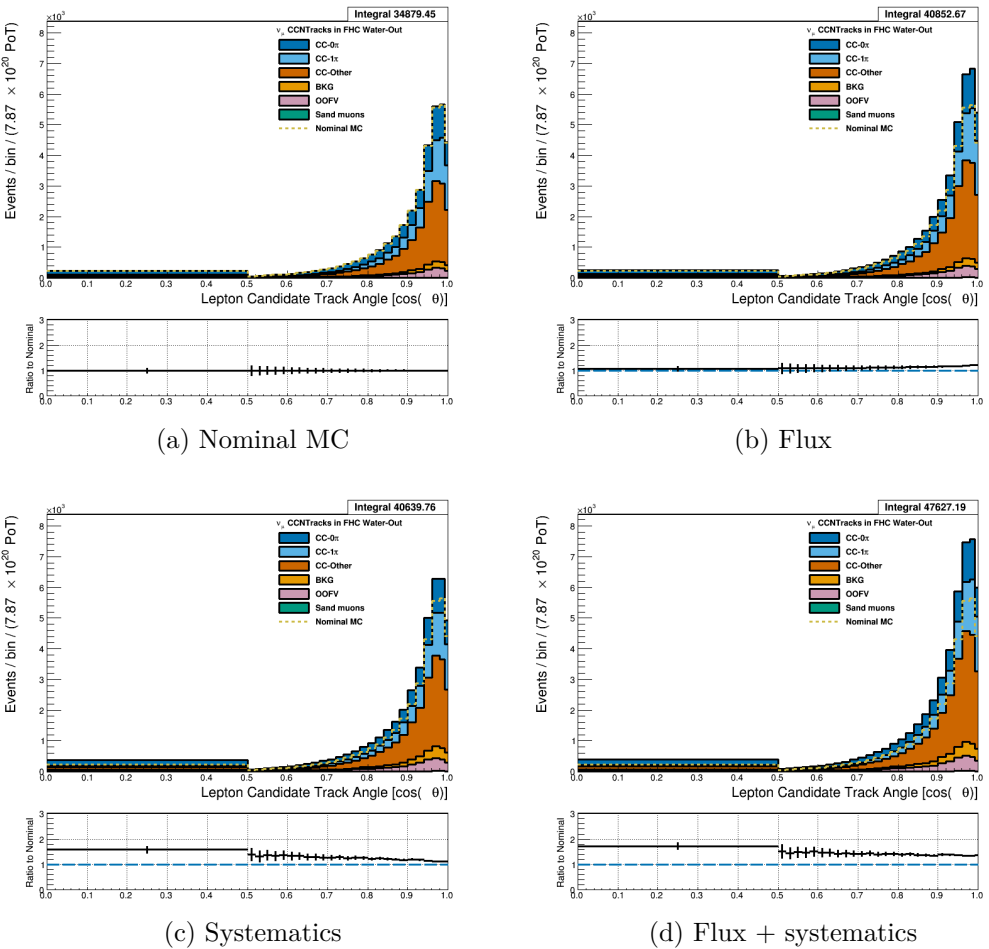


Figure 3.41: Reconstructed lepton candidate  $\cos \theta$  separated by topology for FHC  $\nu_\mu$  CC N-Tracks events occurring in the PØD in water-out mode. (a) The nominal MC prediction without any weights applied. (b) The flux tuning are applied. (c) The systematic weighting are applied. (d) Both flux and systematic weighting are applied.

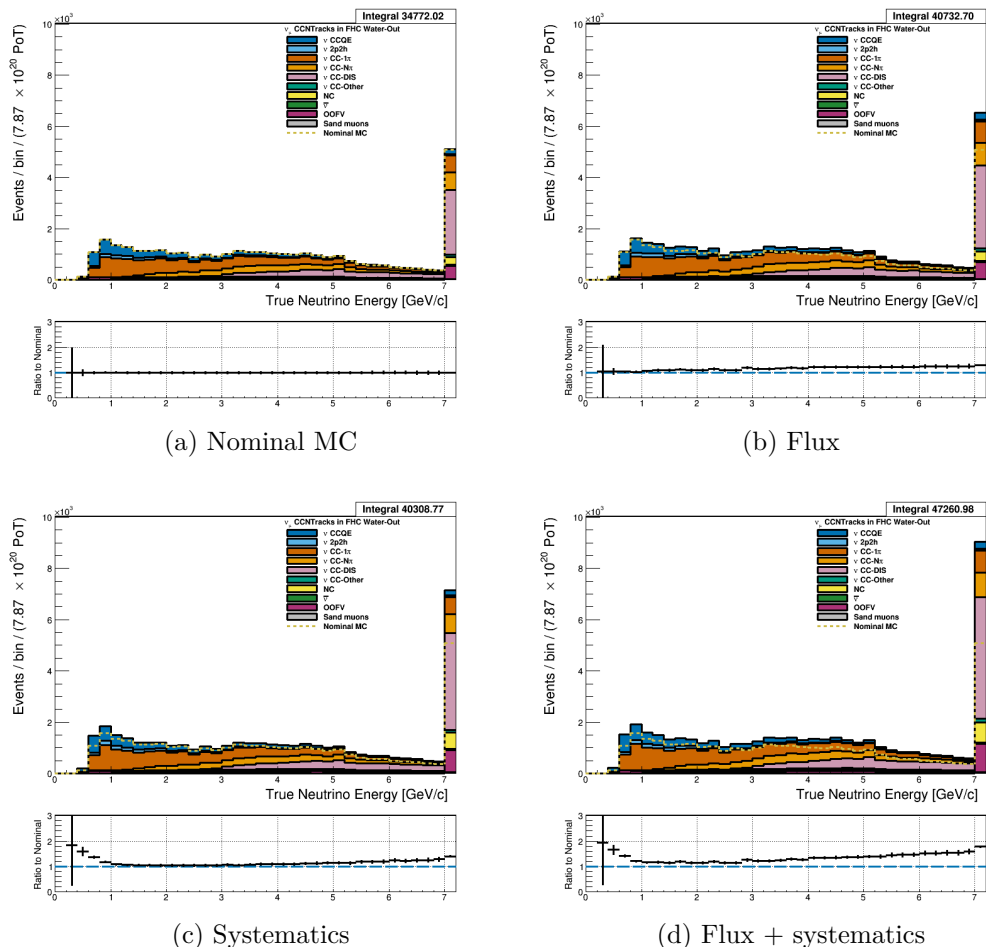


Figure 3.42: True neutrino energy associated with the lepton candidate separated by NEUT model interaction mode for FHC  $\nu_\mu$  CC N-Tracks events occurring in the PØD in water-out mode. (a) The nominal MC prediction without any weights applied. (b) The flux tuning are applied. (c) The systematic weighting are applied. (d) Both flux and systematic weighting are applied.

### 3.4.3.2 $\bar{\nu}_\mu$ Selection in RHC Mode: Text goes here

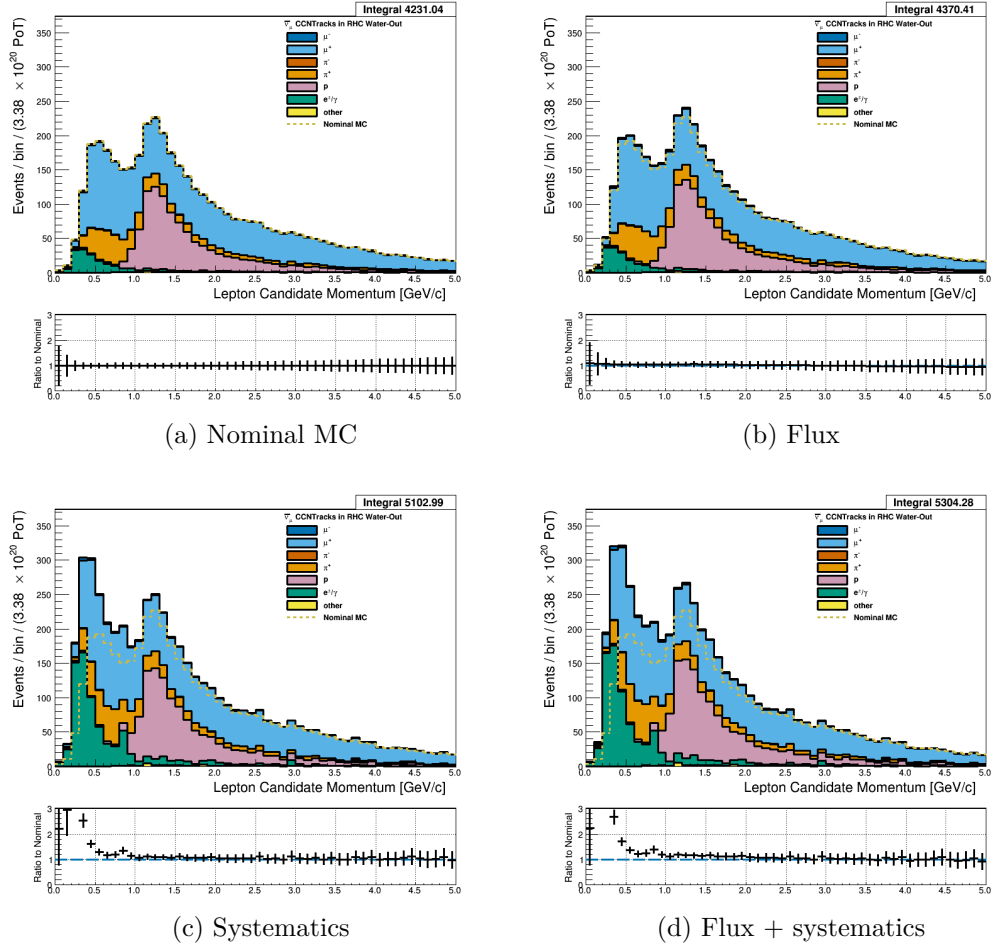


Figure 3.43: Reconstructed lepton candidate momentum separated by true particle species for RHC  $\bar{\nu}_\mu$  CC N-Tracks events occurring in the PØD in water-out mode. Reconstructed lepton candidate angle separated by true particle species for RHC  $\bar{\nu}_\mu$  CC N-Tracks events occurring in the PØD in water-in mode. (a) The nominal MC prediction without any weights applied. (b) The flux tuning are applied. (c) The systematic weighting are applied. (d) Both flux and systematic weighting are applied.

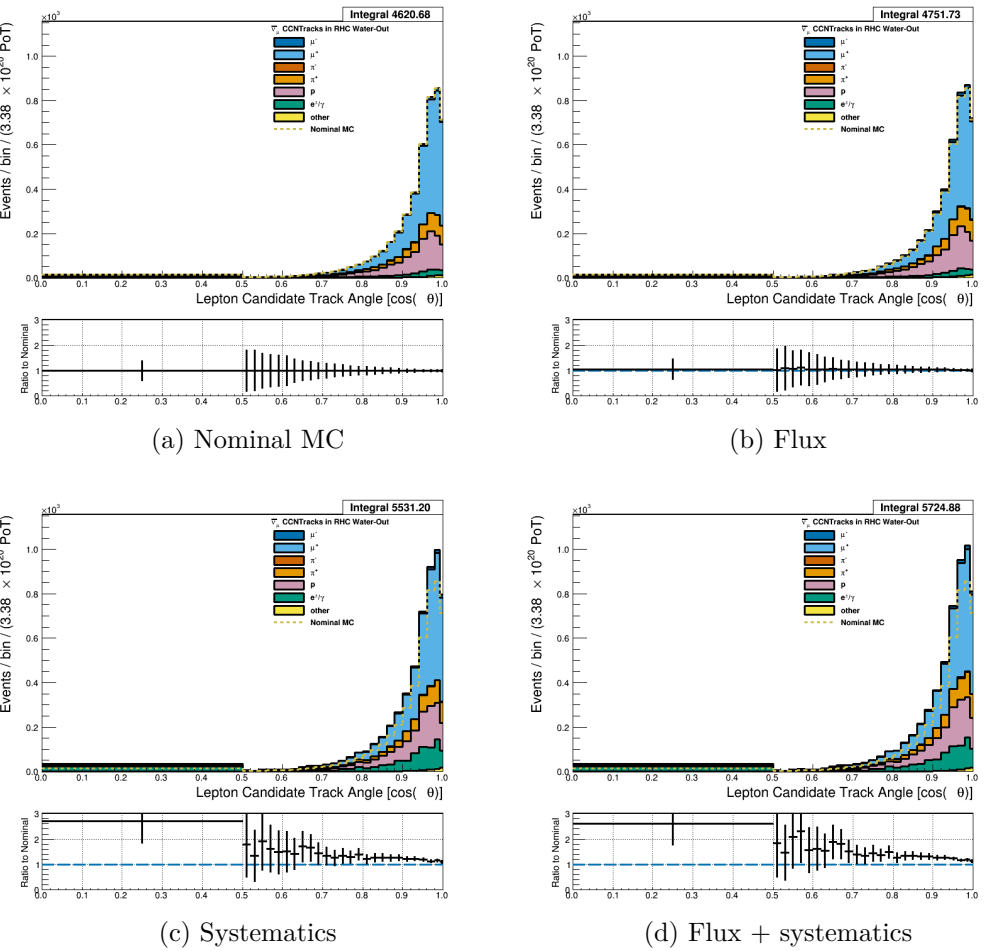


Figure 3.44: Reconstructed lepton candidate angle separated by true particle species for RHC  $\bar{\nu}_\mu$  CC N-Tracks events occurring in the PØD in water-out mode. (a) The nominal MC prediction without any weights applied. (b) The flux tuning are applied. (c) The systematic weighting are applied. (d) Both flux and systematic weighting are applied.

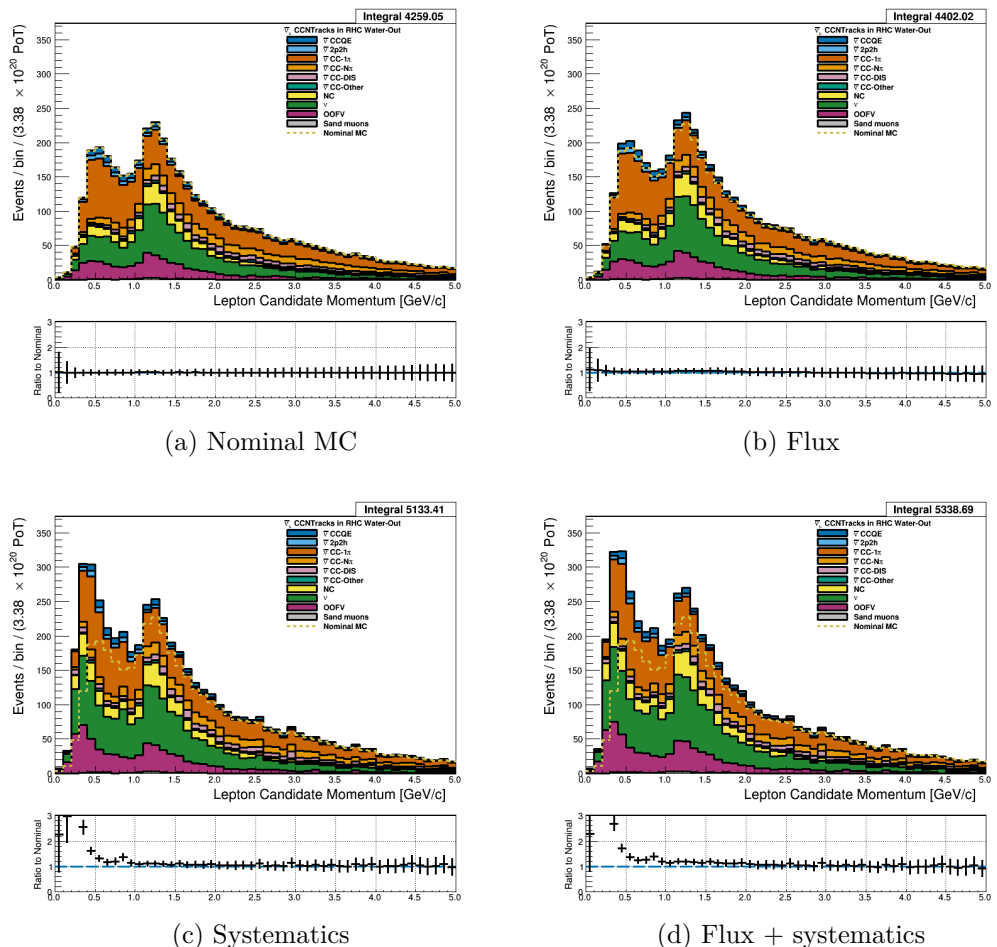


Figure 3.45: Reconstructed lepton candidate momentum separated by NEUT model interaction mode for RHC  $\bar{\nu}_\mu$  CC N-Tracks events occurring in the PØD in water-out mode. (a) The nominal MC prediction without any weights applied. (b) The flux tuning are applied. (c) The systematic weighting are applied. (d) Both flux and systematic weighting are applied.

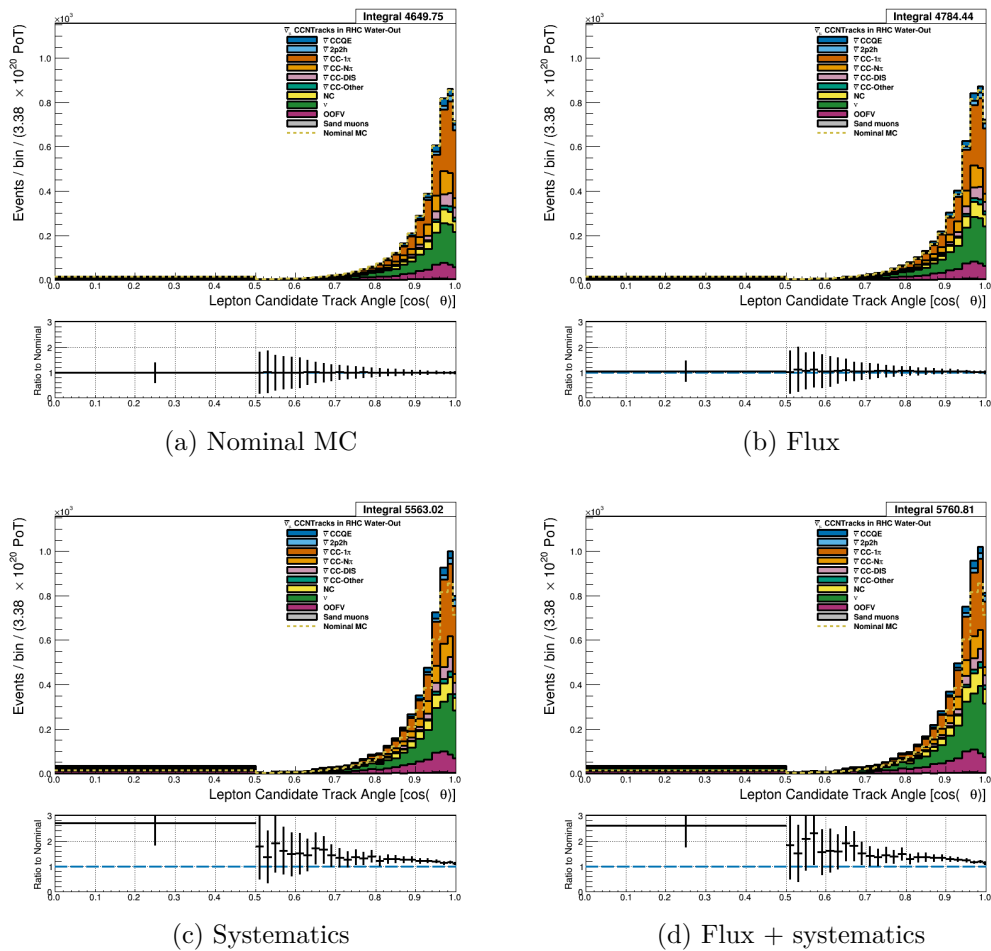


Figure 3.46: Reconstructed lepton candidate  $\cos \theta$  separated by NEUT model interaction mode for RHC  $\bar{\nu}_\mu$  CC N-Tracks events occurring in the PØD in water-out mode. (a) The nominal MC prediction without any weights applied. (b) The flux tuning are applied. (c) The systematic weighting are applied. (d) Both flux and systematic weighting are applied.

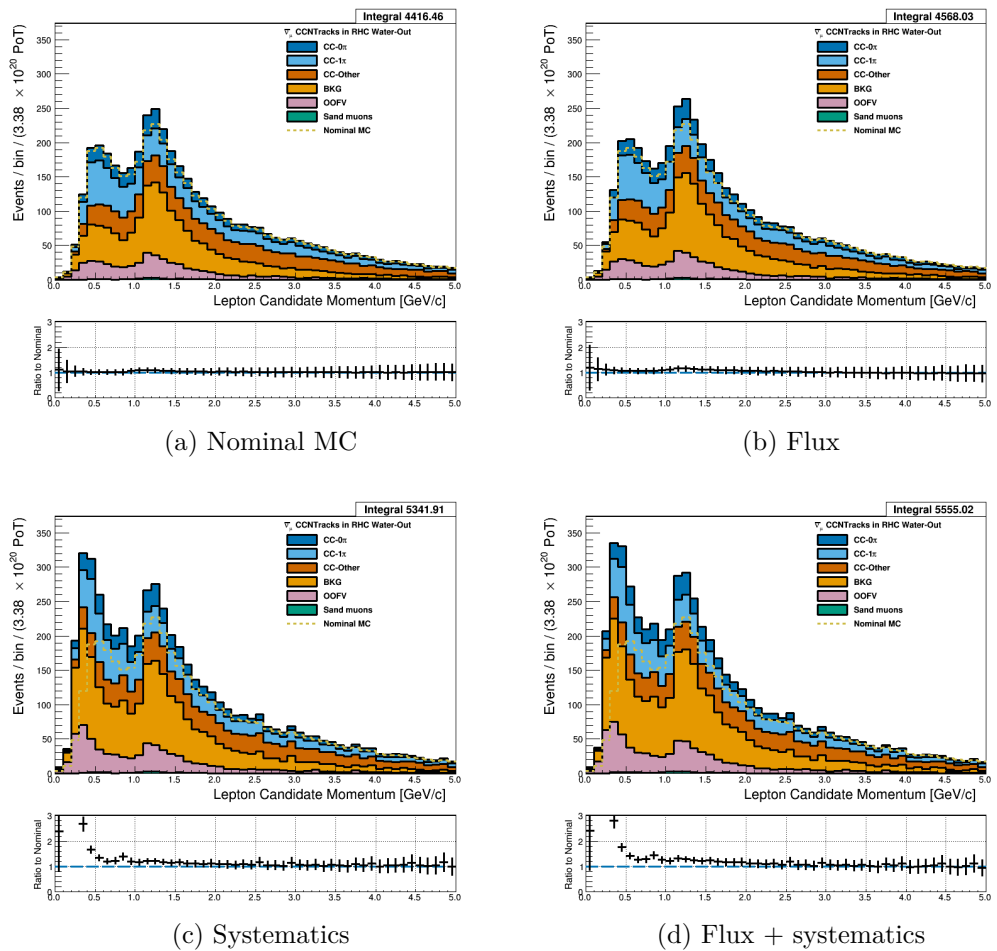


Figure 3.47: Reconstructed lepton candidate momentum separated by topology for RHC  $\bar{\nu}_\mu$  CC N-Tracks events occurring in the PØD in water-out mode. (a) The nominal MC prediction without any weights applied. (b) The flux tuning are applied. (c) The systematic weighting are applied. (d) Both flux and systematic weighting are applied.

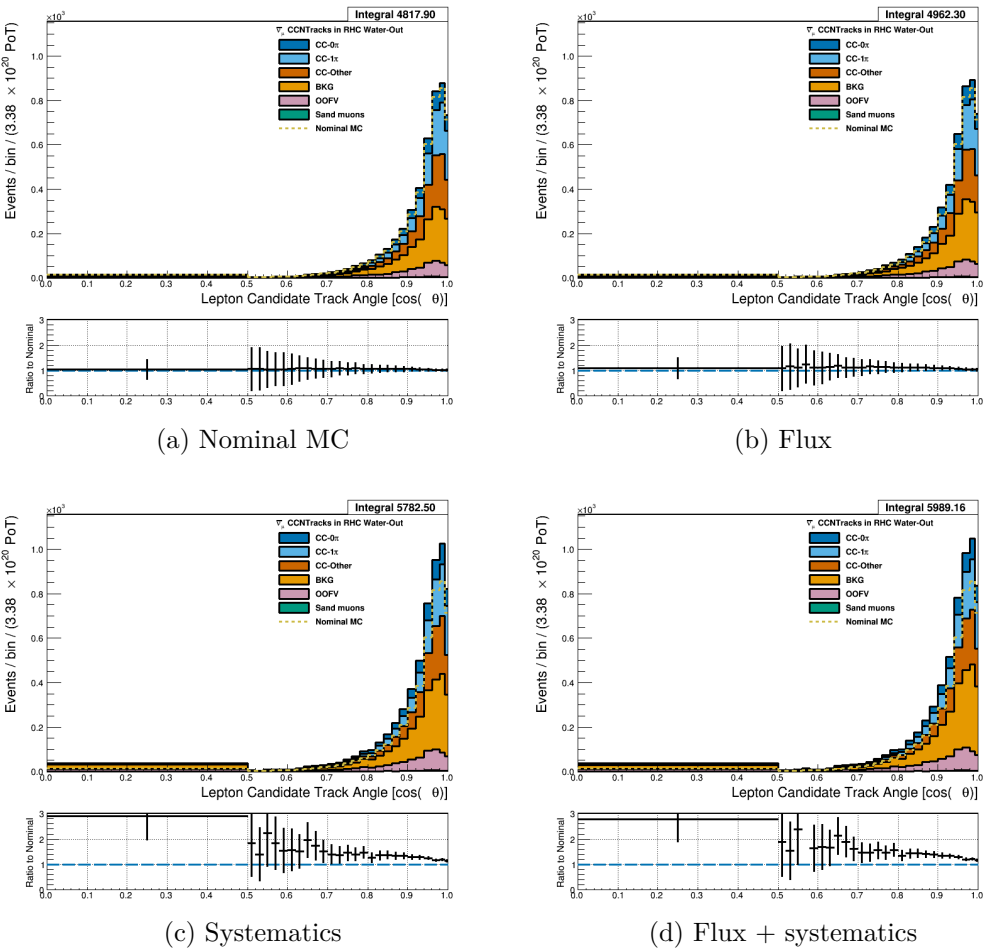


Figure 3.48: Reconstructed lepton candidate  $\cos \theta$  separated by topology for RHC  $\bar{\nu}_\mu$  CC N-Tracks events occurring in the PØD in water-out mode. (a) The nominal MC prediction without any weights applied. (b) The flux tuning are applied. (c) The systematic weighting are applied. (d) Both flux and systematic weighting are applied.

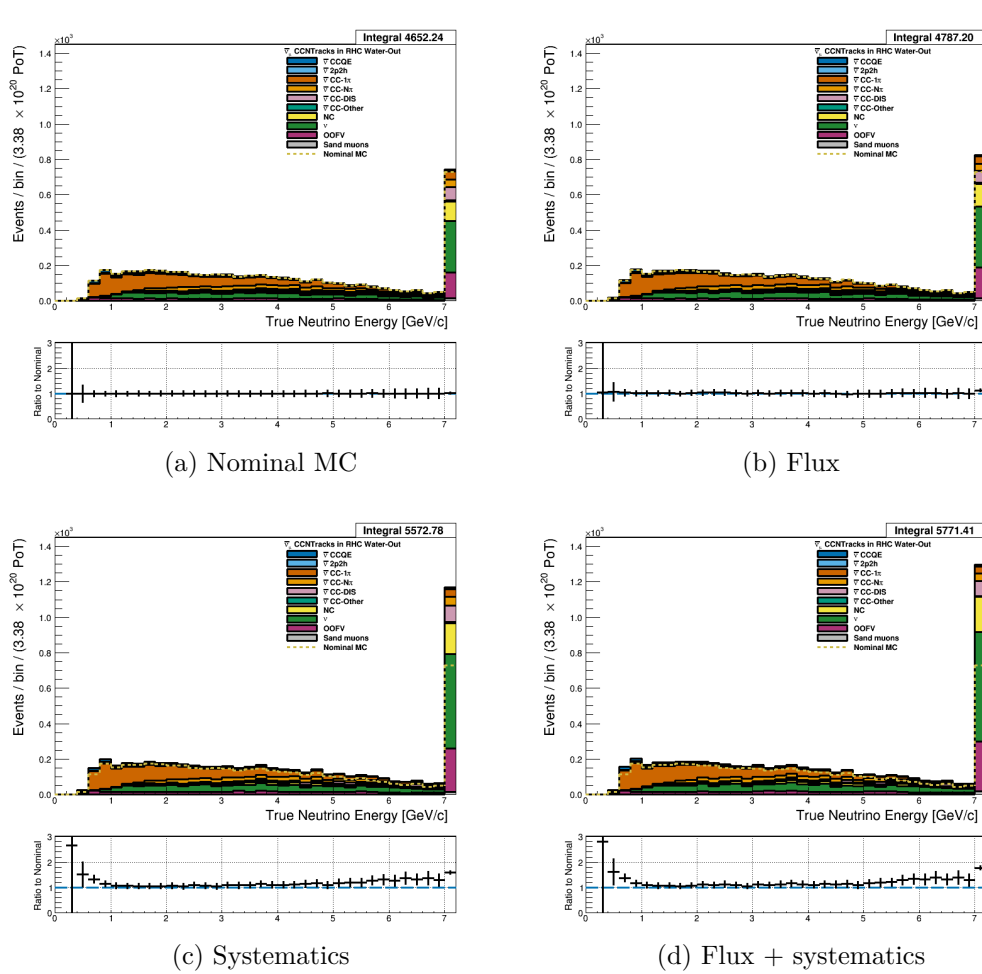


Figure 3.49: True neutrino energy associated with the lepton candidate separated by NEUT model interaction mode for RHC  $\bar{\nu}_\mu$  CC N-Tracks events occurring in the PØD in water-out mode. (a) The nominal MC prediction without any weights applied. (b) The flux tuning are applied. (c) The systematic weighting are applied. (d) Both flux and systematic weighting are applied.

543 **3.4.3.3  $\nu_\mu$  Background Selection in RHC Mode:** Text

544 **3.5 PØD Water-In Samples**

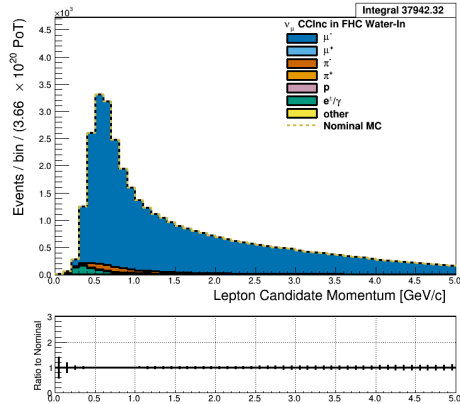
545 This section shows the kinematic distributions for the PØD water-in samples. These samples  
 546 will demonstrate the similarities between it and water-out modes. First an examination of  
 547 the CC Inclusive samples and the effects of the systematic weights will be explored. The

548 samples are then examined as CC 1-track and CC N-tracks.

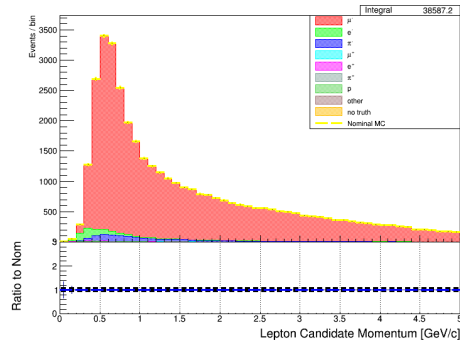
549 **3.5.1 CC Inclusive**

550 The CC Inclusive sample cuts are discussed 3.2.1. Since both flux and detector systematic  
551 weights are applied to all MC events in BANFF, it is important to validate the event weights.  
552 Using neither set of weights is referred to as the nominal MC.

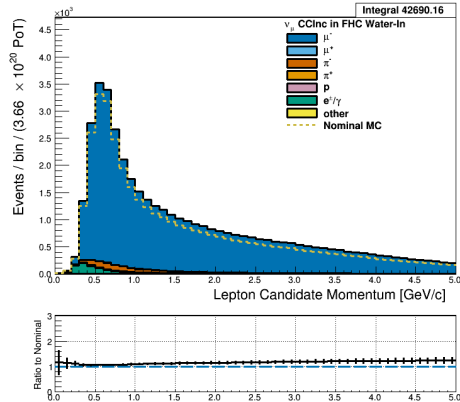
553 **3.5.1.1  $\nu_\mu$  Selection in FHC Mode:** Shown in Figures 3.50 to 3.56 are the momentum  
554 and  $\cos\theta$  distributions for  $\nu_\mu$ CC Inclusive events in FHC mode. There are three pairs of  
555  $P, \theta$  figures with the same truth information break down accompanied by one of neutrino  
556 energy. The truth information categories are lepton candidate particle, NEUT reaction, and  
557 topology. Each figure consists of a set of four sub-figures which illustrate the application of  
558 flux and detector systematic weights.



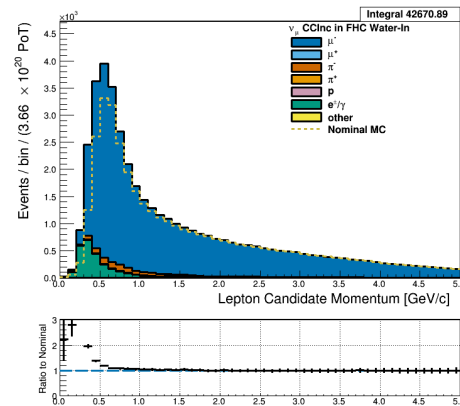
(a) Nominal MC



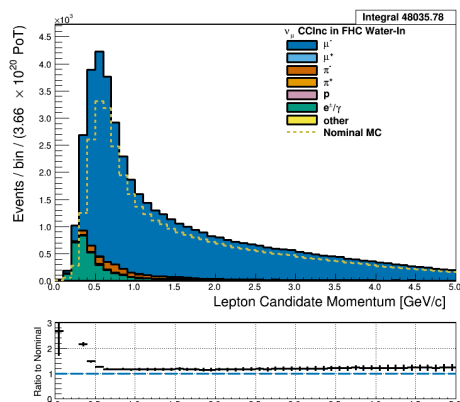
(b) Nominal MC from Highland2



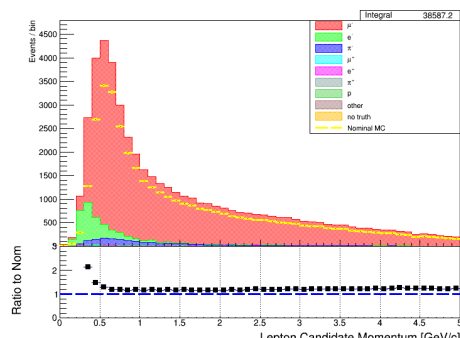
(c) Flux



(d) Systematics



(e) Flux + systematics



(f) Fully weighted in Highland2

Figure 3.50: Reconstructed lepton candidate momentum separated by true particle species for FHC  $\nu_\mu$  CC Inc. events occurring in the PØD in water-in mode. (a) The nominal MC prediction without any weights applied. (b) Highland2 comparison for (a) without any weights applied using the “NOW” draw option. (c) The flux tuning are applied. (d) The systematic weighting are applied. (e) Both flux and systematic weighting are applied. (f) Highland2 comparison for (e).

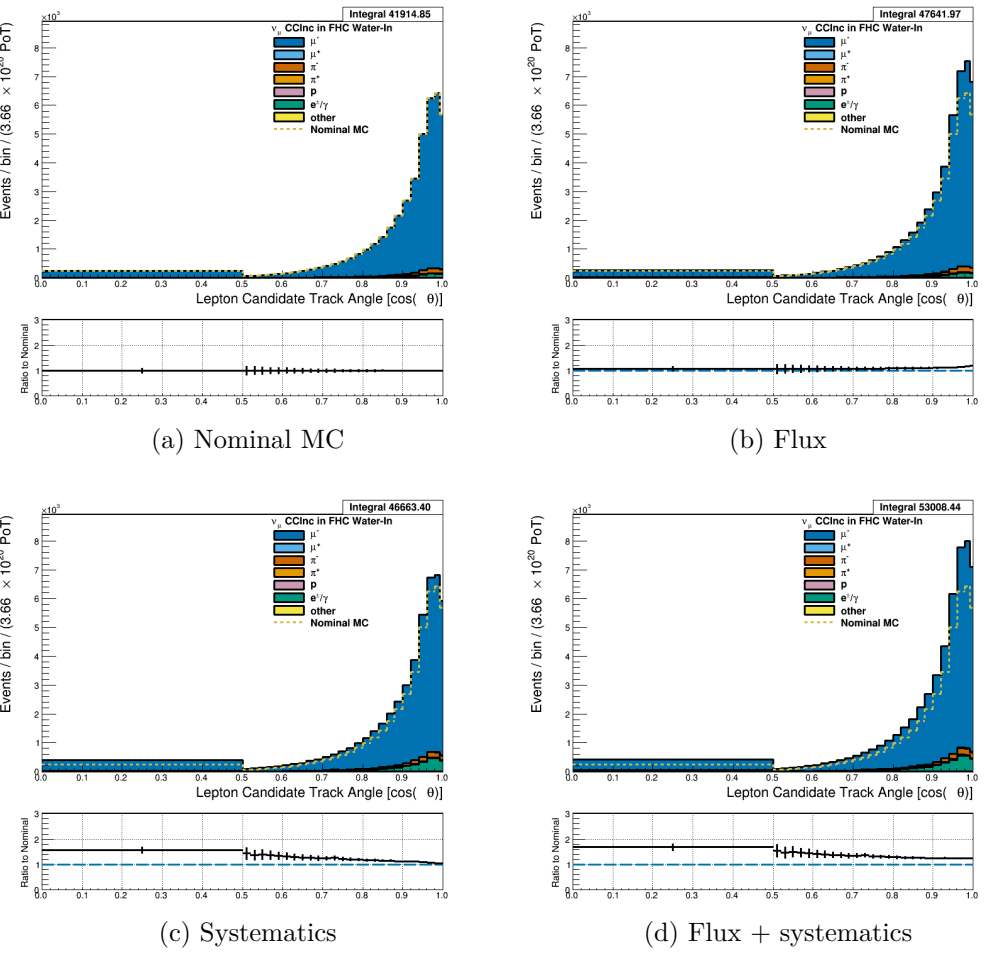


Figure 3.51: Reconstructed lepton candidate angle separated by true particle species for FHC  $\nu_\mu$  CC Inc. events occurring in the PØD in water-in mode. (a) The nominal MC prediction without any weights applied. (b) The flux tuning are applied. (c) The systematic weighting are applied. (d) Both flux and systematic weighting are applied.

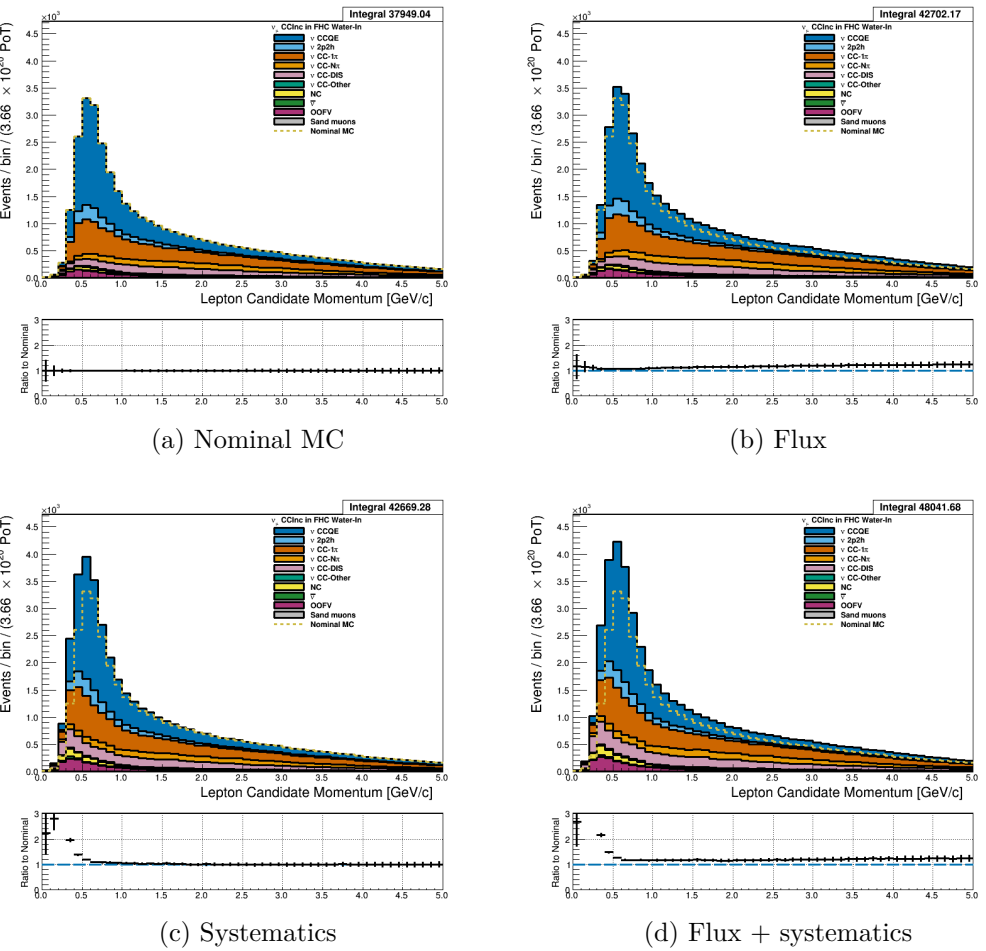


Figure 3.52: Reconstructed lepton candidate momentum separated by NEUT model interaction mode for FHC  $\nu_\mu$  CC Inc. events occurring in the PØD in water-in mode. (a) The nominal MC prediction without any weights applied. (b) The flux tuning are applied. (c) The systematic weighting are applied. (d) Both flux and systematic weighting are applied.

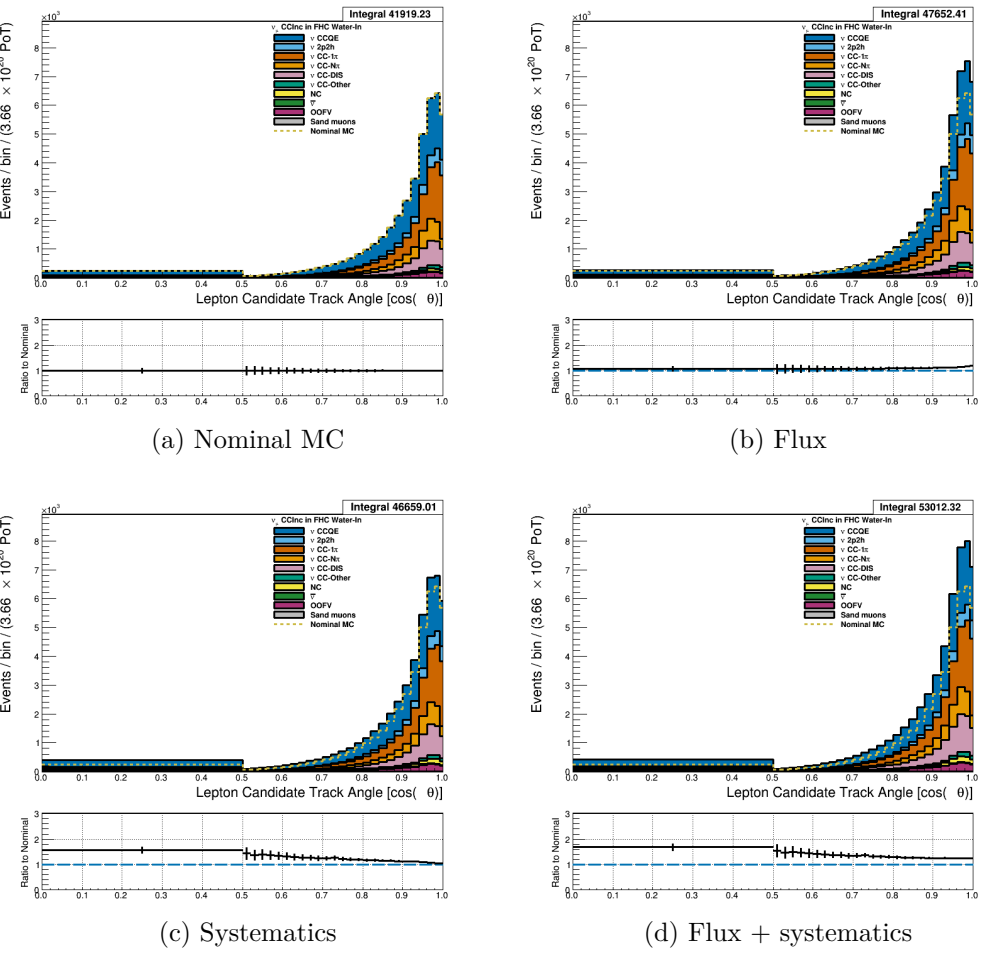


Figure 3.53: Reconstructed lepton candidate  $\cos \theta$  separated by NEUT model interaction mode for FHC  $\nu_\mu$  CC Inc. events occurring in the PØD in water-in mode. (a) The nominal MC prediction without any weights applied. (b) The flux tuning are applied. (c) The systematic weighting are applied. (d) Both flux and systematic weighting are applied.

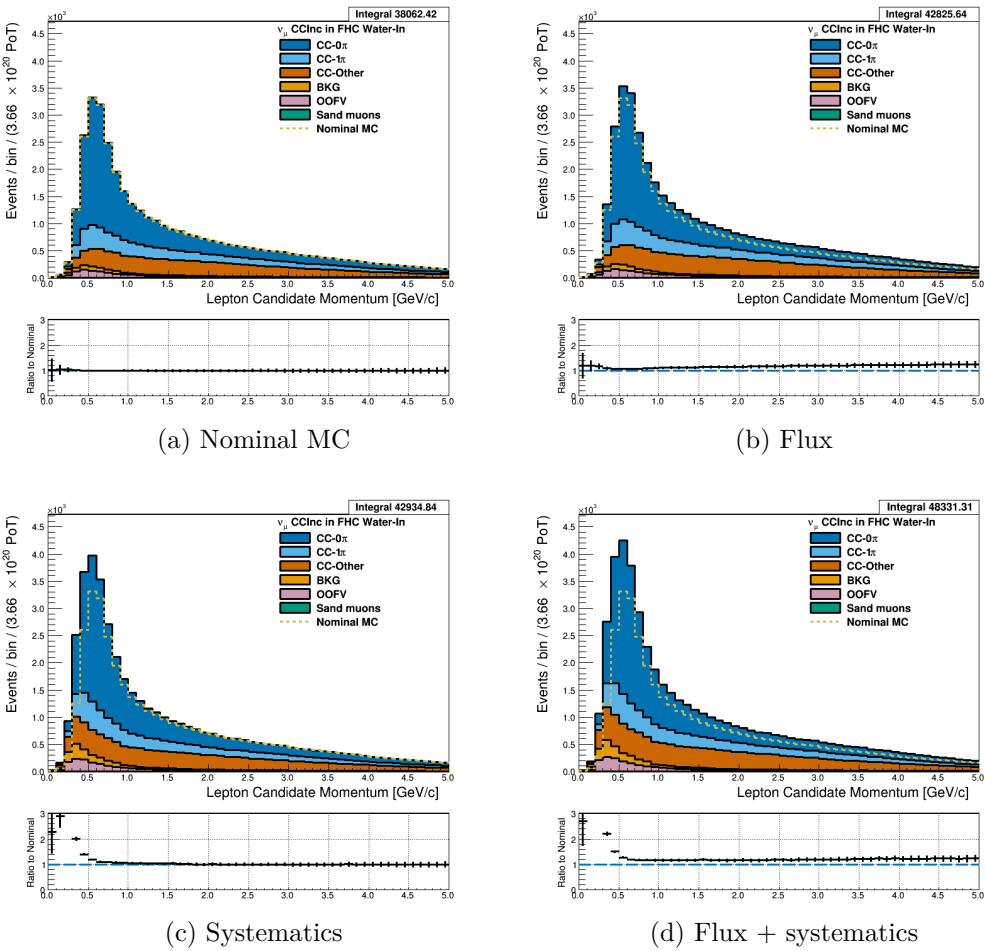


Figure 3.54: Reconstructed lepton candidate momentum separated by topology for FHC  $\nu_\mu$  CC Inc. events occurring in the PØD in water-in mode. (a) The nominal MC prediction without any weights applied. (b) The flux tuning are applied. (c) The systematic weighting are applied. (d) Both flux and systematic weighting are applied.

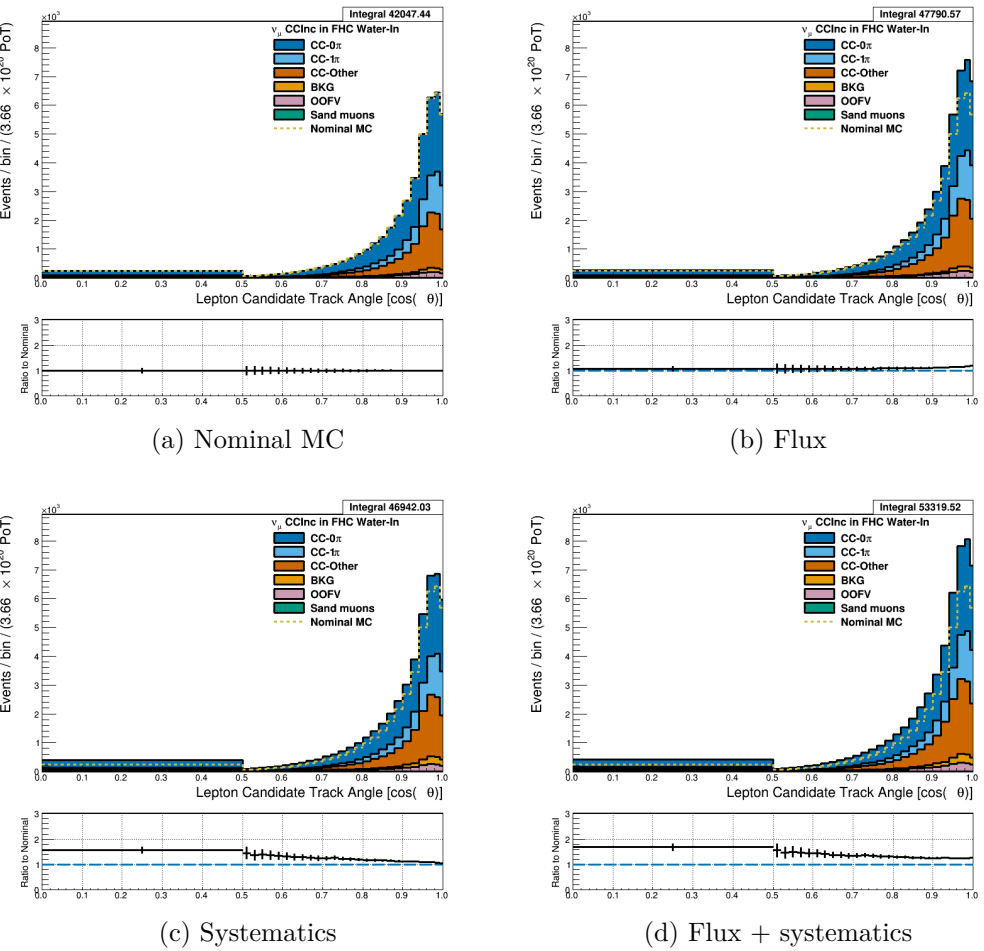


Figure 3.55: Reconstructed lepton candidate  $\cos \theta$  separated by topology for FHC  $\nu_\mu$  CC Inc. events occurring in the PØD in water-in mode. (a) The nominal MC prediction without any weights applied. (b) The flux tuning are applied. (c) The systematic weighting are applied. (d) Both flux and systematic weighting are applied.

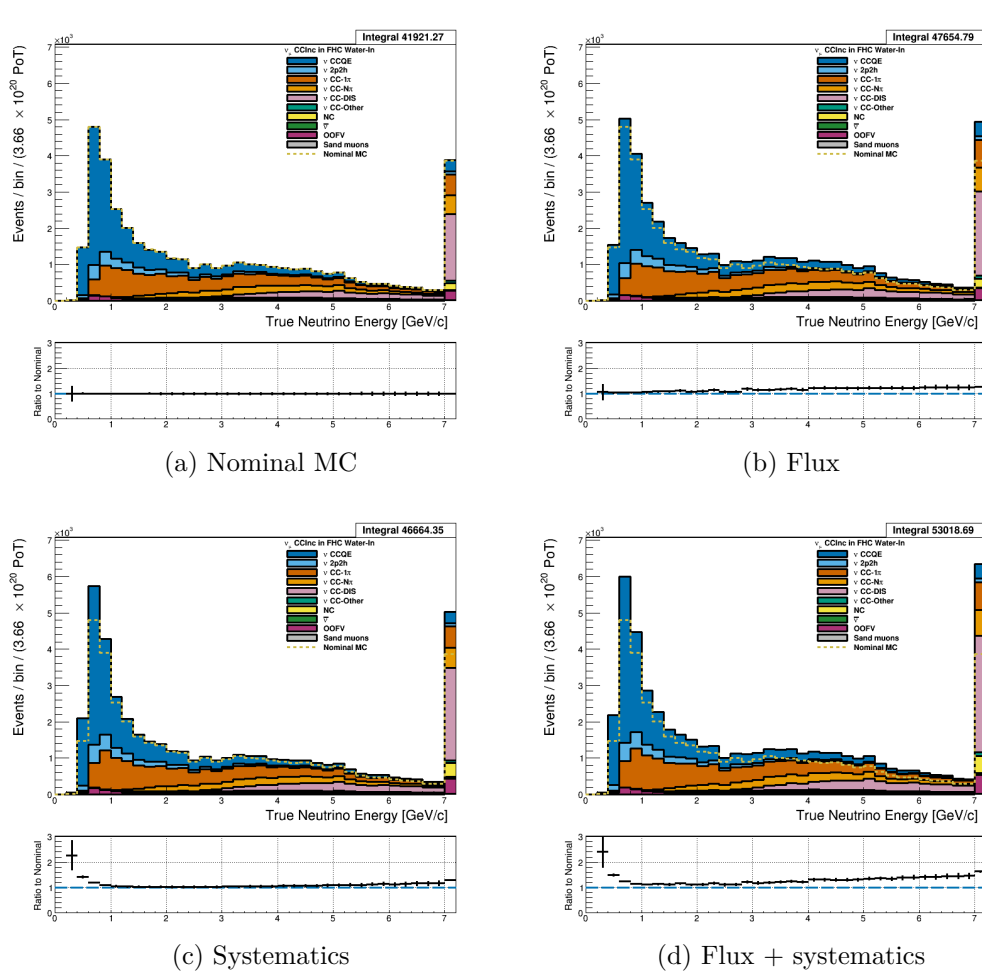


Figure 3.56: True neutrino energy associated with the lepton candidate separated by NEUT model interaction mode for FHC  $\nu_\mu$  CC Inc. events occurring in the PØD in water-out mode. (a) The nominal MC prediction without any weights applied. (b) The flux tuning are applied. (c) The systematic weighting are applied. (d) Both flux and systematic weighting are applied.

559 **3.5.1.2  $\bar{\nu}_\mu$  Selection in RHC Mode:** Shown in Figures 3.57 to 3.63 for  $\bar{\nu}_\mu$  CC Inclusive  
 560 events in RHC mode. There are three pairs of  $P, \theta$  figures with the same truth information  
 561 break down accompanied by one of neutrino energy. The truth information categories are  
 562 lepton candidate particle, NEUT reaction, and topology. Each figure consists of a set of four  
 563 sub-figures which illustrate the application of flux and detector systematic weights.

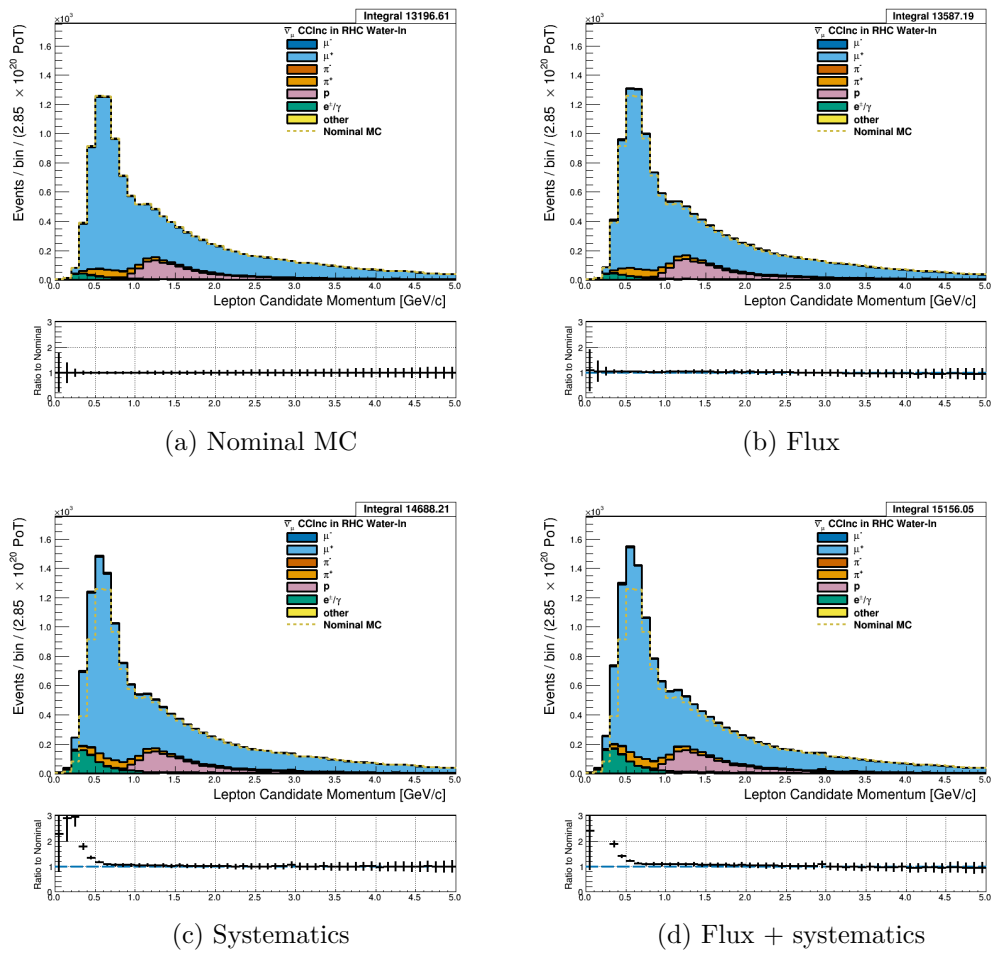


Figure 3.57: Reconstructed lepton candidate momentum separated by true particle species for RHC  $\bar{\nu}_\mu$  CC Inc. events occurring in the PØD in water-out mode. (a) The nominal MC prediction without any weights applied. (b) The flux tuning are applied. (c) The systematic weighting are applied. (d) Both flux and systematic weighting are applied.

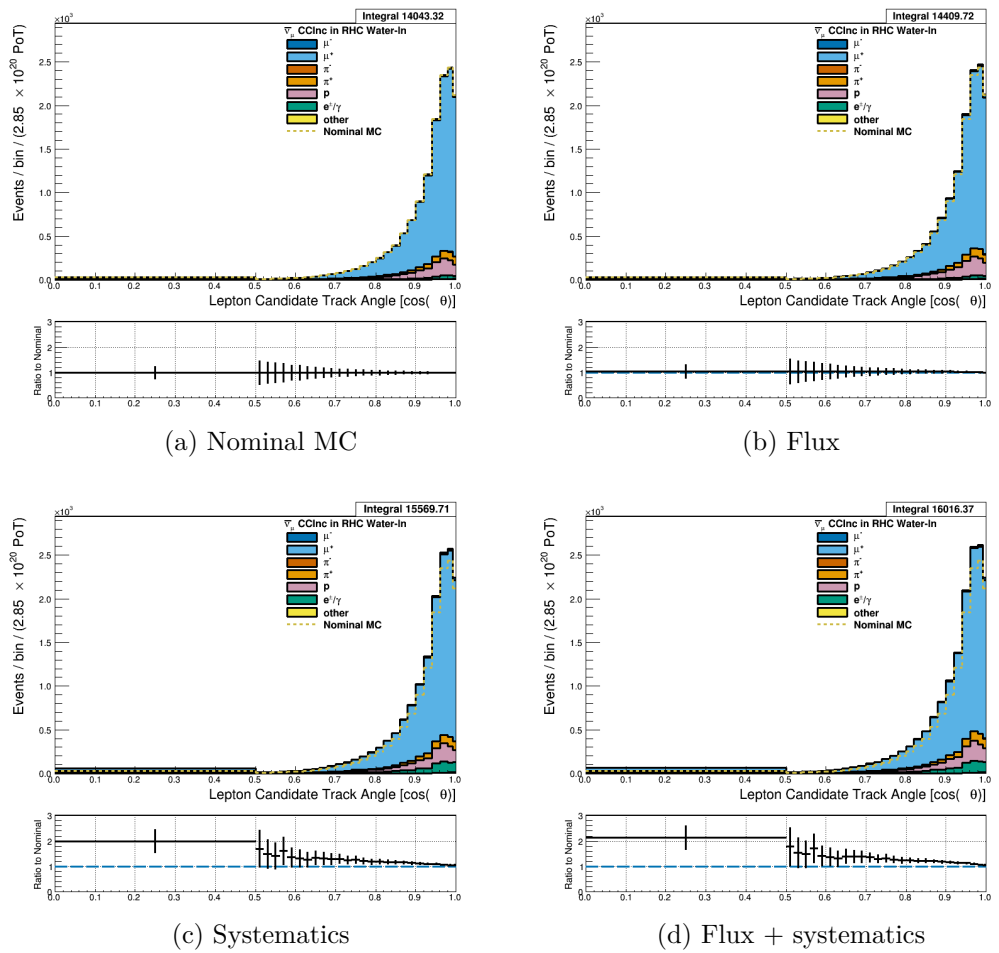


Figure 3.58: Reconstructed lepton candidate angle separated by true particle species for RHC  $\bar{\nu}_\mu$  CC Inc. events occurring in the PØD in water-in mode. (a) The nominal MC prediction without any weights applied. (b) The flux tuning are applied. (c) The systematic weighting are applied. (d) Both flux and systematic weighting are applied.

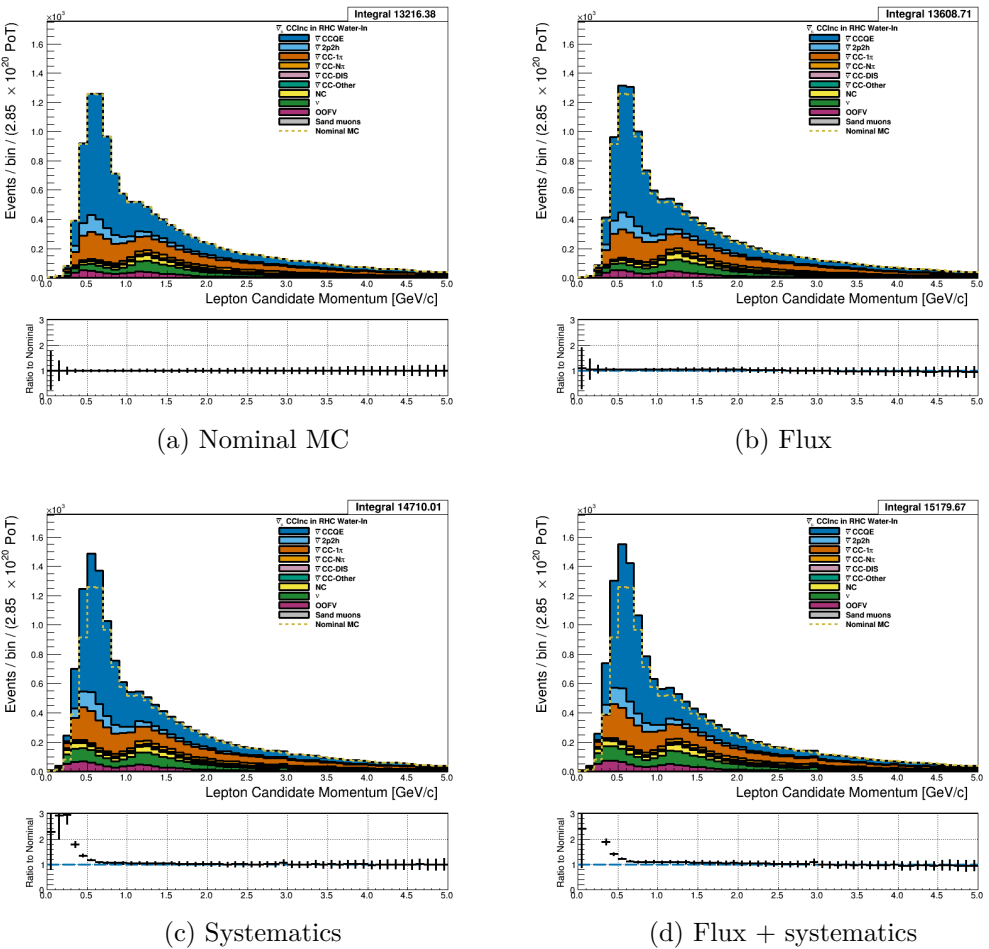


Figure 3.59: Reconstructed lepton candidate momentum separated by NEUT model interaction mode for RHC  $\bar{\nu}_\mu$  CC Inc. events occurring in the PØD in water-out mode. (a) The nominal MC prediction without any weights applied. (b) The flux tuning are applied. (c) The systematic weighting are applied. (d) Both flux and systematic weighting are applied.

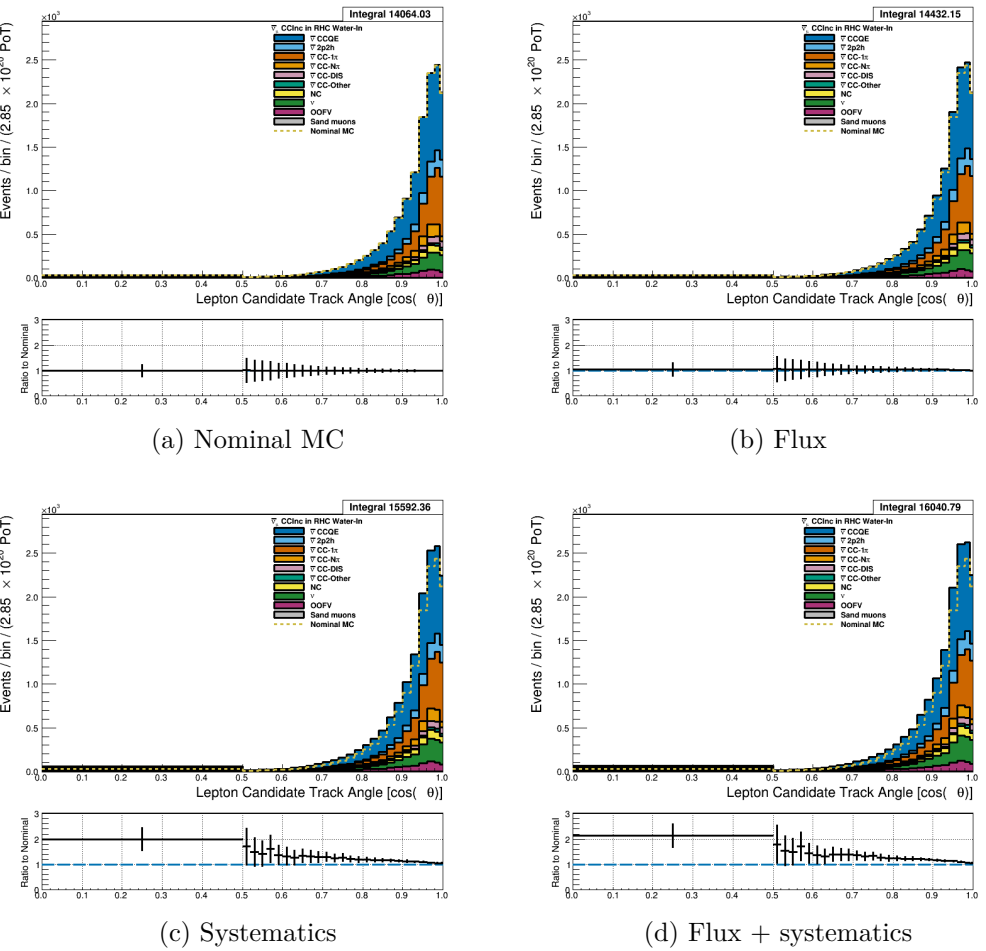


Figure 3.60: Reconstructed lepton candidate  $\cos \theta$  separated by NEUT model interaction mode for RHC  $\bar{\nu}_\mu$  CC Inc. events occurring in the PØD in water-out mode. (a) The nominal MC prediction without any weights applied. (b) The flux tuning are applied. (c) The systematic weighting are applied. (d) Both flux and systematic weighting are applied.

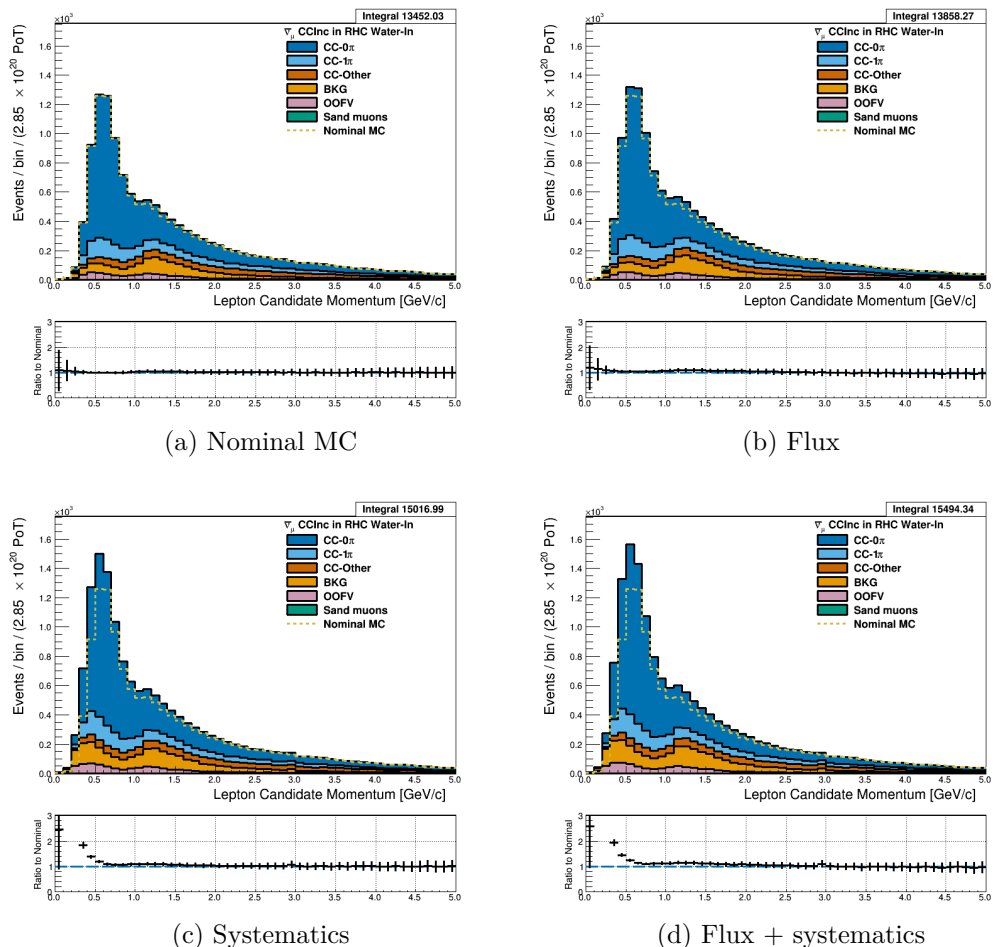


Figure 3.61: Reconstructed lepton candidate momentum separated by topology for RHC  $\bar{\nu}_\mu$  CC Inc. events occurring in the PØD in water-out mode. (a) The nominal MC prediction without any weights applied. (b) The flux tuning are applied. (c) The systematic weighting are applied. (d) Both flux and systematic weighting are applied.

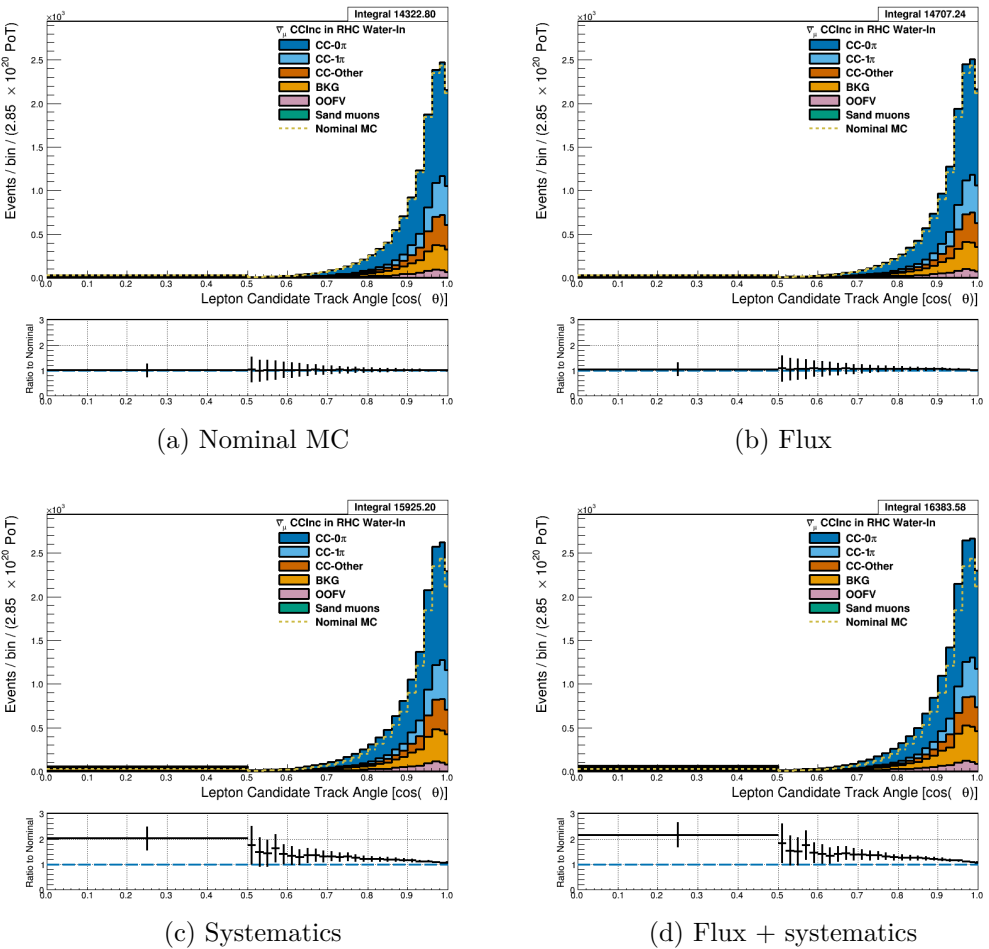


Figure 3.62: Reconstructed lepton candidate  $\cos \theta$  separated by topology for RHC  $\bar{\nu}_\mu$  CC Inc. events occurring in the PØD in water-out mode. (a) The nominal MC prediction without any weights applied. (b) The flux tuning are applied. (c) The systematic weighting are applied. (d) Both flux and systematic weighting are applied.

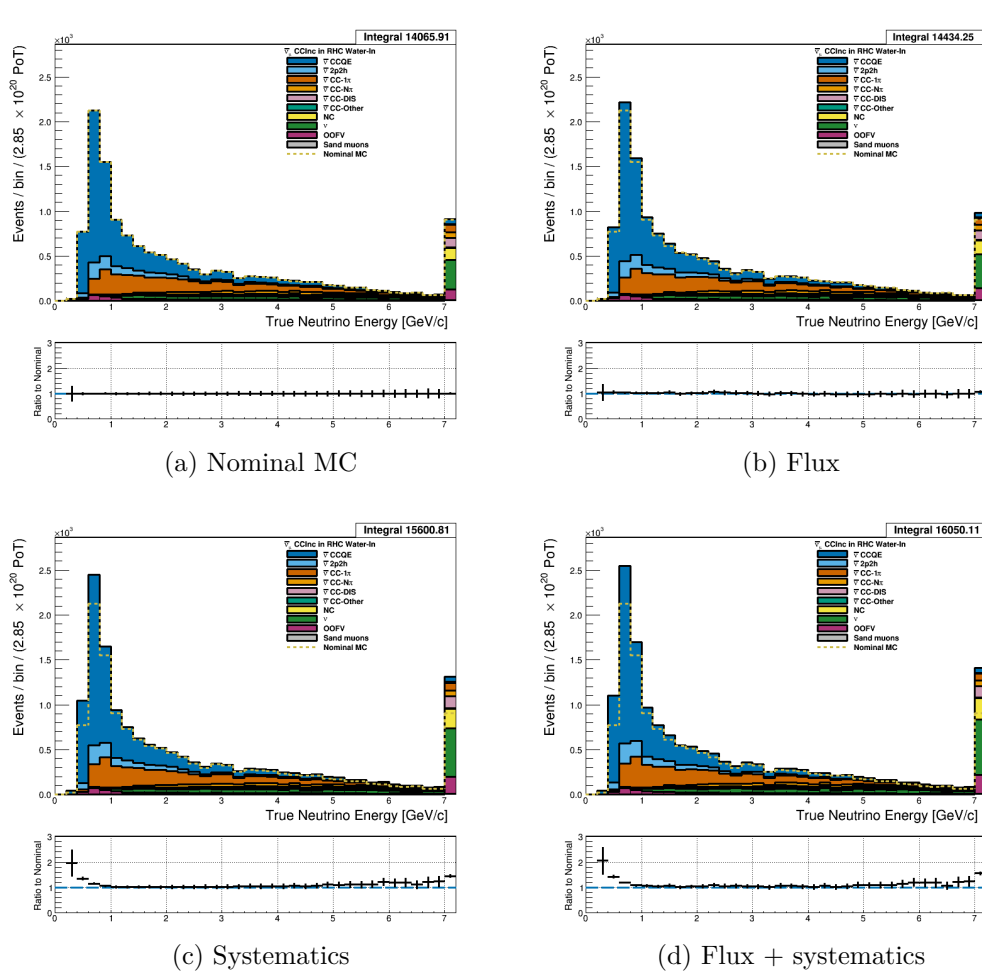


Figure 3.63: True neutrino energy associated with the lepton candidate separated by NEUT model interaction mode for RHC  $\bar{\nu}_\mu$  CC Inc. events occurring in the PØD in water-out mode. (a) The nominal MC prediction without any weights applied. (b) The flux tuning are applied. (c) The systematic weighting are applied. (d) Both flux and systematic weighting are applied.

564 **3.5.1.3  $\nu_\mu$  Background Selection in RHC Mode:** Add figures here

565 **3.5.2 CC 1-Track (CCQE Enhanced)**

566 Text

567 **3.5.2.1  $\nu_\mu$  Selection in FHC Mode:** Text

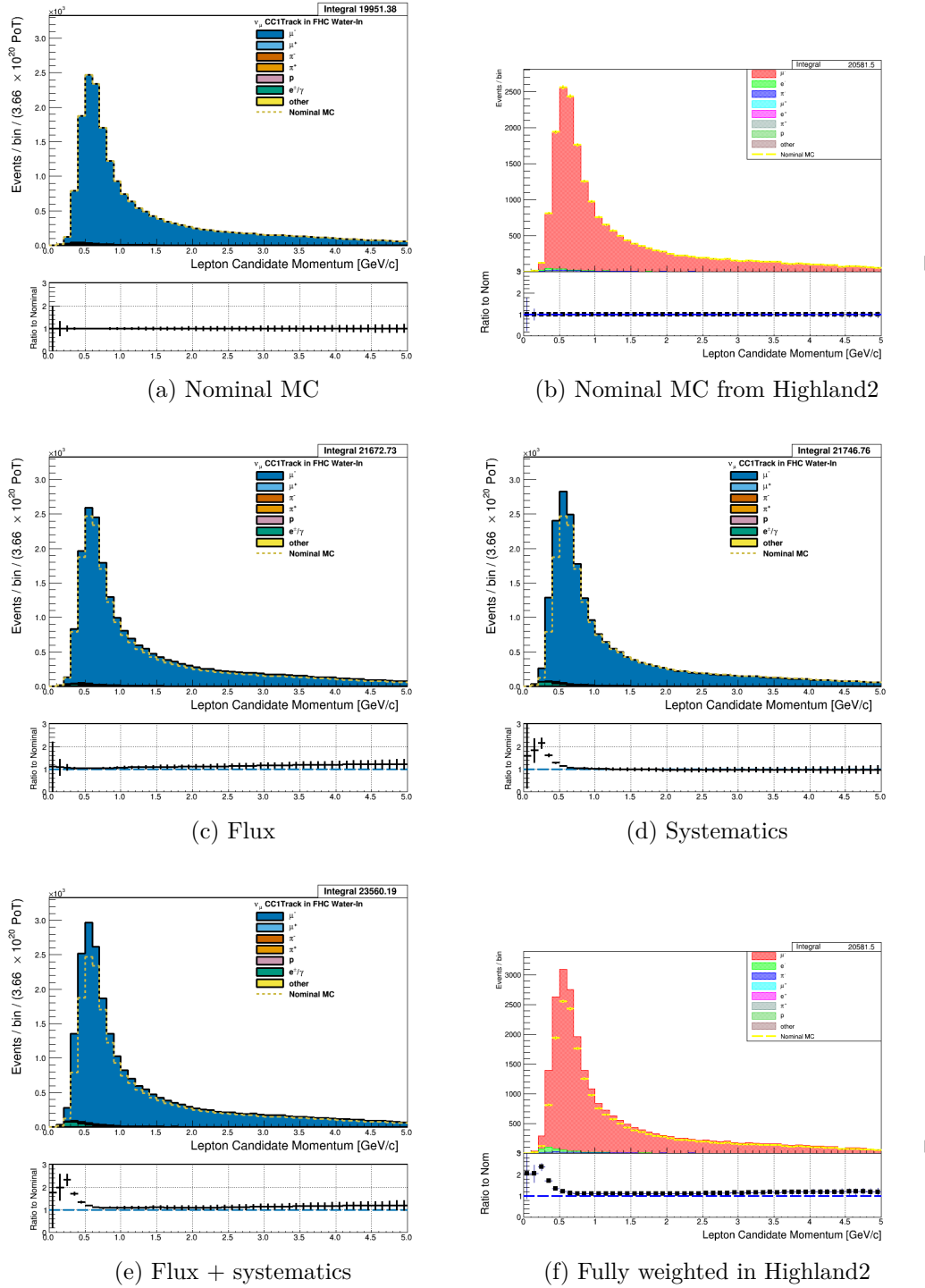


Figure 3.64: Reconstructed lepton candidate momentum separated by true particle species for FHC  $\nu_\mu$  CC 1-Track events occurring in the PØD in water-in mode. (a) The nominal MC prediction without any weights applied. (b) Highland2 comparison for (a) without any weights applied using the “NOW” draw option. (c) The flux tuning are applied. (d) The systematic weighting are applied. (e) Both flux and systematic weighting are applied. (f) Highland2 comparison for (e).

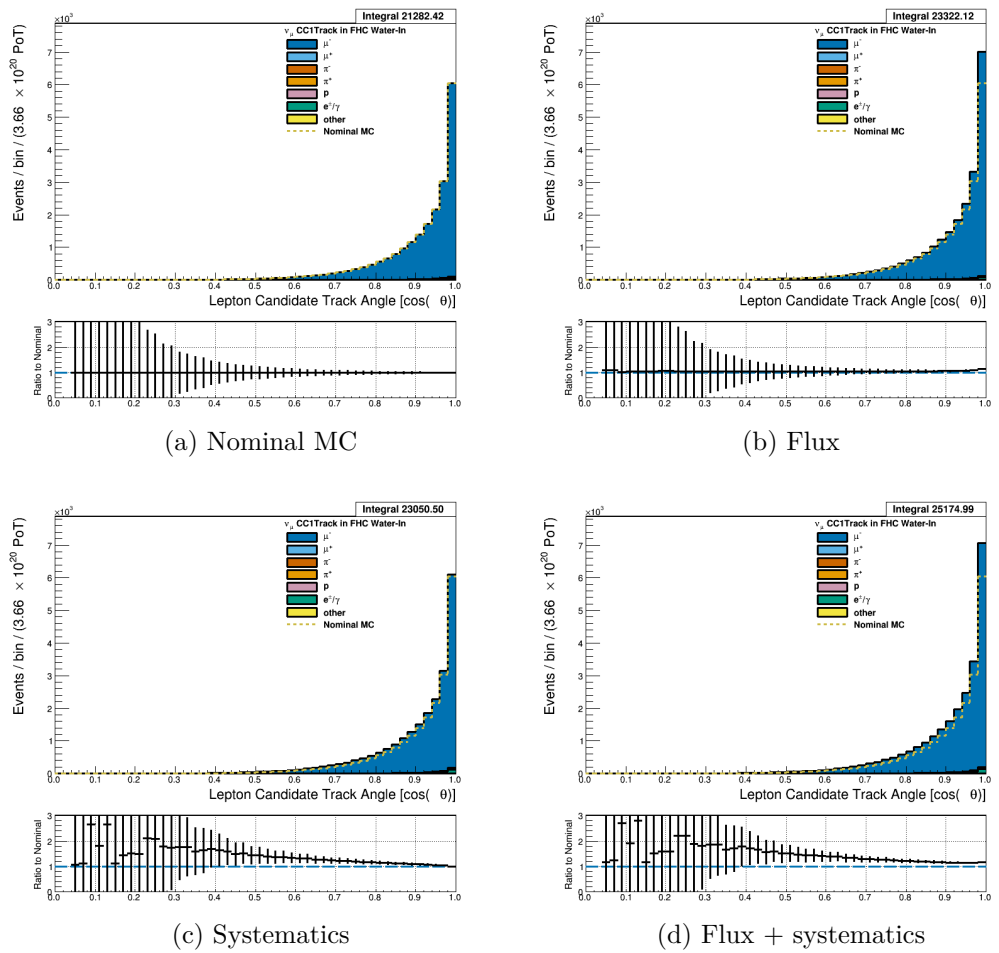


Figure 3.65: Reconstructed lepton candidate angle separated by true particle species for FHC  $\nu_\mu$  CC 1-Track events occurring in the PØD in water-in mode. (a) The nominal MC prediction without any weights applied. (b) The flux tuning are applied. (c) The systematic weighting are applied. (d) Both flux and systematic weighting are applied.

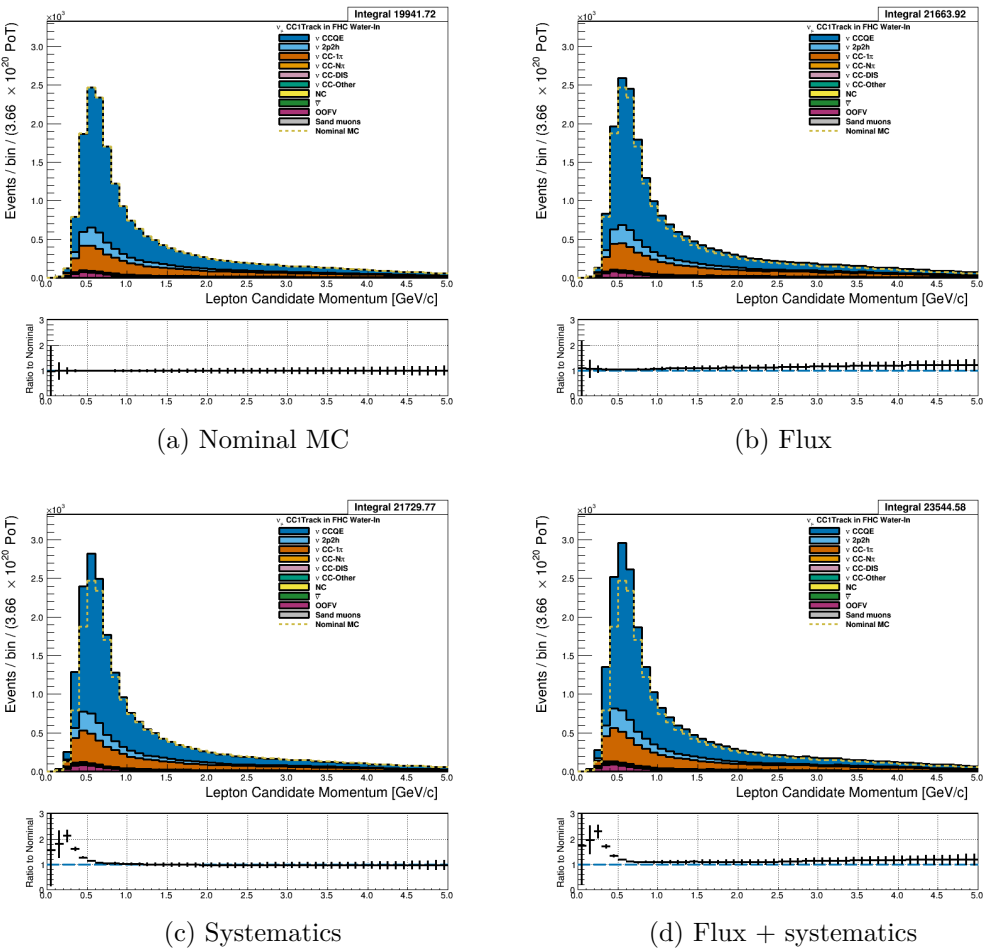


Figure 3.66: Reconstructed lepton candidate momentum separated by NEUT model interaction mode for FHC  $\nu_\mu$  CC 1-Track events occurring in the PØD in water-in mode. (a) The nominal MC prediction without any weights applied. (b) The flux tuning are applied. (c) The systematic weighting are applied. (d) Both flux and systematic weighting are applied.

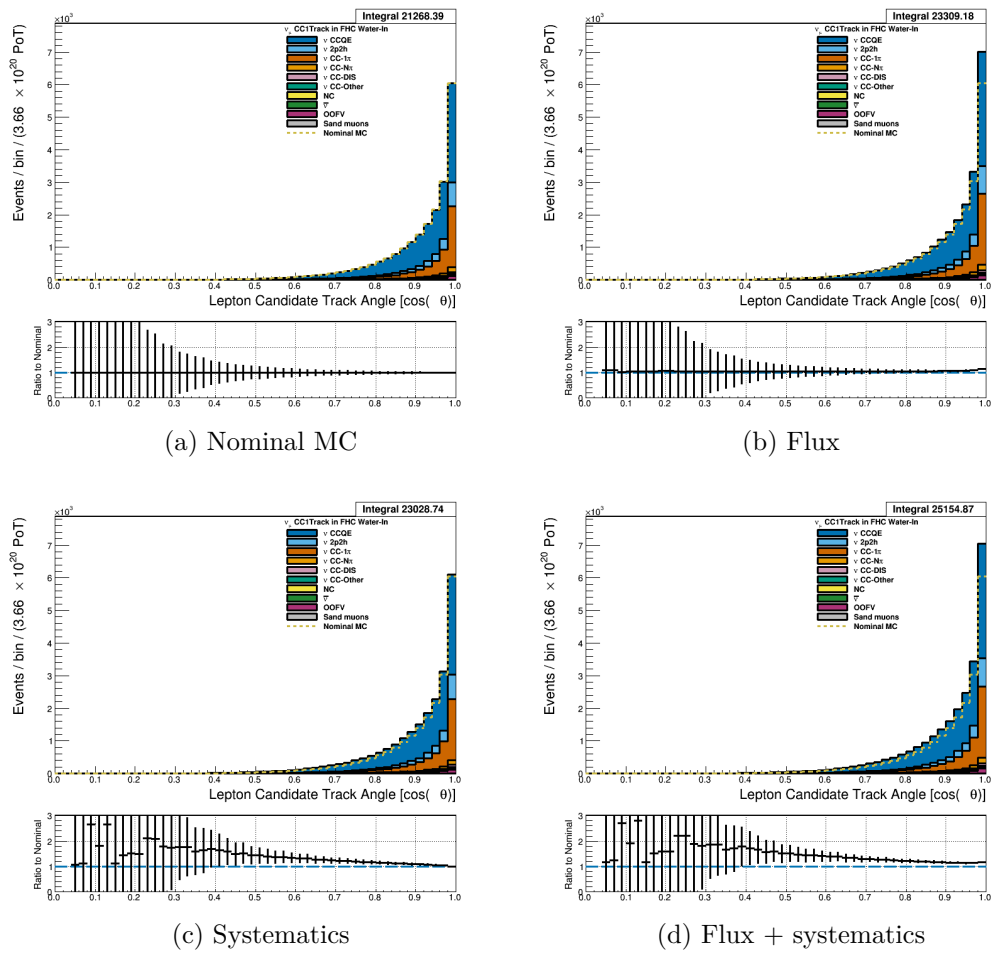


Figure 3.67: Reconstructed lepton candidate  $\cos \theta$  separated by NEUT model interaction mode for FHC  $\nu_\mu$  CC 1-Track events occurring in the PØD in water-in mode. (a) The nominal MC prediction without any weights applied. (b) The flux tuning are applied. (c) The systematic weighting are applied. (d) Both flux and systematic weighting are applied.

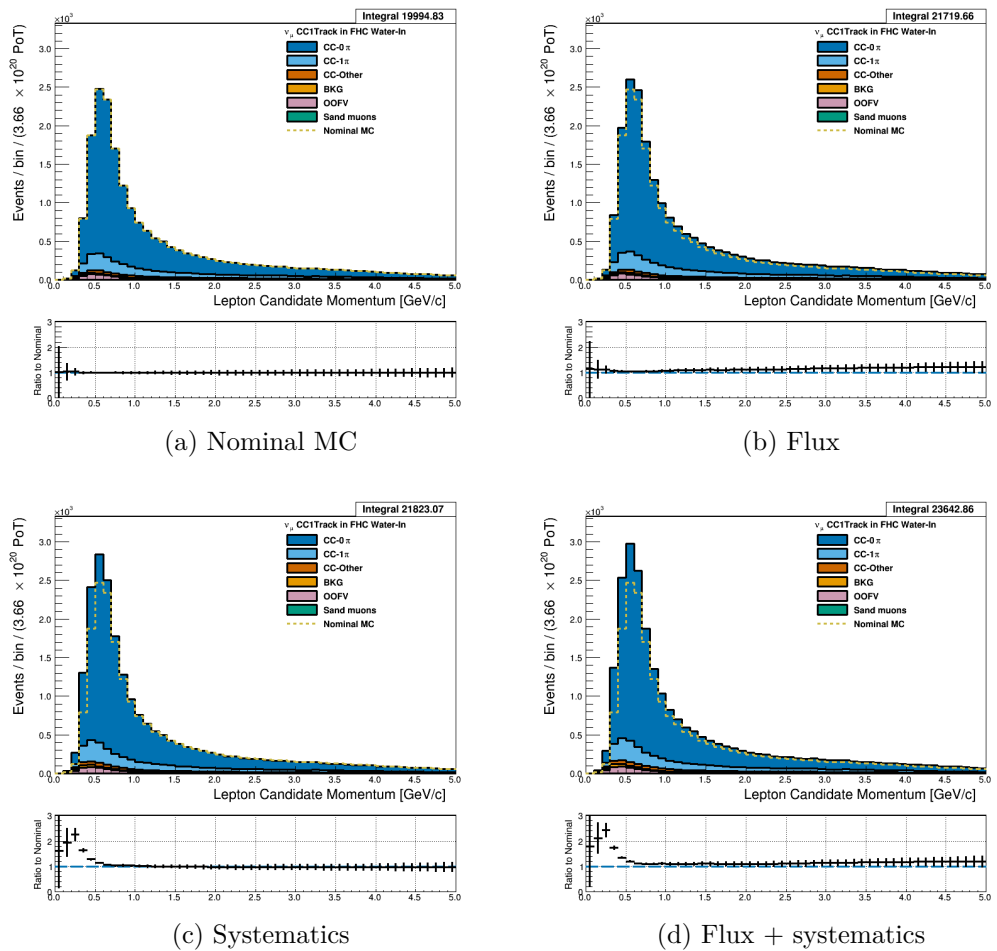


Figure 3.68: Reconstructed lepton candidate momentum separated by topology for FHC  $\nu_\mu$  CC 1-Track events occurring in the PØD in water-in mode. (a) The nominal MC prediction without any weights applied. (b) The flux tuning are applied. (c) The systematic weighting are applied. (d) Both flux and systematic weighting are applied.

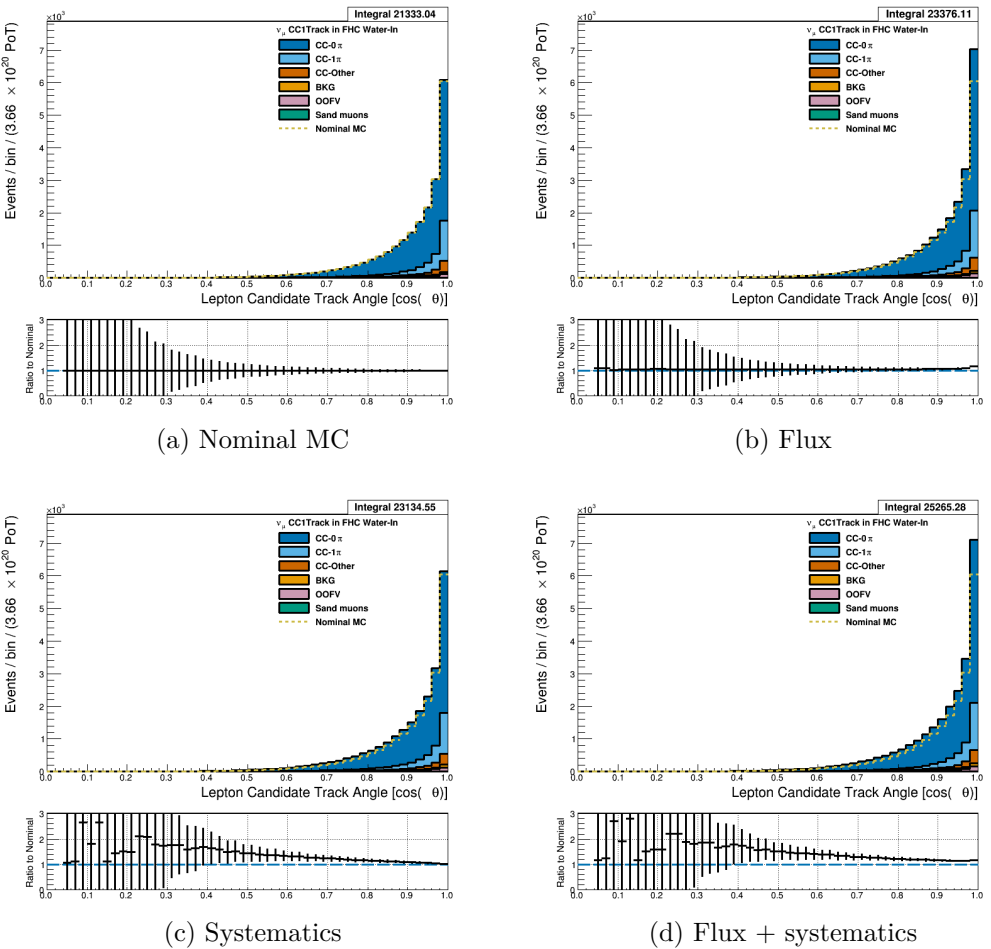


Figure 3.69: Reconstructed lepton candidate  $\cos \theta$  separated by topology for FHC  $\nu_\mu$  CC 1-Track events occurring in the PØD in water-in mode. (a) The nominal MC prediction without any weights applied. (b) The flux tuning are applied. (c) The systematic weighting are applied. (d) Both flux and systematic weighting are applied.

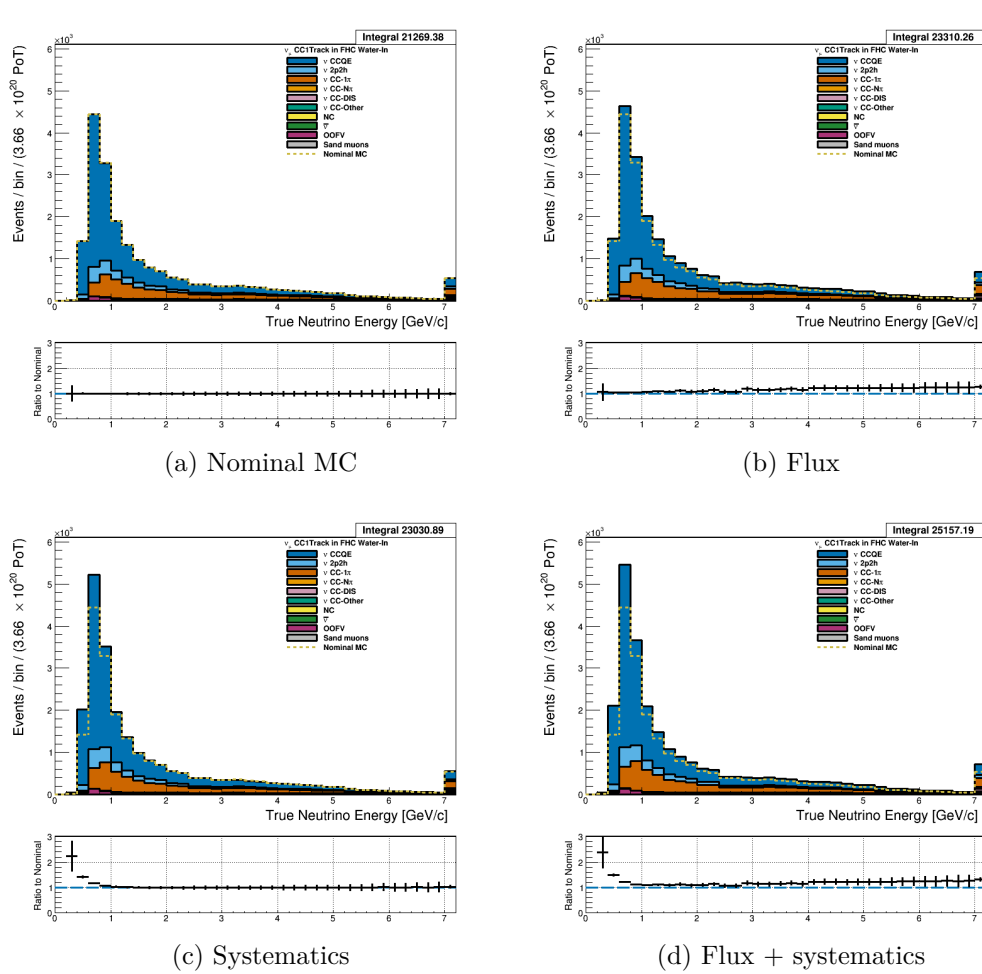


Figure 3.70: True neutrino energy associated with the lepton candidate separated by NEUT model interaction mode for FHC  $\nu_\mu$  CC 1-Track events occurring in the PØD in water-out mode. (a) The nominal MC prediction without any weights applied. (b) The flux tuning are applied. (c) The systematic weighting are applied. (d) Both flux and systematic weighting are applied.

### 3.5.2.2 $\bar{\nu}_\mu$ Selection in RHC Mode: Text

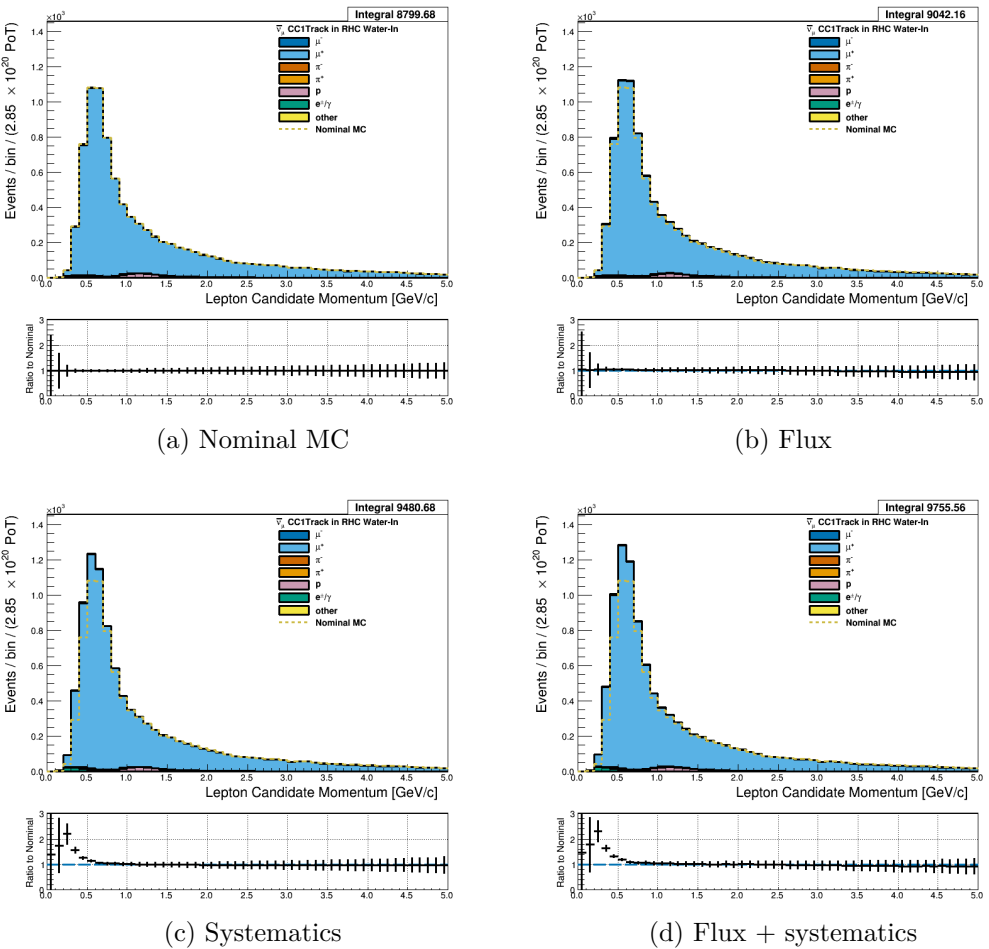


Figure 3.71: Reconstructed lepton candidate momentum separated by true particle species for RHC  $\bar{\nu}_\mu$  CC 1-Track events occurring in the PØD in water-out mode. (a) The nominal MC prediction without any weights applied. (b) The flux tuning are applied. (c) The systematic weighting are applied. (d) Both flux and systematic weighting are applied.

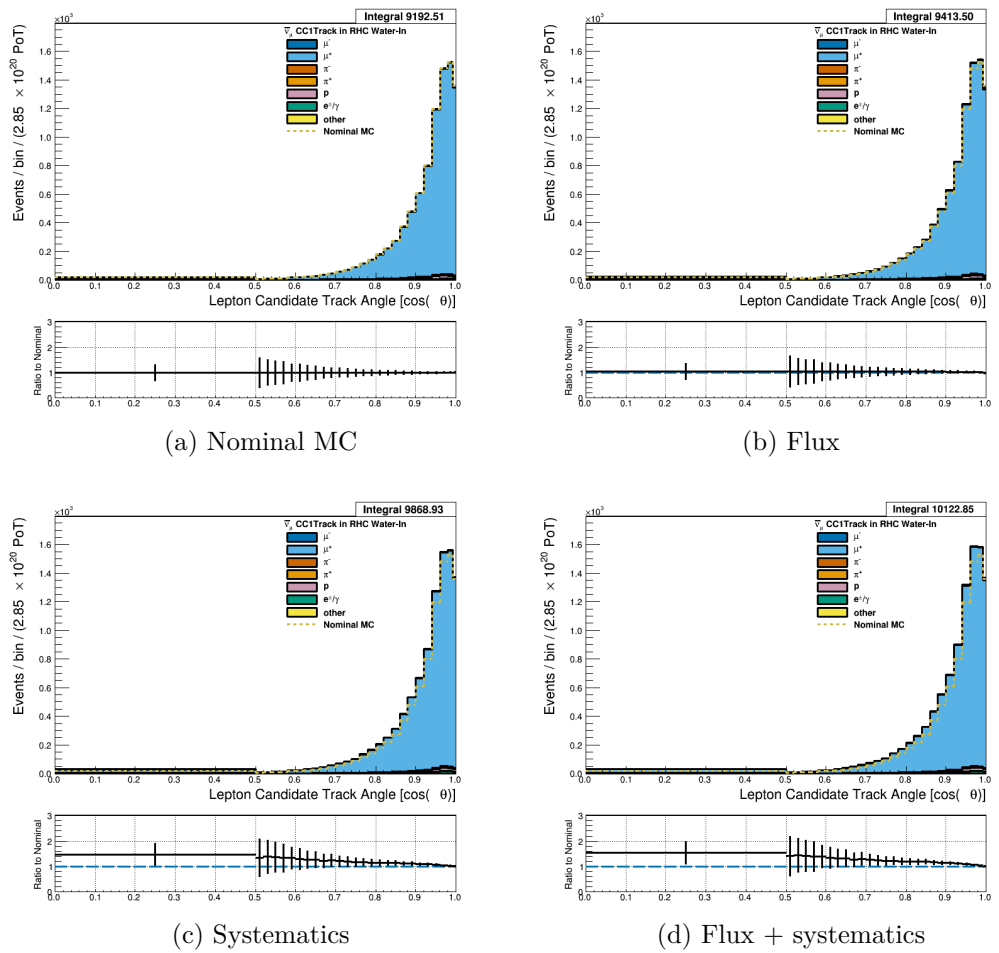


Figure 3.72: Reconstructed lepton candidate angle separated by true particle species for RHC  $\bar{\nu}_\mu$  CC 1-Track events occurring in the PØD in water-in mode. (a) The nominal MC prediction without any weights applied. (b) The flux tuning are applied. (c) The systematic weighting are applied. (d) Both flux and systematic weighting are applied.

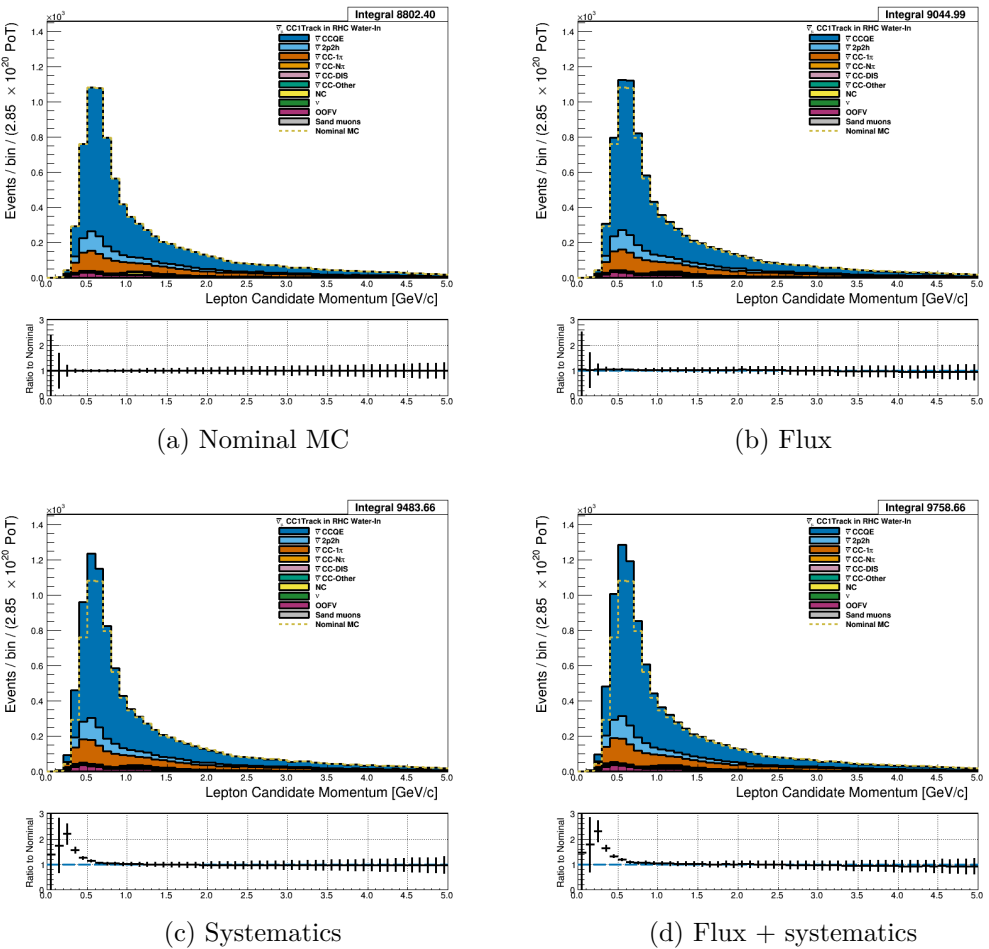


Figure 3.73: Reconstructed lepton candidate momentum separated by NEUT model interaction mode for RHC  $\bar{\nu}_\mu$  CC 1-Track events occurring in the PØD in water-out mode. (a) The nominal MC prediction without any weights applied. (b) The flux tuning are applied. (c) The systematic weighting are applied. (d) Both flux and systematic weighting are applied.

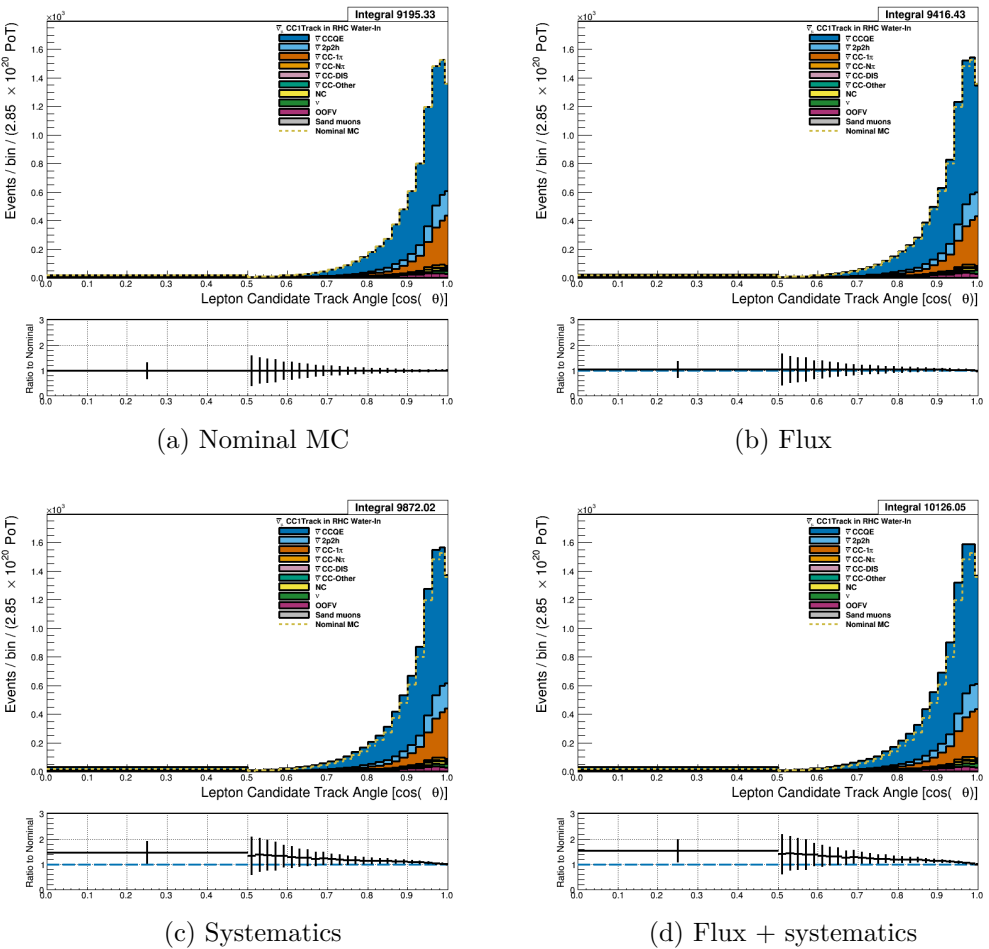


Figure 3.74: Reconstructed lepton candidate  $\cos \theta$  separated by NEUT model interaction mode for RHC  $\bar{\nu}_\mu$  CC 1-Track events occurring in the PØD in water-out mode. (a) The nominal MC prediction without any weights applied. (b) The flux tuning are applied. (c) The systematic weighting are applied. (d) Both flux and systematic weighting are applied.

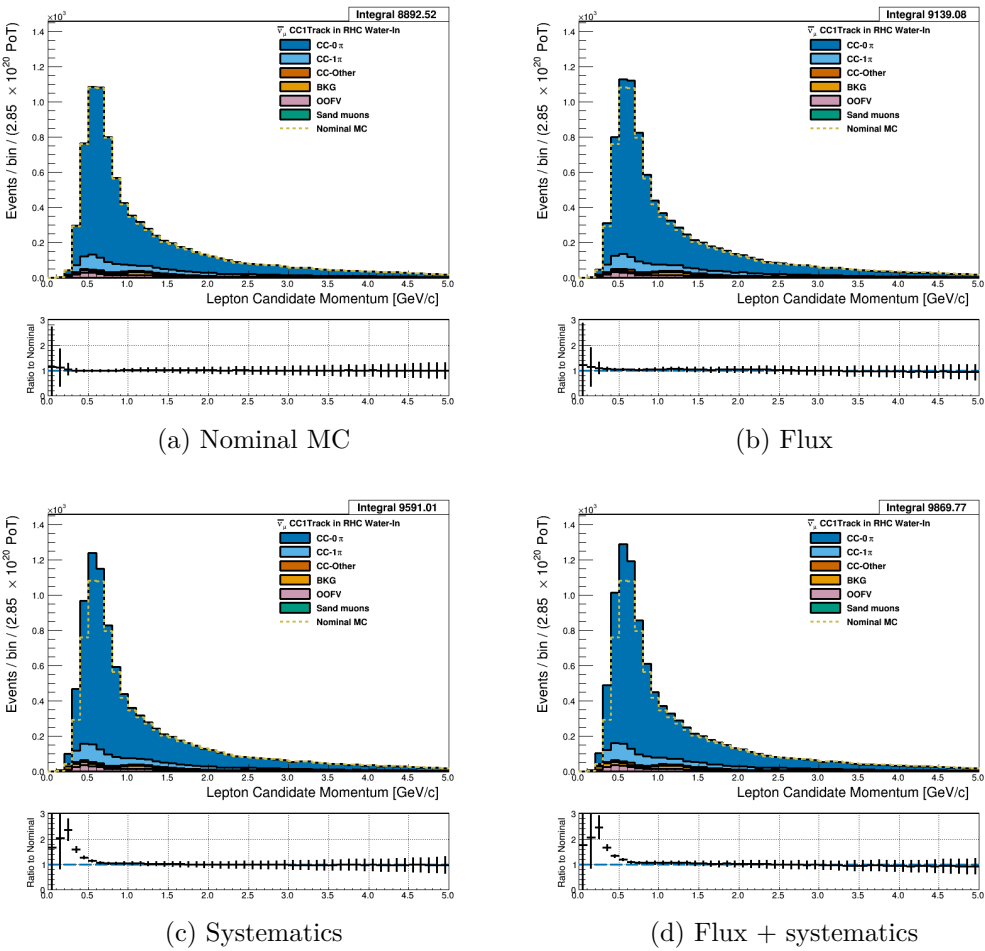


Figure 3.75: Reconstructed lepton candidate momentum separated by topology for RHC  $\bar{\nu}_\mu$  CC 1-Track events occurring in the PØD in water-out mode. (a) The nominal MC prediction without any weights applied. (b) The flux tuning are applied. (c) The systematic weighting are applied. (d) Both flux and systematic weighting are applied.

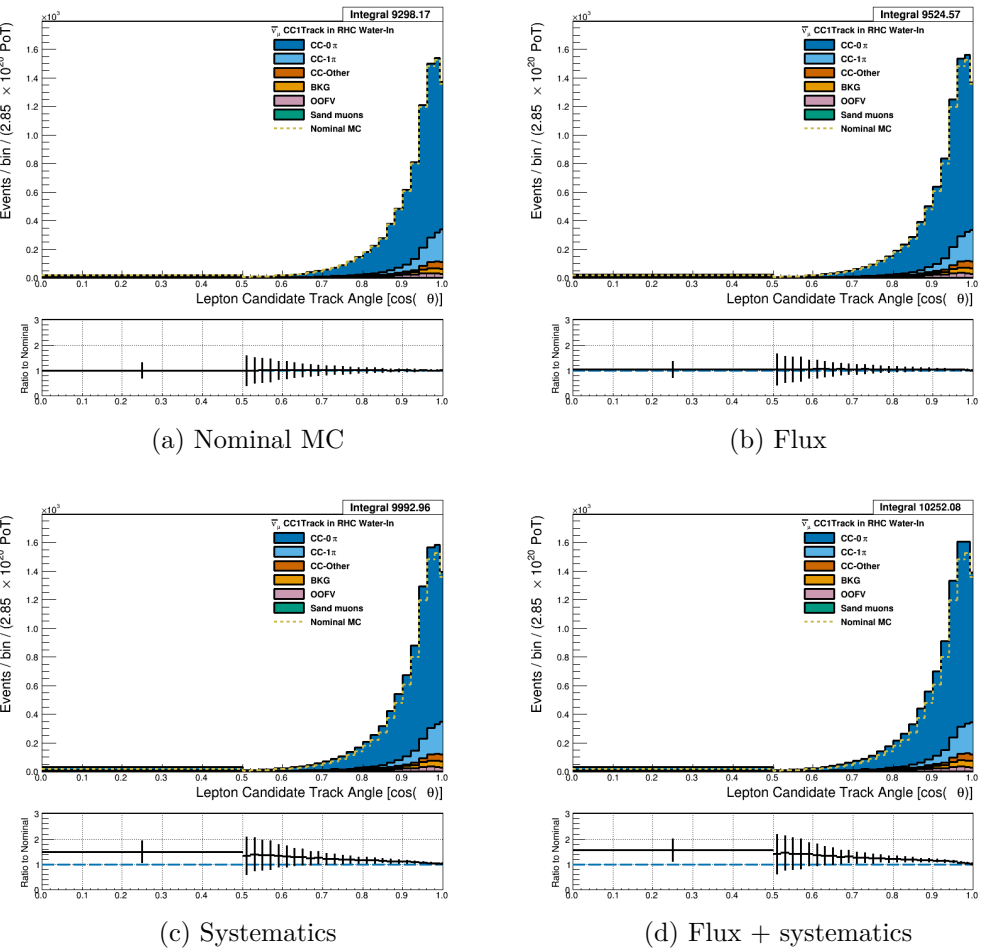


Figure 3.76: Reconstructed lepton candidate  $\cos \theta$  separated by topology for RHC  $\bar{\nu}_\mu$  CC 1-Track events occurring in the PØD in water-out mode. (a) The nominal MC prediction without any weights applied. (b) The flux tuning are applied. (c) The systematic weighting are applied. (d) Both flux and systematic weighting are applied.

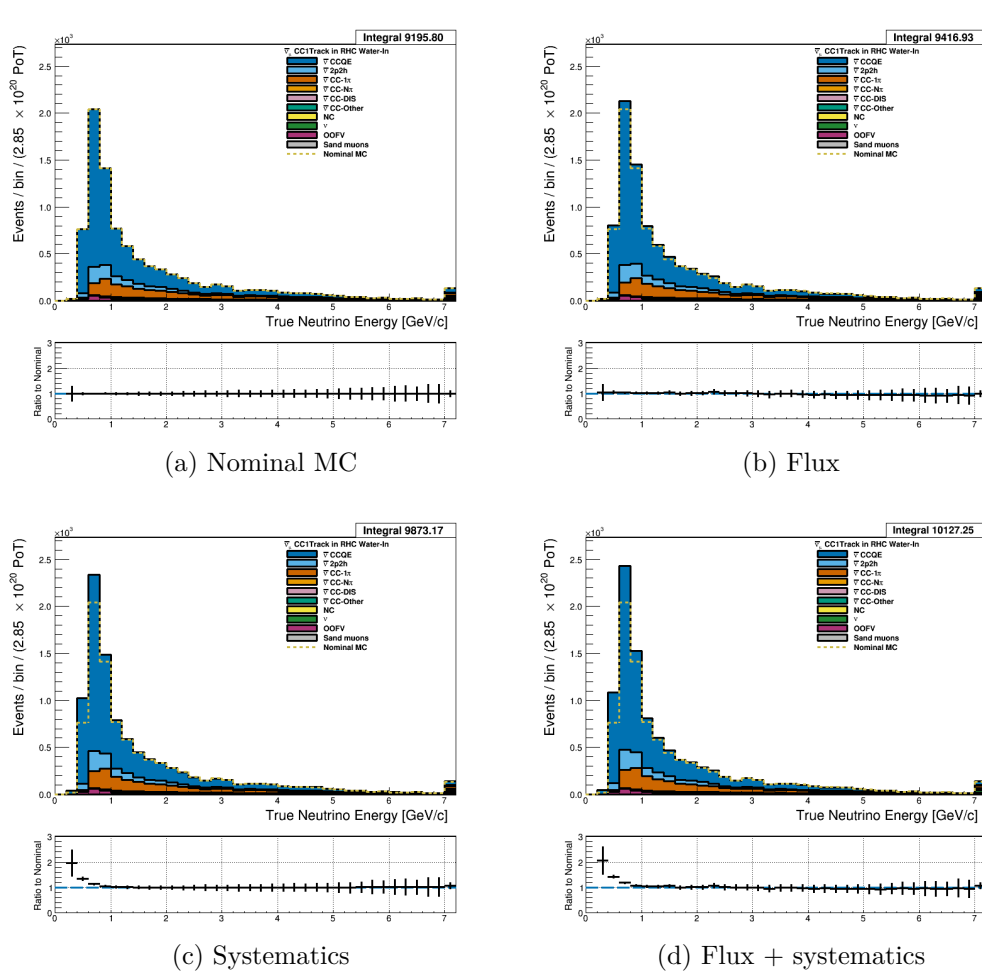


Figure 3.77: True neutrino energy associated with the lepton candidate separated by NEUT model interaction mode for RHC  $\bar{\nu}_\mu$  CC 1-Track events occurring in the PØD in water-out mode. (a) The nominal MC prediction without any weights applied. (b) The flux tuning are applied. (c) The systematic weighting are applied. (d) Both flux and systematic weighting are applied.

569   **3.5.2.3  $\nu_\mu$  Background Selection in RHC Mode:** Text

570   **3.5.3 CC N-Tracks (CCnQE Enhanced)**

571   Text

572   **3.5.3.1  $\nu_\mu$  Selection in FHC Mode:** Text

<sup>573</sup> **3.5.3.2  $\bar{\nu}_\mu$  Selection in RHC Mode:** Text

<sup>574</sup> **3.5.3.3  $\nu_\mu$  Background Selection in RHC Mode:** Text

<sup>575</sup> **3.5.4 Differences Between Water-Out and Water-In Samples**

576 **4 PØD-Only BANFF Parameterization**

577 **4.1 PØD Samples Fit Binning**

578 The PØD ND280 BANFF fit uses the samples described in 3. The bin edges are tabulated  
579 below.

- 580 • FHC  $\nu_\mu$ CC 1-Track bin edges:

581  $p$  [GeV/c]: 0, 0.3, 0.4, 0.5, 0.6, 0.7, 0.8, 1, 1.25, 1.5, 2, 3, 4, 5.5, 30

582  $\cos\theta$  : -1, 0.7, 0.8 , 0.88, 0.94, 0.96, 0.975, 0.99, 1

- 583 • FHC  $\nu_\mu$ CC N-Tracks bin edges:

584  $p$  [GeV/c]: 0, 0.4, 0.5, 0.6, 0.7, 0.8, 1, 1.2, 1.5, 1.8, 2.2, 2.7, 3.5, 5, 10, 30

585  $\cos\theta$  : -1, 0.65, 0.77, 0.85, 0.9, 0.94, 0.97, 0.99, 1

- 586 • RHC  $\bar{\nu}_\mu$ CC 1-Track bin edges:

587  $p$  [GeV/c]: 0, 0.4, 0.5, 0.6, 0.7, 0.8, 1, 1.25, 1.5, 2, 3, 30

588  $\cos\theta$  : -1, 0.82, 0.87, 0.9, 0.93, 0.95, 0.97, 0.99, 1

- 589 • RHC  $\bar{\nu}_\mu$ CC N-Tracks bin edges:

590  $p$  [GeV/c]: 0, 0.5, 0.9, 1.25, 1.6, 2, 3, 8, 30

591  $\cos\theta$  : -1, 0.8, 0.89, 0.95, 0.97, 0.99, 1

- 592 • RHC  $\nu_\mu$ CC 1-Track bin edges:

593  $p$  [GeV/c]: 0, 0.4, 0.6, 0.8, 1.1, 2, 10

594  $\cos\theta$  : -1, 0.78, 0.84, 0.89, 0.92, 0.95, 0.97, 0.98, 0.99, 1

- 595 • RHC  $\nu_\mu$ CC N-Tracks bin edges:

596  $p$  [GeV/c]:0, 0.4, 0.6, 0.8, 1, 1.5, 2, 3, 10

597  $\cos\theta$  : -1, 0.7, 0.8, 0.85, 0.9, 0.94, 0.965, 0.98, 0.99, 1

598 **4.1.1 Fit Binning Determination**

599 The fit binning is designed to optimized to ensure at least 1 predicted Monte Carlo (MC)  
600 event in each bin when scaled to the collected data POT. The fit bins must also account  
601 for detector smearing effects. In order to mitigate smearing and event migration, the recon-  
602 structed kinematics were examined to their MC truth value using only correctly identified  
603 leptons in one-dimensional kinematic slices. Since the MC provides about  $10\times$  the data  
604 statistics, the statistical uncertainty for each bin should be negligible for high statistics re-  
605 gions. The kinematics are scanned across their full relevant spaces in order to understand the  
606 needed width for a fit bin. The first fit bin is always defined from the kinematic maximum.

607 For the momentum bins, the momentum resolution is compared to MC truth . The  
608 momentum resolution is defined as

$$R(r, t) = \frac{r - t}{t},$$

609 where  $r$  is the reconstructed momentum and  $t$  is the true value. The momentum was scanned  
610 in finite bin widths with the mean and standard deviation of the resolution  $R$  extracted. The  
611 mean and standard deviation are used as a proxy for the true bias and true resolution, re-  
612 spectively. In addition, a bootstrapping algorithm was employed to understand the accuracy  
613 of the sample estimates. Bootstrapping in this context is sampling over all relevant values  
614 of true momentum and randomly replacing the values. For each scanned bin, at least 1000  
615 bootstrapping sampling with replacement was performed. In the case of large variances in  
616 the bootstrapping samples, additional 10000 sampling with replacement were performed.  
617 The results for analyzing the FHC  $\nu_\mu$ CC 1-Track selection is shown in Figure 4.1 on page

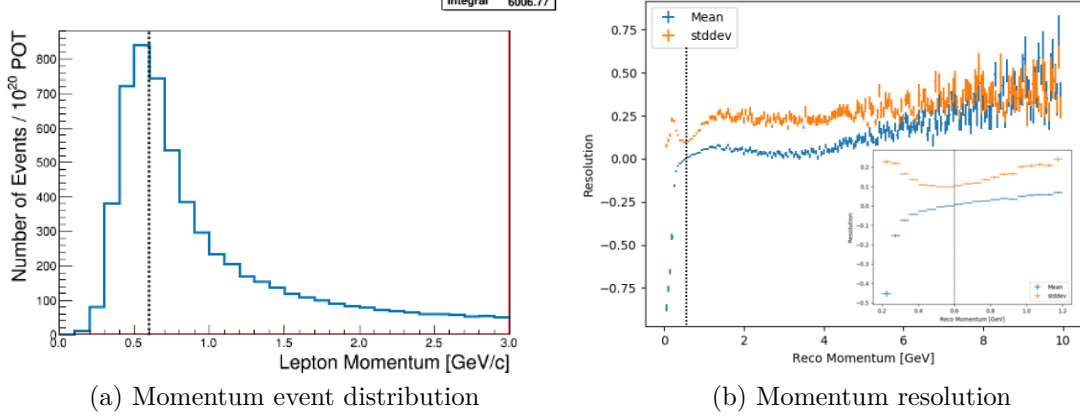


Figure 4.1: The momentum event distribution and uncertainty for FHC  $\nu_\mu$ CC 1-Track events is shown above. Only correctly identified muons are shown. (a) The number of events per unit momentum is scaled to  $10^{20}$  POT which is the approximate scale for all the samples in this analysis. A dashed line indicates the maximum of the peak. (b) The resolution of the momentum measurement is shown for a wide region of momenta. In the inset is the resolution zoomed near the momentum distribution maximum. Like in (a), a dashed line shows the momentum maximum.

618 114.

619     The angle bins are treated in an almost identical manner. While the fit bins and physics  
 620 parameterized in  $\cos \theta$ , the angle with respect to the z-axis, the detector smearing is a  
 621 function of the angle  $\theta$ . In addition, since the angle can be nearly zero for the most forward-  
 622 going tracks, the resolution was not used to characterize the angular uncertainties. Instead,  
 623 the difference between the true and reconstructed angle were analyzed as shown in . The  
 624 mean and standard deviation were studied. Bootstrapping was again used to quantify the  
 625 accuracy of the mean and standard deviation.

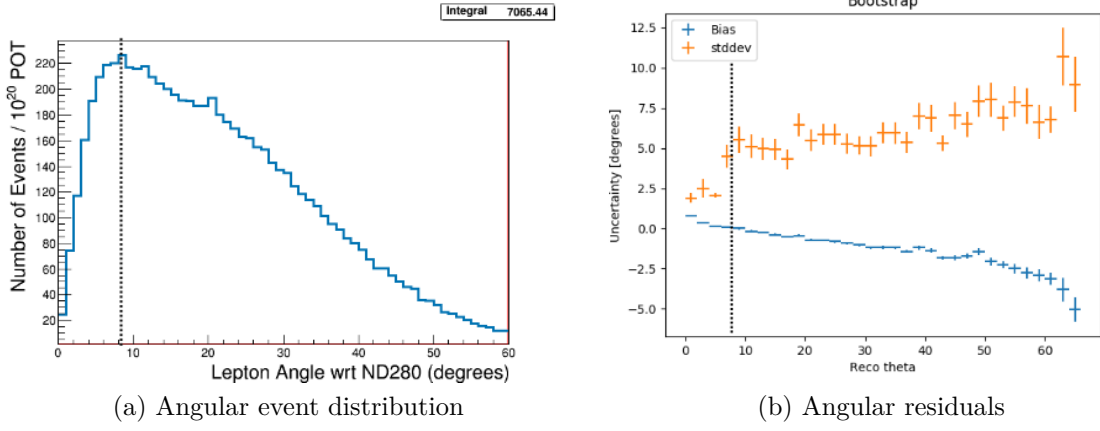


Figure 4.2: The angular event distribution and uncertainty for FHC  $\nu_\mu$ CC 1-Track events is shown above. Only correctly identified muons are shown. (a) The number of angular events is scaled to  $10^{20}$  POT which is the approximate scale for all the samples in this analysis. A dashed line indicates the maximum of the peak. (b) The residual of the angular measurement is shown up to where there are sufficient statistics. Like in (a), a dashed line shows the momentum maximum.

626

## 5 Detector Systematics

627

Text goes here

628

## 6 Fitter Validation

629

Fitter validation

630

## 7 Fitter Results

631

Fitter results

632 **8 Discussion**

633 Discussion

634

## References

- 635 [1] K. Abe et al. The T2K Experiment. *Nucl. Instrum. Meth.*, A659:106–135, 2011. 25
- 636 [2] S. Baker and R. D. Cousins. Clarification of the use of Chi-Square and Likelihood  
637 Functions in Fits to Histograms. *Nucl. Instrum. Meth.*, A221:437–442, 1983. 16
- 638 [3] S. Bienstock et al. Assessing the effect of cross-section model uncertainties on the T2K  
639 oscillation analyses with simulated data studies using the BANFF, MaCh3, P-Theta  
640 and VALOR frameworks, May 2018. T2K-TN-331 v5. 14
- 641 [4] S. Bienstock and Others. Constraining the Flux and Cross Section Models with Data  
642 from the ND280 Detector using FGD1 and FGD2 for the 2017 Joint Oscillation Analysis,  
643 August 2017. T2K-TN-324 v3. 14, 21
- 644 [5] S. Bolognesi and Others. Niwg model and uncertainties for 2017 oscillation analysis,  
645 April 2017. T2K-TN-315 v5. 21
- 646 [6] T. Campbell. Measurement of the  $\nu_\mu$  cc- $0\pi$  double differential cross section on water in  
647 the pød, February 2018. T2K-TN-328. 24
- 648 [7] T. Campbell and Others. Analysis of  $\nu_\mu$  charged current inclusive events in the pød in  
649 runs 1+2+3+4, Mar 2014. T2K-TN-80 v4. 24, 26, 27
- 650 [8] R. Das and Others. Measurement of induced charged current cross section on water  
651 using the pød and tpc, November 2014. T2K-TN-100. 24
- 652 [9] K. Gilje. Geometry and mass of the  $\pi^0$  detector in the nd280 basket, Apr 2012. T2K-  
653 TN-73 v3.1. 27

- 654 [10] M. Hartz and Others. Constraining the flux and cross section models with data from  
655 the nd280 detector for the 2014/15 oscillation analysis, May 2015. T2K-TN-220 v4. 14,  
656 16
- 657 [11] M. Hartz and Others. Constraining the Flux and Cross Section Models with Data from  
658 the ND280 Detector using FGD1 and FGD2 for the 2016 Joint Oscillation Analysis,  
659 June 2016. T2K-TN-230 v3. 14
- 660 [12] A. Hillairet and Others. Nd280 reconstruction, Nov 2011. T2K-TN-72 v1. 27
- 661 [13] T. Koga. Comparison between banff post fit results and on-axis detectors, 2017. 10
- 662 [14] K. Mahn and Others. Implementation of new cross section parameters for the 2017  
663 oscillation analysis, 2017. T2K-TN-307. 21
- 664 [15] G. Wikström and A. Finch. Global kalman vertexing in nd280, Feb 2018. T2K-TN-46  
665 v3. 26
- 666 [16] T. Yuan and Others. Double differential measurement of the flux averaged  $\nu_\mu$  cc0pi  
667 cross section on water, Aug 2016. T2K-TN-258 v4.6.1. 24, 26

668 **Nomenclature**

- 669 BANFF The **beam and near detector task force** is the group responsible for providing near  
670 detector constraints on cross section and flux model parameters.
- 671 CC-0 $\pi$  A **charged current zero pion selection** is an exclusive selection that selects neutrino  
672 interaction topologies only one MIP-like particle.
- 673 CC-Inclusive A **charged current event selection** that selects all neutrino interaction topolo-  
674 gies with an outgoing charged lepton.
- 675 FD The **far detector** refers to the particle detector in a long baseline neutrino oscilla-  
676 tion experiment that is located far away from the neutrino production source where  
677 oscillated neutrinos are observed.
- 678 FGD A **fine grain detector** is a detector made of closely spaced, small scintillating bars  
679 designed to provide precise resolution of charged particle tracks
- 680 FHC The **forward horn current beam configuration** that focuses positively charged particles  
681 into the particle decay pipe. This configuration produces a very pure  $\nu_\mu$  neutrino beam
- 682 HMNT The **highest momentum negatively-charged track** in the bunch
- 683 HMPT The **highest momentum positively-charged track** in the bunch
- 684 MIP A **minimum ionizing particle**
- 685 ND280 The **Near Detector** of T2K which is **280** meters away from the neutrino source.
- 686 ND The **near detector** refers to the particle detector in a long baseline neutrino oscillation  
687 experiment that is located close to the neutrino production source before neutrino  
688 oscillations occur.

689 CECal The **Central ECal** detector which is a part of the PØD inside ND280

690 PØD The  $\pi^0$  detector (**pi-Q** detector)

691 PØDule A collection of two active scintillator bar layers inside the PØD

692 RHC The **reverse horn current** beam configuration that focuses negatively charged particles  
693 into the particle decay pipe. This configuration produces a  $\bar{\nu}_\mu$  enriched neutrino beam  
694 with a significant  $\nu_\mu$  contribution.

695 FV The **fiducial volume** of a detector is the region where the detector response is well  
696 understood

697 TPC A **time projection chamber** is a device that detects and tracks charged particles with  
698 the application of strong electric fields

699 Tracker The region of ND280 consisting of two FGDs and TPCs

700 Global The **Global reconstruction module** responsible for making joined tracks between the  
701 subdetectors inside ND280

702 USECal The **Upstream ECal** which is a part of the PØD inside ND280